

# UNCLASSIFIED

AD NUMBER
AD917132
NEW LIMITATION CHANGE
TO Approved for public release, distribution unlimited
FROM Distribution authorized to U.S. Gov't. agencies only; Administrative/Operational Use; FEB 1974. Other requests shall be referred to Space and Missile Systems Organization, Norton AFB, CA 92409.
AUTHORITY
AFWL ltr, 23 May 1983

THIS PAGE IS UNCLASSIFIED

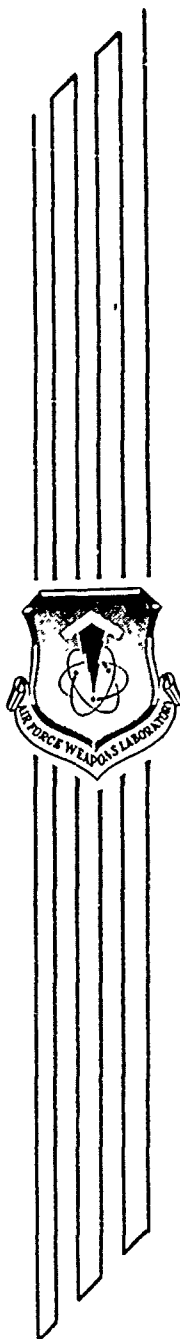
THIS REPORT HAS BEEN DELIMITED  
AND CLEARED FOR PUBLIC RELEASE  
UNDER DOD DIRECTIVE 5200.20 AND  
NO RESTRICTIONS ARE IMPOSED UPON  
ITS USE AND DISCLOSURE.

DISTRIBUTION STATEMENT A

APPROVED FOR PUBLIC RELEASE;  
DISTRIBUTION UNLIMITED.

L

AD917132



## ELECTROMAGNETIC PULSE COUPLING AND PROPAGATION TO POWER LINES: THEORY AND EXPERIMENTS

W. E. Scharfman      E. F. Vance  
Stanford Research Institute  
Menlo Park, CA 94025

February 1974

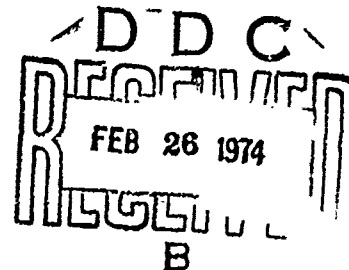
Final Report for Period 1 May 1972 through  
1 November 1973

Distribution limited to US Government agencies only because test and evaluation information concerning electromagnetic pulse coupling and propagation is discussed in the report (Feb 74). Other requests for this document must be referred to AFWL (ELA), Kirtland AFB, NM, 87117.

Prepared for

SPACE AND MISSILE SYSTEMS ORGANIZATION  
Norton Air Force Base, CA 92409

AIR FORCE WEAPONS LABORATORY  
Air Force Systems Command  
Kirtland Air Force Base, NM 87117



AIR FORCE WEAPONS LABORATORY  
Air Force Systems Command  
Kirtland Air Force Base  
New Mexico 87117

When US Government drawings, specifications, or other data are used for any purpose other than a definitely related Government procurement operation, the Government thereby incurs no responsibility nor any obligation whatsoever, and the fact that the Government may have formulated, furnished, or in any way supplied the said drawings, specifications, or other data, is not to be regarded by implication or otherwise, as in any manner licensing the holder or any other person or corporation, or conveying any rights or permission to manufacture, use, or sell any patented invention that may in any way be related thereto.

DO NOT RETURN THIS COPY. RETAIN OR DESTROY.

AFWL-TR-73-287

ELECTROMAGNETIC PULSE COUPLING AND PROPAGATION  
TO POWER LINES: THEORY AND EXPERIMENTS

W. E. Scharfman      E. F. Vance  
Stanford Research Institute  
Menlo Park, CA 94025

TECHNICAL REPORT NO. AFWL-TR-73-287

Final Report for Period 1 May 1972 through 1 November 1973

Distribution limited to US Government agencies only because test and evaluation information concerning electromagnetic pulse coupling and propagation is discussed in the report (Feb 74). Other requests for this document must be referred to AFWL (ELA), Kirtland AFB, NM, 87117.

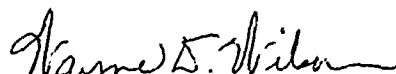
FOREWORD

This report was prepared by the Stanford Research Institute, Menlo Park, California, under Contract F29601-69-C-0127. The research was performed under Program Element 11213F, Project 133B, and was funded by the Space and Missiles Systems Organization (SAMSO).

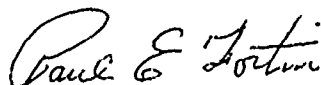
Inclusive dates of research were 1 May 1972 through 1 November 1973. The report was submitted 10 December 1973 by the Air Force Weapons Laboratory Project Officer, Captain Wayne D. Wilson (ELA).

The Contractor's report number is: SRI Project 7995.

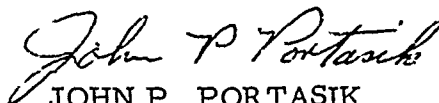
This technical report has been reviewed and is approved.



WAYNE D. WILSON  
Captain, USAF  
Project Officer



PAUL E. FORTIN  
Lt Colonel, USAF  
Chief, Aircraft and Missiles  
Branch



JOHN P. PORTASIK  
Colonel, USAF  
Chief, Electronics Division

ABSTRACT

(Distribution Limitation Statement B)

Coupling of transients to aboveground transmission lines is analyzed and measured experimentally. Measurements were made using scale models approximately 1-foot high to represent power transmission lines. The coupling to the line and the propagation characteristics of the line were measured. The effects of bends and junctions on the transmitted signals were measured and analyzed. Periodically, grounded lines and multiconductor lines were also examined. The variation of the induced-voltage waveforms with soil conductivity, line height, and pulse width were calculated.

# CONTENTS

I	INTRODUCTION . . . . .	1
A.	Background . . . . .	1
1.	Previous Work . . . . .	1
2.	Use of Scale Models . . . . .	2
3.	Experimental Verification of Coupling to Transmission Line . . . . .	3
B.	Other Aspects of Coupling to Power Lines . . . . .	5
C.	Purpose of this Report . . . . .	6
D.	Summary of Results . . . . .	6
1.	Common-Mode Coupling to the Transmission Line . . . . .	6
2.	Propagation Characteristics of Transmission Line . . . . .	7
3.	Effects of Bends and Junctions on Propagation . . . . .	8
4.	Multiconductor Transmission Lines . . . . .	9
5.	Periodically Grounded Conductor . . . . .	10
II	COMMON-MODE CURRENT AND VOLTAGE INDUCED IN TRANSMISSION LINES . . . . .	11
A.	General . . . . .	11
B.	Open-Circuit Voltage Induced by a Space Wave . . . . .	13
C.	Parametric Variation of the Open-Circuit Voltage . . . . .	17
D.	Vertically Polarized Wave at Grazing Incidence . . . . .	24
1.	General . . . . .	24
2.	Current Induced in Wire . . . . .	26
E.	Response of Vertical Element . . . . .	33
III	PROPAGATION OF CURRENTS INDUCED IN POWER LINES . . . . .	36
A.	Introduction . . . . .	36
B.	Real-Earth Effects . . . . .	36

III	PROPAGATION OF CURRENTS INDUCED IN POWER LINES (Continued)	
C.	Measurements of Propagation Effects . . . . .	43
D.	Step-Function Response . . . . .	43
E.	Low-Frequency Attenuation . . . . .	48
IV	DISCONTINUITIES ON POWER LINES . . . . .	51
A.	Bends . . . . .	51
B.	Symmetrical Junctions . . . . .	55
C.	Rise-Time Characteristics . . . . .	59
V	COUPLING TO MULTI-WIRE LINES . . . . .	61
VI	CONCLUSIONS AND RECOMMENDATIONS . . . . .	70
APPENDICES		
A	COMPARISON OF TRANSMISSION-LINE APPROXIMATION WITH THE EXACT SOLUTION . . . . .	73
B	THEORY OF ELECTROMAGNETIC SCALING . . . . .	81
C	ESTIMATED ACCURACY OF THE MODEL DATA . . . . .	87
REFERENCES . . . . .		89
DISTRIBUTION LIST . . . . .		91

## ILLUSTRATIONS

1	Coordinates Defining Azimuth and Elevation Angles of Incidence . . . . .	15
2	Open-Circuit Voltage at the End of a Semi-Infinite Line for Various Soil Conductivities . . . . .	17
3	Open-Circuit Voltage at the End of a Semi-Infinite Line for Various Line Heights . . . . .	18
4	Open-Circuit Voltage at the End of a Semi-Infinite Line for Various Incident Pulse Decay Time Constants . . . . .	20
5	Variation of the Directivity Function $D_v(\psi, 0)$ with Elevation Angle $\psi$ for Selected Values of the Parameter $\alpha/k$ . . . . .	21
6	Variation of the Directivity Function $D_h(\psi, 90)$ with Elevation Angle for $\alpha/k \ll 1$ . . . . .	22
7	Physical Arrangement That Produces a Vertically Polarized Wave with End-on Incidence . . . . .	24
8	Geometry for Analysis of the Coupling Configuration of Figure 7 . . . . .	28
9	Short-Circuit Current at the Terminals of a Line 1000 Meters Long and 1000 Meters from the Source with 1 V/m Incident on the End Nearest the Source ( $Z_0 = 300 \Omega$ , $z_1 = 1000$ m, $z_2 = 2000$ m). . . . .	31
10	Current Delivered to a Matched Load at the Top of a Vertical Riser by a Vertically Polarized Incident Wave . . . . .	35
11	Attenuation Constant of a Line Over Ground as a Function of Frequency, Where $h = 17$ Feet Full-Scale . . . . .	40
12	Attenuation Constant of a Line Over Ground as a Function of Frequency, Where $h = 100$ Feet Full-Scale . . . . .	41
13	Equipmental Set-up for Measurement of Current Waveforms of a Line Over Ground . . . . .	44
14	Current Waveform of a Single-Wire Line 1600 Feet (Full-Scale) from the Feed Point, Where $h = 17$ Feet Full-Scale . . . . .	45

# ILLUSTRATIONS (Continued)

15	Current Waveform of a Single-Wire Line 4000 Feet (Full-Scale) from the Feed Point, Where $h = 100$ Feet Full-Scale . . . . .	46
16	Current Waveform of a Three-Wire Line 1600 Feet (Full-Scale) from the Feed Point, Where $h = 17$ Feet Full-Scale . . . . .	47
17	Current Waveform of a Three-Wire Line 640 Feet (Full-Scale) from the Feed Point, Where $h = 29$ Feet Full-Scale . . . . .	47
18	Experimental Set-up for Measurement of Attenuation of a Wire over Ground . . . . .	48
19	Phase Constant as a Function of Frequency for a Single-Wire Line over Ground . . . . .	50
20	Two-Wire Line with a Bend . . . . .	52
21	Reflection and Transmission Coefficient of a Bend in a Single-Wire Line over Ground as a Function of Bend Angle . . . . .	53
22	Comparison of Calculated and Measured Reflection Coefficients of a Bend as a Function of Bend Angle . . . . .	54
23	Reflection Coefficient for a $90^\circ$ Bend as a Function of Radius of Curvature . . . . .	55
24	Reflection and Transmission Coefficient at a Symmetrical Junction, Where $h = 2$ Feet . . . . .	56
25	Reflection Coefficient at a Symmetrical Junction, Where $h = 1$ Foot . . . . .	58
26	Current Waveform on Side-Arm Line of a Junction . . . . .	60
27	Experimental Configuration for Coupling to Multi-Wire Lines over Ground . . . . .	62
28	Currents Coupled to Two-Wire Lines over Ground . . . . .	63
29	Currents Coupled to a Four-Wire Line with $400\text{-}\Omega$ Loads and Horizontal Polarization . . . . .	66
30	Phase to Neutral Currents on a Four-Wire Line with $400\text{-}\Omega$ Loads and Horizontal Polarization . . . . .	67

# ILLUSTRATIONS (Continued)

15	Current Waveform of a Single-Wire Line 4000 Feet (Full-Scale) from the Feed Point, Where $h = 100$ Feet Full-Scale . . . . .	46
16	Current Waveform of a Three-Wire Line 1600 Feet (Full-Scale) from the Feed Point, Where $h = 17$ Feet Full-Scale . . . . .	47
17	Current Waveform of a Three-Wire Line 640 Feet (Full-Scale) from the Feed Point, Where $h = 29$ Feet Full-Scale . . . . .	47
18	Experimental Set-up for Measurement of Attenuation of a Wire over Ground . . . . .	48
19	Phase Constant as a Function of Frequency for a Single-Wire Line over Ground . . . . .	50
20	Two-Wire Line with a Bend . . . . .	52
21	Reflection and Transmission Coefficient of a Bend in a Single-Wire Line over Ground as a Function of Bend Angle . . . . .	53
22	Comparison of Calculated and Measured Reflection Coefficients of a Bend as a Function of Bend Angle . . . . .	54
23	Reflection Coefficient for a $90^\circ$ Bend as a Function of Radius of Curvature . . . . .	55
24	Reflection and Transmission Coefficient at a Symmetrical Junction, Where $h = 2$ Feet . . . . .	56
25	Reflection Coefficient at a Symmetrical Junction, Where $h = 1$ Foot . . . . .	58
26	Current Waveform on Side-Arm Line of a Junction . . . . .	60
27	Experimental Configuration for Coupling to Multi-Wire Lines over Ground . . . . .	62
28	Currents Coupled to Two-Wire Lines over Ground . . . . .	63
29	Currents Coupled to a Four-Wire Line with 400- $\Omega$ Loads and Horizontal Polarization . . . . .	66
30	Phase to Neutral Currents on a Four-Wire Line with 400- $\Omega$ Loads and Horizontal Polarization . . . . .	67

# ILLUSTRATIONS (Continued)

31	Currents Coupled to a Four-Wire Line with 400- $\Omega$ Loads, Multiply-Grounded Neutral, and Horizontal Polarization . .	68
32	Currents Coupled to a Four-Wire Line with 400- $\Omega$ Loads, Multiply-Grounded Neutral, and Vertical Polarization . . .	69
A-1	Comparison of the Transmission-Line Approximation and the Exact Solution for the Current in a Wire over a Perfectly Conducting Ground Plane--Step-Function Incident Field, Vertically Polarized . . . . .	75
A-2	Comparison of the Transmission-Line Approximation and the Exact Solution for the Current in a Wire over a Perfectly Conducting Ground Plane--Step-Function Incident Field, Horizontally Polarized . . . . .	76
A-3	Comparison of the Transmission-Line Approximation and the Exact Solution for the Current in a Wire over a Perfectly Conducting Ground Plane--Impulse Incident Field, Vertically Polarized . . . . .	78
A-4	Comparison of the Transmission-Line Approximation and the Exact Solution for a Vertically Polarized Incident Exponential Pulse . . . . .	79
A-5	Comparison of the Induced-Current Spectra for Horizontal Polarization . . . . .	80
C-i	Scale-Model Experiment to Study Coupling to Transmission Line . . . . .	88

## SECTION I

### INTRODUCTION

#### A. Background

##### 1. Previous Work

The coupling of the EMP wave to power transmission lines was initially analyzed using a low-frequency version of Sunde's theory,<sup>1</sup> which was valid for a long, straight transmission line whose height was smaller than the longest wavelength of interest. The analysis of transmission lines using this approach was reported in Technical Memorandum 22 for this contract.<sup>2</sup> Because of its apparent limitation to the low frequency portion of the EMP spectrum, however, two programs were initiated to improve the understanding of the coupling to the transmission lines. The first was a more rigorous analysis of the coupling to the transmission line that was not limited to a height-to-wavelength ratio less than one ( $h/\lambda < 1$ ). The details of this effort will be reported in a separate document; however, some of the important results are contained in Appendix A. The second was an experimental determination of the actual coupling to a transmission line when the height-to-wavelength ratio  $h/\lambda$  is not smaller than one. To study coupling to a power transmission line in such a manner that directional effects, propagation characteristics, radiation, and scattering effects could be adequately assessed, however, would require an extensive effort, a large test site, and a large mobile transmitter. The cost of a thorough evaluation of the coupling would have been prohibitive, and the results that could have been obtained from a simple test would have answered fewer questions than they left unanswered. Because of the limitations in the practical ability to experimentally examine the coupling to full scale power transmission lines, and because it was anticipated that the results of the rigorous analysis of the

coupling might not be available soon enough to meet the immediate requirements of the Air Force, it was proposed to use scale modelling of the power lines to study the coupling experimentally.

## 2. - Use of Scale Models

The use of scale models to obtain engineering solutions to complicated electromagnetic problems is an old but powerful technique. It is, in essence, an analog computer technique used for problems that are very difficult to solve accurately (or with confidence) by conventional approaches used in mathematics and physics either because they entail complicated geometries or because the relative importance of the various factors thought to influence the solution is unknown. These problems can be solved, however, by constructing electromagnetic models of the structures, surroundings, and excitation sources, and measuring the solution. A classic example of the use of scale models is the use of electrolytic tanks to map the fields or equipotential surfaces about irregular-shaped bodies that are (or were) difficult to analyze. A more current example is the use of models to study aircraft antenna performance. Since the typical airframe is much too complicated to permit an analytical determination of antenna patterns and impedances with sufficient economy (even with modern computation methods) to justify aircraft antenna design based on analytical techniques alone, aircraft (and other vehicular) antenna design has, for the last two decades, relied on the scale model method of determining radiation patterns.

Electromagnetic scale modelling is useful primarily because the technique

- Is economical.
- Allows timely determination of engineering solutions.
- Provides solutions to problems too difficult to solve analytically.

- Permits greater control to be exercised over the experiment under laboratory conditions.
- Allows flexibility to modify the model to study the effects of changes in geometry, an advantage that is particularly useful when the exact geometry is unknown.

The technique is particularly well suited to the solution of problems that are too complicated, because of the geometry or parameters involved, to solve in a timely manner by analytical methods, yet simple enough structurally that a scale model can be constructed quickly and economically. Power transmission lines and airframes are good examples of structures that can be constructed quickly and economically. The interior of the aircraft or the structure inside a power transformer are much more difficult to build into scale models; hence they are not good candidates for analysis using scale models (at least not with the same models used to study the power line and the airframe).

### 3. Experimental Verification of Coupling to Transmission Line

The scale model facility used to study the common mode coupling to the transmission line consisted of an area of soil that was salted to increase its conductivity to about 0.2 mho/m. The test area was illuminated with a pulse radiated by a dipole antenna. The radiated pulse was essentially a two-exponential pulse with a rise time of less than 0.3 ns, and a decay time that could be varied from a fraction of a nanosecond to about 35 ns, so that responses ranging from the impulse response to the step-function response could be obtained. Both vertical polarization and horizontal polarization of the wave were used, and azimuth angles of incidence from 0 to 180 degrees relative to the direction of the transmission line were examined. Elevation angles of 0 and about 30 degrees with respect to the horizontal were used for most of the experiments. The experiments were based on a nominal scale of 20:1, so that a 20-foot

high transmission line over soil of conductivity  $10^{-2}$  mho/m would be simulated by a 1-foot-high transmission line over salted earth with conductivity 0.2 mho/m. This basic model could also be interpreted as a 40:1 scale model of a 40-foot-high transmission line over soil of conductivity  $5 \times 10^{-3}$  mho/m, however. In fact, in the course of the parametric study of coupling, the model line height was varied from 0 to 2 feet, so that a range of line heights (or by a different interpretation, a range of soil conductivities) was studied. The scaling considerations for electromagnetic modeling are discussed in detail in Appendix B.

The results of the scale-model studies of common mode coupling to the transmission line indicated that, for the full scale rise times of 5 to 10 ns, the low-frequency analysis developed in Technical Report 5 for this contract<sup>3</sup> is adequate to describe all significant features of the transmission line response. This result was somewhat surprising in view of how far beyond the limits of validity of the low-frequency analysis the spectrum of a pulse with 5 ns rise time extends. The low frequency analysis represents the induced current so accurately because (1) the field strength of the wave scattered from the wire and reflected back to the wire by the ground is small, so that the current it induces in the wire is small compared to that induced by the direct wave, and (2) over the pulse spectrum, the "scattering impedance" (i.e., the ratio of the axial component of the incident field to the current induced in the wire) is nearly equal to twice the characteristic impedance of the wire over ground, so that the induced current is almost the same whether the wire is viewed in early times as a transmission line (low-frequency model) or as a scattering cylinder in space. (For much faster rise times there should be a noticeable difference, however, because, for frequencies considerably higher than those contained in the pulse spectrum, the "scattering impedance" is significantly smaller than  $2Z_0$ , so that the induced current at very early times would be significantly larger than that predicted by the low-frequency transmission-line theory.)

The experimental studies of coupling to long, straight transmission lines thus demonstrated that the hypothesized coupling mechanisms were correct and that the effect of line height, soil conductivity, and angle of incidence predicted by the low-frequency transmission-line theory were adequate throughout the pulse spectrum of interest (i.e., 10 kHz to 100 MHz). In addition, the effect of coupling to a vertical element such as a transformer ground wire or a service entrance conduit were studied using the scale model, and the transmission-line theory was adapted to the analysis of coupling to these elements.

#### B. Other Aspects of Coupling to Power Lines

A typical power-distribution transmission line is not, however, a long straight line. The typical distribution line contains bends necessary to follow the right of way and spur lines that branch off from the main line to serve other loads within the distribution area. In addition, the transmission line contains three or four conductors instead of the single conductor assumed in the common-mode model, and in the four-wire wye system, the neutral wire is sometimes grounded periodically along the transmission line. Since these features of practical distribution lines may affect the coupling to the lines or the propagation of the coupled signal to the customer's terminals, additional model studies, accompanied by analyses, were made to evaluate the effects of these phenomena.

In addition, the analysis of the coupling presented in Technical Report 5<sup>3</sup> was in the frequency domain, and much of the scale model work was performed with pulses approximating a step function because the step function response is readily analyzed and interpreted. The exponential pulse response is more representative of the EMP, however. Now that the coupling theory has been validated using the model studies, the

response of the transmission line to exponential pulses for various line heights and soil conductivities can be calculated to assess the effects of these parameters on the waveform and peak values of the induced current or voltage.

#### C. Purpose of this Report

The purpose of this report is to examine the effect of the coupling parameters on the induced waveform and to examine the effects of the non-ideal aspects of practical transmission lines on the coupling and propagation of the induced signals. In addition, the status of the power-line coupling was to be reviewed to determine the requirements for full-scale testing on a power transmission line, if such testing is deemed necessary.

#### D. Summary of Results

##### 1. Common-Mode Coupling to the Transmission Line

The maximum common-mode coupling to the transmission line, as measured by the open-circuit voltage or short-circuit current at the end of a long, straight line, is obtained for a vertically polarized wave incident along the axis of the transmission line and propagating toward the terminals. For a truly semi-infinite line length, the peak voltage is limited only by the attenuation of the transmission line, but for the more likely case of a finite length of straight line a few kilometers long, the peak voltage is limited by line length. The waveform of the short circuit current induced at the end of a finite length of straight line by the vertically polarized exponential wave incident along the axis is a short spike of current having a rise time approximately equal to the rise time of the incident field and a fall time roughly one-tenth that of the incident field (assuming the rise time of the incident field is

much less than its fall time). For other angles of incidence, the rise time of the open-circuit voltage (or short-circuit current) is a few tenths of the fall time of the incident wave, and the fall time is very slow (several fall times of the incident wave). In either case, the peak current or voltage is roughly inversely proportional to the square root of the soil conductivity and only weakly dependent on line height (except when the line is over very highly conducting soils).

For average soil conductivity ( $10^{-2}$  mho/m), a 10-meter line height, and a 1-V/m exponential pulse with a 1- $\mu$ s decay time incident on a 1000-meter long line, the peak induced current will be about 0.93 A for a plane wave and about 0.65 A for a spherical wave (with 1 V/m at the end closest to the source). For the lossless semi-infinite line with the plane 1 V/m wave incident at an elevation angle of 10 degrees, the short-circuit current would be 2.8 A. The corresponding open-circuit voltages for a 300-ohm transmission line are 280, 195, and 840 volts per V/m, respectively. It should be emphasized that these responses are for vertically polarized waves incident at grazing angles along the axes of long straight transmission lines. Whether this combination of source characteristics and transmission line characteristics actually occurs frequently in practical situations of concern should be considered before such coupling characteristics are used as system excitation criteria.

## 2. Propagation Characteristics of Transmission Line

The propagation characteristics of the common mode signal were studied experimentally by observing the change in the leading edge of a fast-rising pulse as it propagated along the line, and by measuring the position and width of the null in the CW standing wave on the line when it was short-circuited at one end. In both cases, the results were found to agree very well with those given by Sunde<sup>1</sup> and Technical Report 5.<sup>3</sup>

It was concluded, therefore, that the dominant parameters affecting the propagation characteristics of the power transmission line were the conductor height and the soil conductivity and that these factors are adequately accounted for (for engineering purposes) by the work of Sunde.<sup>1</sup>

### 3. Effects of Bends and Junctions on Propagation

A bend in the transmission line was found to cause a small reflection of the leading edge of the incident current. The properties of the transmission line can be represented by a distributed decrease in the inductance and capacitance per unit length in the vicinity of the bend, which causes a local decrease in the effective characteristic impedance of the line. The peak reflected current for sharp bends of 90 degrees or less is 6 percent or less of the incident current for full scale current rise times of the order of 10 ns. Because a little of the leading edge of the incident current pulse is reflected, the rise time of the current transmitted beyond the bend is slightly longer, but these effects are quite small and can be neglected without serious error for bends smaller than 90 degrees. If the radius of the bend is increased, the effect of the bend is reduced, so that for a bend radius of 20 feet in a 20-foot-high line, the reflection is reduced from 6 percent to 2 percent for a 90-degree bend.

The effect of a branch in the line formed by the junction of two load lines with a source line is, to a first approximation, represented well by classical transmission line theory. When a source line of characteristic impedance  $Z_0$  is loaded by two identical transmission lines in parallel, the current transmitted to each of the load lines is two thirds of the current incident on the junction from the source line, and the current reflected back down the source line from the junction is one third the incident current. When the angle between the two load lines

is small, there is some deviation from this ideal line behavior because of mutual coupling between the load lines. The current transmitted to the load lines decreases when mutual coupling is significant, however, so that the maximum transmitted current occurs when the lines are behaving as ideal transmission lines.

#### 4. Multiconductor Transmission Lines

The studies of multiconductor transmission lines indicate that differential currents whose magnitude is related to the wire spacing and angle of incidence of the wave are induced in the transmission lines. The results are generally consistent with those predicted by Harrison et al., but their work was for two-wire transmission lines in free space, while the cases of interest here are for two or more wires above a ground plane. Because the ground-reflected wave incompletely cancels the direct wave, the late-time differential current does not go to zero as might be expected for two wires over a perfect ground. Instead, a residual differential current of about 20 percent of the peak value continues to flow at late times. For typical line heights and wire spacings the peak differential current for a 45-degree angle of incidence can be of the order of one-tenth of the common mode current with a perfect ground for horizontal polarization incident at broadside. At smaller angles of incidence the fraction can be larger, because the common mode coupling decreases and the differential mode coupling increases as the elevation angle decreases. The differential mode coupling tends to be smallest when the common mode coupling is largest, however, so that the maximum differential current is quite small compared to the maximum common mode current. Thus, for example, the maximum differential current for 1 V/m incident on a two-wire line with one-meter spacing is of the order of 6 to 10 mA, whereas maximum common mode currents of the order of 1 to 3 A (at a different angle of incidence) were calculated.

For a four-wire system with the neutral periodically grounded, however, the differential current between the three phase conductors and the neutral can be almost as large as the common mode current, apparently because the neutral is maintained at approximately ground potential, while the phase conductors assume approximately the potential they would have if the neutral conductor were not present.

##### 5. Periodically Grounded Conductor

The common mode propagation characteristics of a periodically grounded conductor were found to behave as a transmission line with many spurs in early times (before the reflections from the bottoms of the ground wires returned to the horizontal conductor) and as a conductor in contact with the soil at late times. In early times, the transmitted current was roughly  $(2/3)^n$  times the incident current, where  $n$  is the number of ground leads along the line. At late times, the series impedance per unit length can be represented by  $Z_g/l$ , where  $Z_g$  is the impedance of the ground rods at the base of the ground leads, and  $l$  is the spacing between the ground leads. At an intermediate frequency associated with the line height and the spacing between grounds, there was a minimum in the line attenuation, and for long sections of periodically grounded line, this frequency tended to dominate the transmitted current.

## SECTION II

### COMMON-MODE CURRENT AND VOLTAGE INDUCED IN TRANSMISSION LINES

#### A. General

The analysis of the common-mode coupling to transmission lines is described in considerable detail in Technical Memorandum 22.<sup>2</sup> There the detailed analysis of the coupling and experimental verification of the analytical results are presented. In this section the analytical procedures developed in Technical Memorandum 22<sup>2</sup> will be used to calculate the common-mode voltage and current waveforms for various angles of incidence, soil conductivities, line heights, and incident pulse durations.

In Sections B and C, the effect of these parameters is investigated for the semi-infinite horizontal conductor. There it is shown that the strongest coupling occurs for vertical polarization incident on a poorly conducting soil at small angles of incidence. Because the length of line effective in producing a current or voltage waveform of duration  $t$  is of the order of  $ct/(1 - \cos \psi \cos \phi)$ , the semi-infinite transmission line model is valid for small angles  $\psi$  and  $\phi$  only if the line is very long, and for  $\psi = \phi = 0$  the line length must be truly infinite.

A more realistic model for the transmission line when  $\psi = \phi = 0$  is a line of finite length with the incident field strength varying as  $1/z$  along its length. This case is examined in Section II-D, where it is known that the major coupling is due to the horizontal electric field induced in the soil. The waveform of the induced current or voltage is then a function of the incident pulse shape and the electrical properties of the soil. The waveforms for this end-fire coupling ( $\psi = \phi = 0$ ) are calculated for a two-exponential incident pulse waveform for soil conductivities between  $10^{-1}$  and  $10^{-3}$  mho/m. As in the case of the semi-infinite

line, the induced current increases as the soil conductivity decreases ( $I\sqrt{\sigma} \approx \text{constant}$ ), but whereas the current induced in a low-loss, semi-infinite transmission line approaches infinity as the line attenuation approaches zero, the current induced in a finite length transmission line is always finite even if there is no line attenuation. The waveform of the induced current for the end-fire condition is also quite different from that for oblique incidence because, in the end-fire case, all of the induced effects arrive at the terminals in synchronism, while, in the case of oblique incidence, there is some dispersion of the induced current.

The current induced in a vertical element, such as a ground wire or service entrance conduit, is calculated for an exponential incident pulse in Section II-E. In Technical Memorandum 22,<sup>2</sup> this current was shown to be significant in comparison with the current induced in a horizontal conductor over a good ground plane. If the soil conductivity is  $10^{-2}$  mho/m or less, however, the current induced in the riser is small compared to the peak current induced in the horizontal conductor by a vertically polarized wave incident at a small angle (relative to the horizontal conductor). The direction of the current induced in the riser is such that a riser at the end of a transmission line tends to reduce the maximum peak current in the combination of horizontal and vertical conductors, but this reduction would not be great for typical-to-poor soils.

The results of this parametric study of the common mode voltages and currents induced in the power transmission system leave little doubt that the maximum coupling for average-to-poor soil conductivity occurs for end-on incidence with vertical polarization. Unless the transmission lines are very long and straight (over 10 kilometers) and subjected to a vertically polarized wave with an angle of incidence of 10 degrees or less, however, it is not possible to achieve the strong coupling reported in Baird, Marable, and Nelson<sup>4</sup> for conductors of infinite length in

line, the induced current increases as the soil conductivity decreases ( $I\sqrt{\sigma} \approx \text{constant}$ ), but whereas the current induced in a low-loss, semi-infinite transmission line approaches infinity as the line attenuation approaches zero, the current induced in a finite length transmission line is always finite even if there is no line attenuation. The waveform of the induced current for the end-fire condition is also quite different from that for oblique incidence because, in the end-fire case, all of the induced effects arrive at the terminals in synchronism, while, in the case of oblique incidence, there is some dispersion of the induced current.

The current induced in a vertical element, such as a ground wire or service entrance conduit, is calculated for an exponential incident pulse in Section II-E. In Technical Memorandum 22,<sup>2</sup> this current was shown to be significant in comparison with the current induced in a horizontal conductor over a good ground plane. If the soil conductivity is  $10^{-2}$  mho/m or less, however, the current induced in the riser is small compared to the peak current induced in the horizontal conductor by a vertically polarized wave incident at a small angle (relative to the horizontal conductor). The direction of the current induced in the riser is such that a riser at the end of a transmission line tends to reduce the maximum peak current in the combination of horizontal and vertical conductors, but this reduction would not be great for typical-to-poor soils.

The results of this parametric study of the common mode voltages and currents induced in the power transmission system leave little doubt that the maximum coupling for average-to-poor soil conductivity occurs for end-on incidence with vertical polarization. Unless the transmission lines are very long and straight (over 10 kilometers) and subjected to a vertically polarized wave with an angle of incidence of 10 degrees or less, however, it is not possible to achieve the strong coupling reported in Baird, Marable, and Nelson<sup>4</sup> for conductors of infinite length in

practical power distribution lines. The current that can be induced in a very long conductor by a wave at grazing incidence has another limitation; the wave cannot be maintained near the surface of the ground because of losses to the soil (the power density lost to the soil is of the order  $\eta/\eta_0$  times that propagating along the surface). For straight transmission lines a few kilometers long, however, it is possible to attain voltages of a few hundred times the incident field strength for the unique end-on case ( $\theta = \phi = 0$ ).

#### B. Open-Circuit Voltage Induced by a Space Wave

The open-circuit voltage induced at the terminals of a semi-infinite transmission line is analyzed in Technical Memorandum 22<sup>2</sup> for arbitrary angles of incidence, soil conductivities, and line heights. The open-circuit voltage and short-circuit current were obtained for impulse and step-function incident fields in that analysis. Here we will present the transient responses of the transmission line for incident exponential pulses, of selected decay time constants, for typical soil conductivities and line heights. Although the high-altitude EMP waveform is usually represented by a two-exponential pulse, the exponential rise time of the pulse contributes very little to the response of the transmission line if the rise time-constant is smaller than the transit time,  $h/c$ , between the ground and the transmission line. Therefore, the responses presented here are for zero-rise-time exponential pulses.

In addition, the results reported in Technical Memorandum 22<sup>2</sup> indicate that the error in assuming that the soil behaves as a good conductor (i.e.,  $\epsilon > \kappa\epsilon$ ) is very small for soils with average or above average conductivity. The slight error resulting from this assumption makes the open-circuit voltages appear to be slightly larger than they would be if the dielectric behavior of the soil at early times were fully accounted for. Because the error is small and on the conservative side from the

EMP vulnerability viewpoint, the results are given for the case when the ground is a good conductor. Neglecting the early-time dielectric behavior of the ground also simplifies the computation to the extent that very good results can be obtained using tabulated functions and hand calculations, which is an important advantage when a quick estimate of the voltage induced in a particular transmission line is required.

The open-circuit voltage developed at the end of a semi-infinite transmission line of height  $h$  above a perfectly conducting ground is

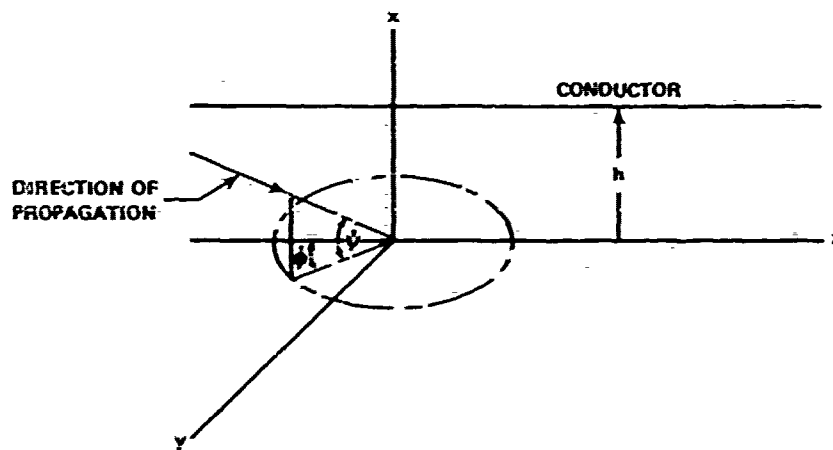
$$V_{\infty}(\omega) = E_0 c D(\psi, \varphi) \frac{1 - e^{-j\omega t_0}}{j\omega(j\omega + \frac{1}{\tau})} \quad (1)$$

when an exponential pulse  $E_0 e^{-t/\tau}$  is incident at an elevation angle  $\psi$  and azimuth angle  $\varphi$  as illustrated in Figure 1. The directivity function  $D(\psi, \varphi)$  is given by

$$\begin{aligned} D(\psi, \varphi) &= \frac{\sin \psi \cos \varphi}{\frac{\alpha c}{j\omega} \div 1 - \cos \psi \cos \varphi} \quad (\text{vertical polarization}) \\ &= \frac{\sin \varphi}{\frac{\alpha c}{j\omega} \div 1 - \cos \psi \cos \varphi} \quad (\text{horizontal polarization}) \end{aligned} \quad (2)$$

and  $t_0 = (2 h \sin \psi)/c$ , where  $c$  is the speed of light. In the expressions for  $D(\psi, \varphi)$ , it is assumed that the phase factor for the transmission line is the same as that for free space, but the line may have some attenuation, represented by  $\alpha$ , if finitely conducting wire is used for the transmission line.

The correction that must be applied to  $V_{\infty}$  to account for the finite conductivity of the soil when  $\sigma \gg \omega \epsilon$  is



LA-7995-61

FIGURE 1 COORDINATES DEFINING AZIMUTH AND ELEVATION ANGLES OF INCIDENCE

$$\begin{aligned} \Delta V &= E_0 \sqrt{\epsilon_c} D(\theta, \varphi) \frac{2}{\sin \theta} \frac{e^{-j\omega t_0}}{\sqrt{j\omega} (j\omega + \frac{1}{\tau})} \quad (\text{vertical polarization}) \\ &= E_0 \sqrt{\epsilon_c} D(\theta, \varphi) 2 \sin \theta \frac{e^{-j\omega t_0}}{\sqrt{j\omega} (j\omega + \frac{1}{\tau})} \quad (\text{horizontal polarization}) \end{aligned} \quad (3)$$

When the propagation factor for the transmission line is dominated by the capacitance and inductance of the line over perfect ground (see Section III), the directivity factor  $D(\theta, \varphi)$  is given by Eq. (2). In Eq. (3) above,  $\tau_c = \epsilon_0 / \sigma$ , where  $\sigma$  is the soil conductivity and  $\epsilon_0$  is the permittivity of free space.

The total open-circuit voltage is then

$$\begin{aligned} V_{oc} &= V_{\infty} + \Delta V \\ &= E_0 \sqrt{\epsilon_c} D(\theta, \varphi) \left[ \frac{1 - e^{-j\omega t_0}}{j\omega (j\omega + 1/\tau)} + 2\sqrt{\epsilon_c} (\sin \theta)^{\pm 1} \frac{e^{-j\omega t_0}}{\sqrt{j\omega} (j\omega + 1/\tau)} \right] \quad (4) \end{aligned}$$

where the exponent  $+1$  is associated with horizontal polarization and  $-1$  is associated with vertical polarization. Taking the inverse transforms, the voltage waveform is

$$\begin{aligned}
 V_{oc}(t) &= E_0 c \tau D(\psi, \varphi) \left[ 1 - e^{-t/\tau} \right] \quad (0 \leq t \leq t_0) \\
 &= E_0 c \tau D(\psi, \varphi) \left\{ \left( e^{t_0/\tau} - 1 \right) e^{-t/\tau} + \frac{4 (\sin \psi)}{\pi} \sqrt{\frac{\epsilon}{\tau}} e^{-t'/\tau} \right. \\
 &\quad \times \left. \int_0^{\sqrt{t'/\tau}} e^{u^2} du \right\} \quad (t \geq t_0)
 \end{aligned} \quad (5)$$

where  $t' = t - t_0$ . The first term in the braces is due to the geometry (line height and angle of incidence) and is independent of the properties of the soil. The second term contains the effect of the soil conductivity in  $\tau_c = \epsilon_0 / \tau$ , as well as geometric effects.

The source impedance for the semi-infinite transmission line is simply its characteristic impedance  $Z_0 = \sqrt{Z/Y}$ . For typical power transmission line configurations, this impedance deviates very little from

$$Z_0 = \frac{\tau_0}{2\pi} \log \frac{2h}{a} \quad (6)$$

where  $a$  is the radius (or effective radius) of the power conductors and  $\tau_0 = \sqrt{-\epsilon_0/\epsilon_0}$  is the intrinsic impedance of free space. The Thevenin equivalent circuit of the transmission line is thus the open-circuit voltage given by Eq. (5) in series with  $Z_0$ . The Norton equivalent circuit is a current source  $V_{oc}/Z_0$  in parallel with  $Z_0$ .

### C. Parametric Variation of the Open-Circuit Voltage

The open-circuit voltage  $V_{oc}(t)$  is plotted in Figure 2 for both polarizations with soil conductivity varying from  $10^{-3}$  to  $\infty$  mho/m. The waveform for  $\sigma = \infty$  ( $\tau_e = 0$ ) is produced by the first term of Eq. (5) alone. The deviations of the other waveforms from that for  $\sigma = \infty$  are caused by imperfect reflection of the incident wave by the ground. It is apparent that the coupling caused by the ground effect is larger than the coupling caused by the line height for vertical polarization and soil conductivities less than  $10^{-2}$  mho/m. It is also apparent that the ground-effect coupling to vertical polarization is considerably greater than the

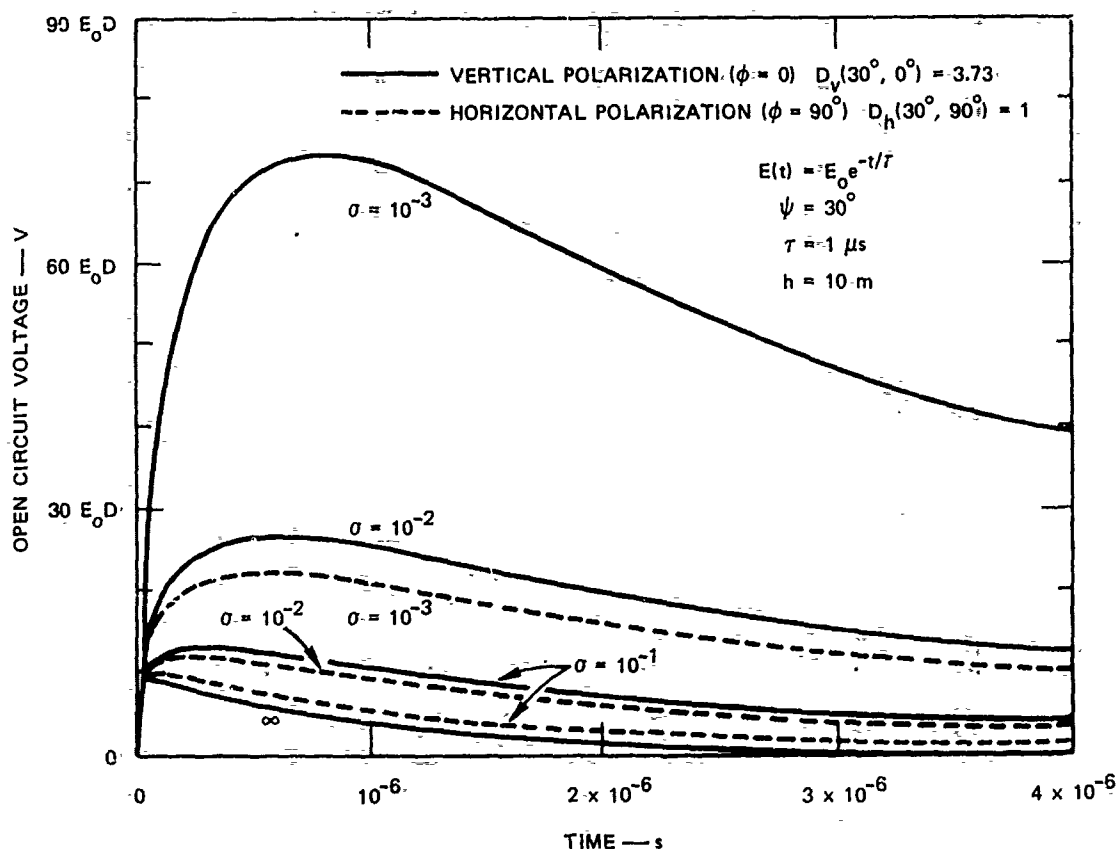


FIGURE 2 OPEN-CIRCUIT VOLTAGE AT THE END OF A SEMI-INFINITE LINE FOR VARIOUS SOIL CONDUCTIVITIES

coupling to horizontal polarization. The difference is even greater than the waveforms in Figure 2 indicate because the directivity function  $D(\psi, \phi)$  is greater for vertical polarization than for horizontal polarization.

The effect of line height on the open-circuit voltage waveform is illustrated in Figure 3, where the waveforms are plotted for vertical polarization incident on soil with a conductivity of  $10^{-2}$  mho/m. Also

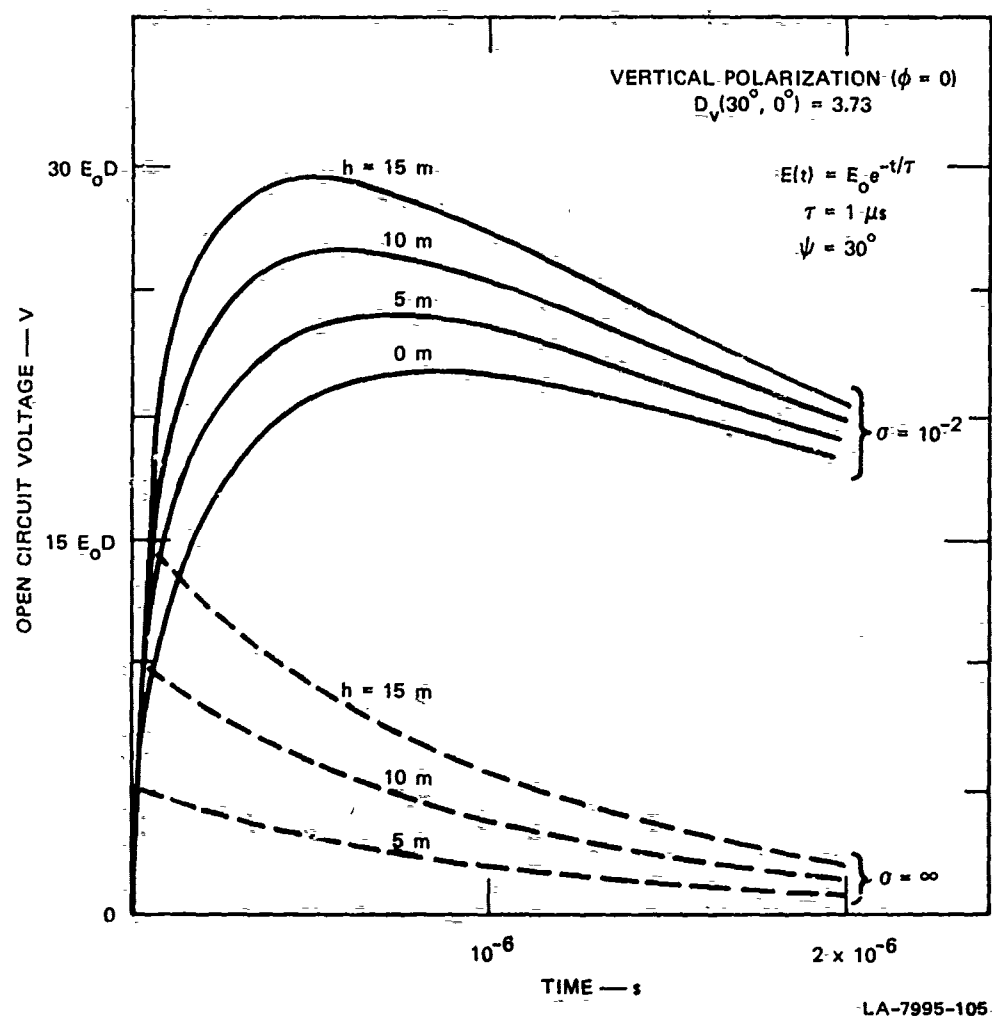
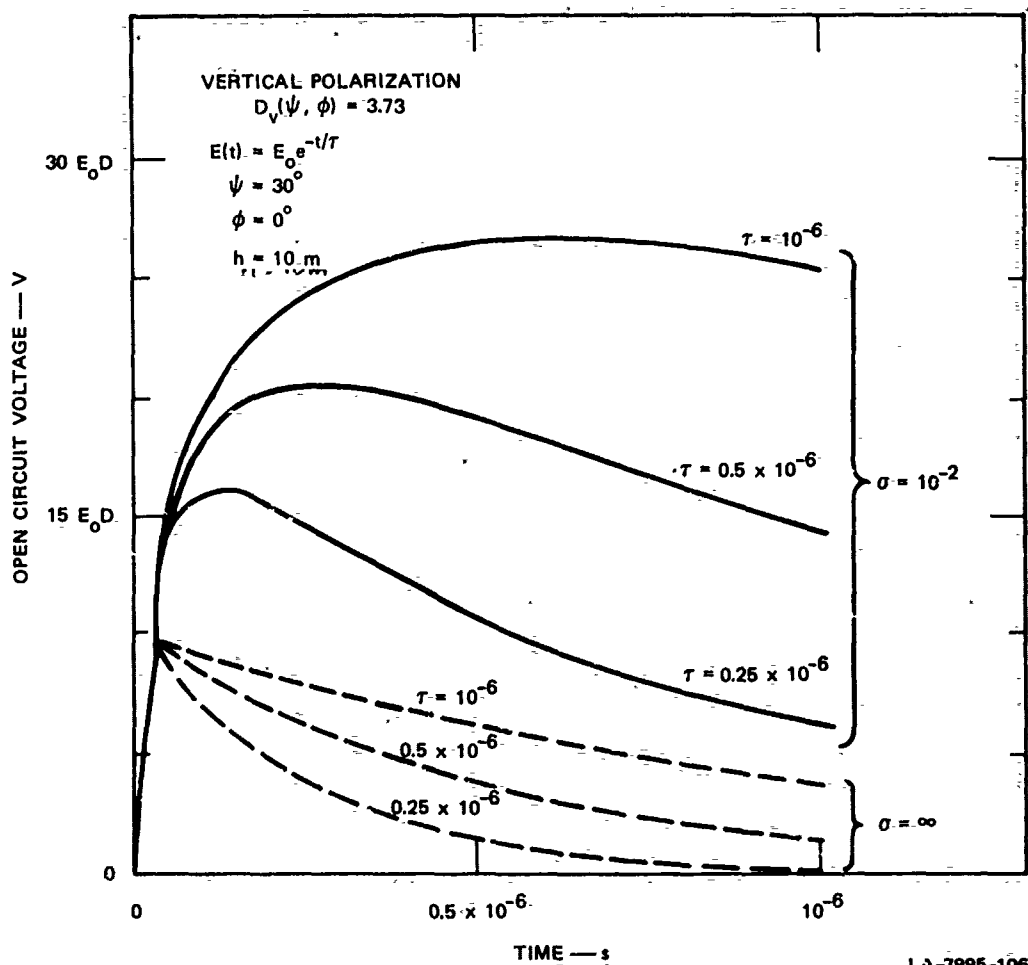


FIGURE 3 OPEN-CIRCUIT VOLTAGE AT THE END OF A SEMI-INFINITE LINE FOR VARIOUS LINE HEIGHTS

shown as dashed curves in Figure 3 are the waveforms with  $\sigma = \infty$ ; only this portion of the waveform is proportional to the line height. For the soil conductivity of  $10^{-2}$  mho/m, the ground effect is larger than the height effect, and changing height of the line does not have a large effect on the peak open-circuit voltage.

The effect of incident pulse duration (decay time constant) on the open-circuit voltage waveform is illustrated in Figure 4, where the open-circuit voltage is plotted for incident pulse decay time constants of 0.25, 0.5, and 1.0 microseconds. As is apparent from Eq. (5), the waveform for a given soil conductivity, line height, and angle of incidence can be plotted as a function of a normalized time  $t/\tau$ , in which case the pulse decay time constant  $\tau$  affects only the relative magnitudes of the two terms in braces in Eq. (5). Plotted in real time as in Figure 4, however, it is apparent that the pulse duration affects both the peak voltage and the time required to reach the peak value. The wider the pulse, the larger the peak voltage because the wider the pulse, the longer the segment of line near the terminals over which the ground-effect is integrated. Note that for perfect ground (dashed curves in Figure 4) the pulse width has little effect on the peak voltage, and the open-circuit voltage waveform is essentially the incident field waveform except for the finite rise time,  $t_0 = (2h \sin \psi)/c$ .

In Figures 2, 3, and 4, the waveforms for vertical polarization have been plotted for an elevation angle  $\psi = 30^\circ$  and an azimuth angle  $\phi = 0^\circ$ , while the waveforms for the horizontally polarized incident wave in Figure 2 were plotted for  $\psi = 30^\circ$  and  $\phi = 90^\circ$  (broadside). In all three illustrations, it was assumed that  $\alpha/k \ll 1$  and that  $\alpha/k$  was not frequency-dependent. When Eq. (5) is reexamined, it is apparent that changing the angles of incidence affects the relative magnitude of the ground-effect through the  $(\sin \psi)^{\pm 1}$  coefficient as well as affecting the



LA-7995-106

FIGURE 4 OPEN-CIRCUIT VOLTAGE AT THE END OF A SEMI-INFINITE LINE FOR VARIOUS INCIDENT PULSE DECAY TIME CONSTANTS

directivity function  $D(\psi, \varphi)$  and the delay time  $t_0$  for the arrival of the ground-reflected wave. In effect, there are two directivity functions--one for the response with perfectly conducting ground,  $D(\psi, \varphi)$ , and one for the correction term,  $(\sin \psi)^{\pm 1} D(\psi, \varphi)$ . The magnitude of these directivity functions for vertical polarization are shown in Figure 5 for various values of  $\alpha/k$ . Note that for  $\alpha/k \rightarrow 0$ , both directivity functions approach  $\infty$  as  $\varphi \rightarrow 0$ , so that for a lossless semi-infinite transmission line, an infinite open-circuit voltage is developed for any finite field

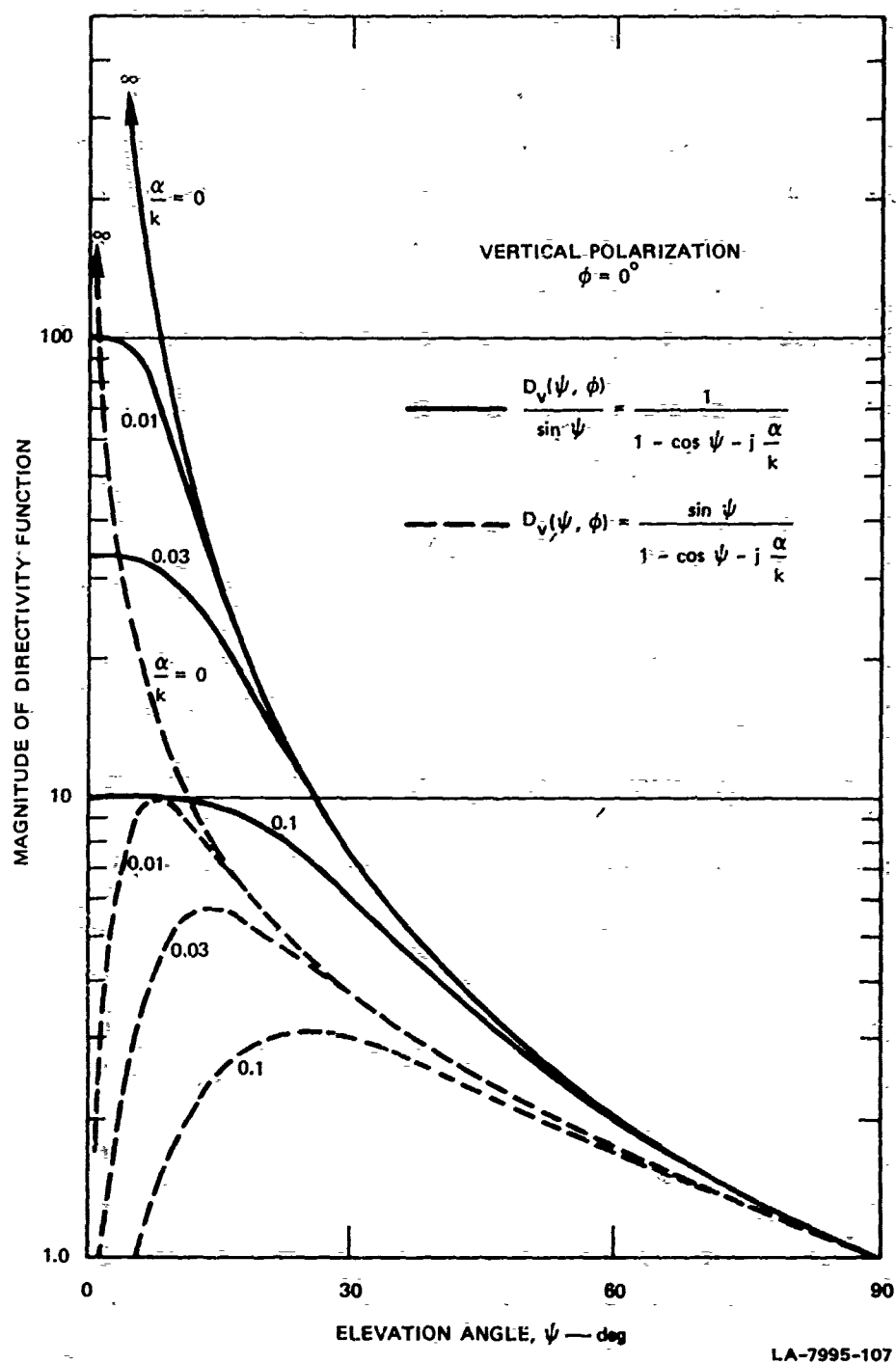


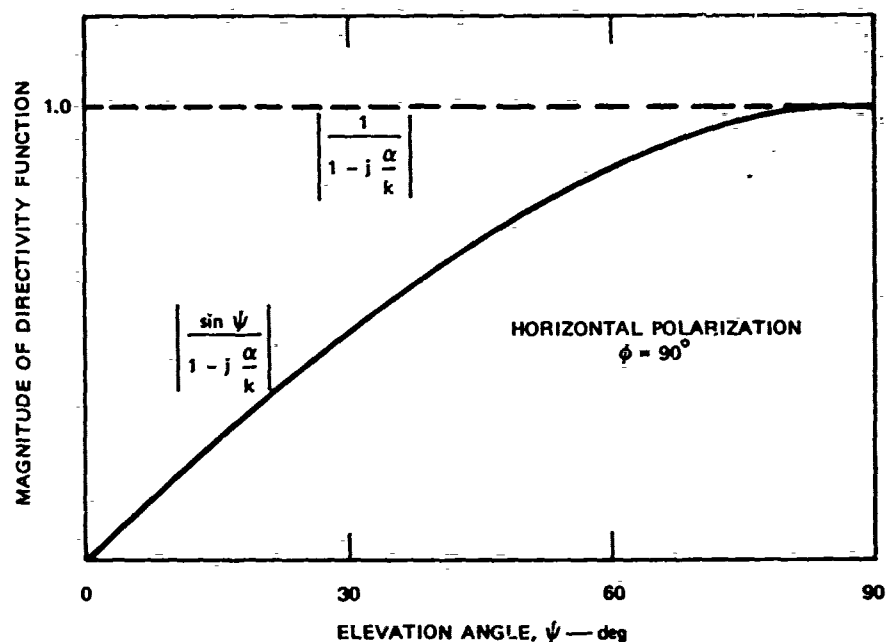
FIGURE 5 VARIATION OF THE DIRECTIVITY FUNCTION;  $D_v(\psi, 0)$  WITH ELEVATION ANGLE  $\psi$  FOR SELECTED VALUES OF THE PARAMETER  $\alpha/k$

incident at  $\varphi = \psi = 0$ . This situation is, of course, an abstract one, because neither lossless nor semi-infinite transmission lines are realizable (nor is the plane wave to illuminate it). Since  $\alpha/k > 0$ , the value of the directivity functions is always finite, and  $D(\psi, \varphi)/\sin \psi \rightarrow j\omega/\alpha c$  as  $\psi, \varphi \rightarrow 0$ , while  $D(\psi, \varphi)$  reaches a maximum value at some value of  $\psi$  that is greater than zero.

The directivity functions for a horizontally polarized wave incident at broadside are shown in Figure 6. For  $\alpha = 0$ ,

$$D(\psi, \varphi) = \frac{\sin \varphi}{1 - \cos \psi \cos \varphi} \quad (7)$$

which approaches  $\infty$  as  $\psi, \varphi \rightarrow 0$ . For any real transmission line, however,  $\alpha \neq 0$ , and  $D(\psi, \varphi)$  is finite. In fact, the behavior of  $D(0, \varphi)$  with  $\varphi$  for



LA-7995-108

FIGURE 6 VARIATION OF THE DIRECTIVITY FUNCTION  $D_h(\psi, 90)$  WITH ELEVATION ANGLE FOR  $\alpha/k \ll 1$

horizontal polarization is identical to the variation of  $D(\psi, 0)$  for vertical polarization, since

$$D(0, \varphi) = \frac{\sin \varphi}{1 - j \frac{\alpha}{k} - \cos \varphi} \quad (\text{horizontal polarization})$$

$$D(\psi, 0) = \frac{\sin \psi}{1 - j \frac{\alpha}{k} - \cos \psi} \quad (\text{vertical polarization}) \quad (8)$$

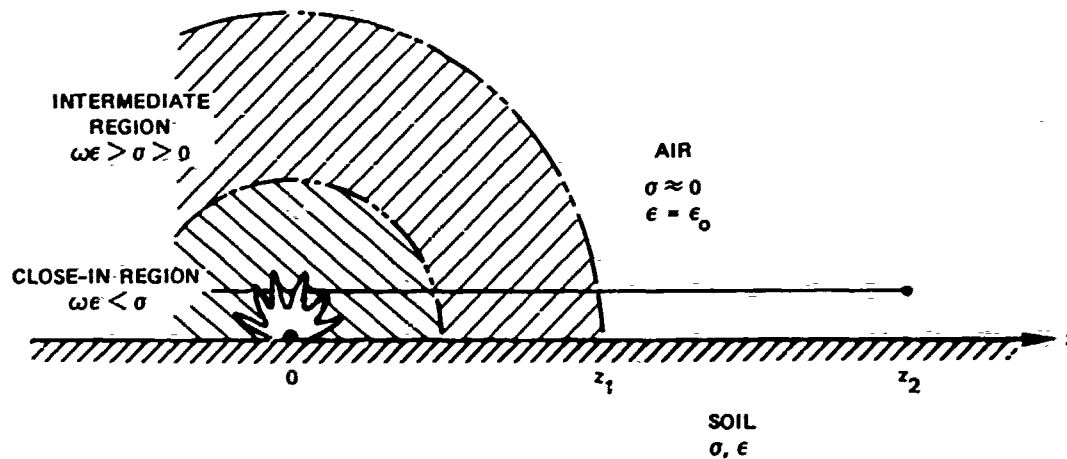
Thus the dashed curves of Figure 5 may be used to illustrate the behavior of  $D(0, \varphi)$  for horizontal polarization if  $\psi$  in Figure 5 is replaced by  $\varphi$ . Figure 6 illustrates that the directivity function for the ground effect,  $\sin \psi D(\psi, 0)$ , illustrated by the solid curve, is always equal to or less than the directivity function  $D(\psi, 0)$  for the wire over perfect ground.

Because the open-circuit voltage is dominated by the ground effect for vertical polarization and average or less-than-average soil conductivity, and because the response to vertical polarization is greater than the response to horizontal polarization, the maximum open-circuit voltage will be developed when the transmission line is subjected to a vertically polarized, end-on illumination ( $\psi = \varphi = 0$ ). Then  $D(\psi, \varphi) / \sin \psi \rightarrow jk / (\gamma - jk)$ , and the problem becomes one of a vertically polarized wave propagating along the transmission line. It is no longer reasonable, in this situation, to assume a uniform plane wave and a semi-infinite line because there exists no practical case in which a uniform field can be generated over a very long line when the wave is incident at a grazing angle ( $\psi = 0$ ). For the case where  $\psi = \varphi = 0$ , therefore, we will assume that the total vertical electric field varies as  $1/z$  and that the length of the transmission line is finite.

#### D. Vertically Polarized Wave at Grazing Incidence

##### 1. General

A case for which a vertically polarized wave incident at  $\psi = \varphi = 0$  is of interest is illustrated in Figure 7. In this case, the EMP is generated by a surface burst on the transmission line (or an extension of the line). Near the source point (in the close-in region), the radiation from the weapon will ionize the air sufficiently to cause it to behave as a conductor ( $\sigma \gg \omega \epsilon_0$ ), and further away (in the intermediate region), the ionization will be weaker but still sufficient to produce significant attenuation of signals propagating away from the source on the line. Although it is evident that there will be coupling to the transmission line in the close-in and intermediate regions, the analysis of the coupling in these regions is beyond the scope of this report. Here we discuss only the coupling that occurs outside these regions, where the EMP wave behaves as a vertically polarized wave propagating outward from the source at the speed of light. The analysis is performed



LA-7995-109

FIGURE 7 PHYSICAL ARRANGEMENT THAT PRODUCES A VERTICALLY POLARIZED WAVE WITH END-ON INCIDENCE

in such a manner that the signals induced in that part of the line closer to the source can be superimposed on the results calculated for the region further from the source.

For our analysis, the transmission line axis is assumed to pass through the source point at  $z = 0$  and is assumed to leave the intermediate region at  $z_1$  and extend to the terminals at  $z_2 > z_1$  as illustrated in Figure 7. The wave emanating from the intermediate region is assumed to propagate as though the ground were a perfect conductor so that  $E_x = \eta_0 H_y$ , where  $\eta_0$  is the intrinsic impedance of free space, and  $E_x = E_0 e^{-jkz/z}$ . To determine the  $z$ -component of the field in the ground, however, we will concede that the ground is not a perfect conductor and observe that for a finitely conducting ground, the  $z$ -component of the electric field at the surface will be  $E_z(0, z) = \eta H_y(0, z)$ , where  $\eta$  is the intrinsic impedance of the soil, and  $\eta \ll \eta_0$ . Since we will need the  $z$ -component of the electric field at the wire height to calculate the current induced in the wire, we can approximate this field by

$$E_z(h, z) \approx E_z(0, z) + h \left. \frac{\partial E_z}{\partial x} \right|_{x=0} \quad (9)$$

where  $\partial E_z / \partial x$  is obtained from the curl  $E$  at the surface:

$$\begin{aligned} \frac{\partial E_z}{\partial x} &= j\omega\mu_0 H_y + \frac{\partial E_x}{\partial z} \\ &= \frac{j\omega\mu_0}{\eta_0} E_x + \left(-jk - \frac{1}{z}\right) E_x \\ &= -\frac{E_x}{z} \end{aligned} \quad (10)$$

since  $E_x = E_o e^{-jkz}/z$  and  $H_y = E_x/\eta_o$ . The field at the wire height is thus

$$E_z(h, z) \approx \left( \frac{\eta}{\eta_o} - \frac{h}{z} \right) \frac{E_o e^{-jkz}}{z} \quad (11)$$

In deriving this field, we have (1) neglected attenuation of the wave due to losses to the ground, and (2) applied a first order correction to the field at the surface to obtain the field at the wire height. In addition it should be pointed out that  $E_o$  is now the total vertical electric field, so that it corresponds to  $2E_o$  in the space wave case discussed in Section II-B.

## 2. Current Induced in Wire

The current induced in the wire may now be obtained for the region between the edge of the intermediate region at  $z_1$  and the terminals at  $z_2$ . This current is obtained from the differential equation

$$\frac{d^2 I}{dz^2} - \gamma^2 I = -Y E_z(h, z) \quad (12)$$

which has a solution

$$I(z) = [K_1 + P(z)] e^{-\gamma z} + [K_2 + Q(z)] e^{\gamma z} \quad (13)$$

where

$$P(z) = \frac{1}{2Z_o} \int_{z_1}^z c^{\gamma v} E_z(h, v) dv$$

$$Q(z) = \frac{1}{2Z_0} \int_z^{z_2} e^{-\gamma v} E_z(h, v) dv$$

$$K_1 = \rho_1 e^{\gamma z_1} \frac{\rho_2 P(z_2) e^{-\gamma z_2} - Q(z_1) e^{\gamma z_2}}{e^{\gamma(z_2 - z_1)} - \rho_1 \rho_2 e^{-\gamma(z_2 - z_1)}}$$

$$K_2 = \rho_2 e^{-\gamma z_2} \frac{\rho_1 Q(z_1) e^{\gamma z_1} - P(z_2) e^{-\gamma z_1}}{e^{\gamma(z_2 - z_1)} - \rho_1 \rho_2 e^{-\gamma(z_2 - z_1)}}$$

$$\rho_i = \frac{Z_i - Z_0}{Z_i + Z_0}$$

$$\gamma = \sqrt{ZY} = \alpha + j\beta$$

We will assume that the coupling to the line extending into the intermediate region can be represented by a current source  $I_1$  and an impedance  $Z_0$  at  $z = z_1$  as illustrated in Figure 8. The effect of this source can be superimposed on the induced current calculated here for that portion of the line between  $z_1$  and  $z_2$  outside the intermediate region. The short circuit current at the terminals at  $z_2$  due to the coupling between  $z_1$  and  $z_2$  will be obtained by letting the impedance at  $z_2$  be zero, so that  $\rho_2 = -1$ . Because the source impedance at  $z_1$  is  $Z_0$ ,  $\rho_1 = 0$  and  $K_1 = 0$ . Also, because  $Q(z_2) = 0$ , the short circuit current at  $z_2$  is

$$I(z_2) = P(z_2) e^{-\gamma z_2} + K_2 e^{\gamma z_2} \quad (14)$$

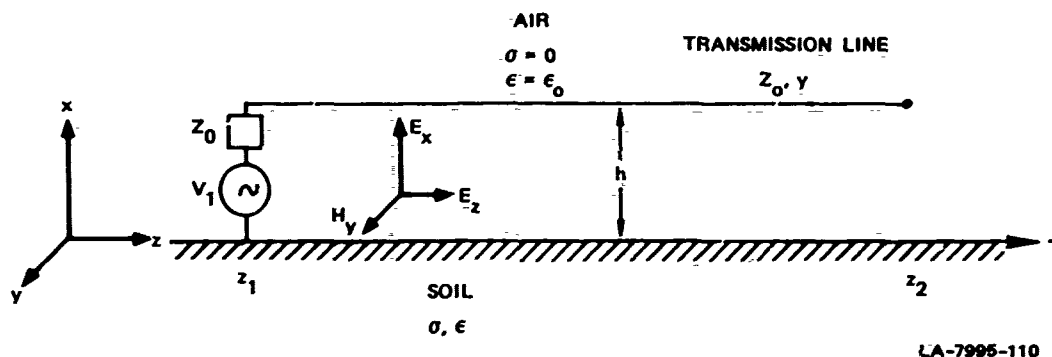


FIGURE 8 GEOMETRY FOR ANALYSIS OF THE COUPLING CONFIGURATION OF FIGURE 7

where

$$K_2 = e^{-2\gamma z_2} P(z_2)$$

or

$$I(z_2) = 2P(z_2) e^{-\gamma z_2}$$

When  $E_z(h, z)$  is substituted into the integral for  $P(z)$ , the short circuit at the terminals induced between  $z_1$  and  $z_2$  by the wave is

$$\begin{aligned} I(z_2) &= \frac{E_o e^{-\gamma z_2}}{Z_o} \left[ \frac{\eta}{\eta_o} \int_{z_1}^{z_2} \frac{e^{(\gamma-jk)v}}{v} dv - h \int_{z_1}^{z_2} \frac{e^{(\gamma-jk)v}}{v^2} dv \right] \\ &= \frac{E_o h e^{-\gamma z_2}}{Z_o} \left\{ e^{\frac{(\gamma-jk)z_2}{2}} - e^{\frac{(\gamma-jk)z_1}{2}} + \left[ \frac{\eta}{h\eta_o} - (\gamma-jk) \right] \right. \\ &\quad \left. \times \int_{z_1}^{z_2} \frac{e^{(\gamma-jk)v}}{v} dv \right\} \end{aligned} \quad (15)$$

The coupling to the wire can now be resolved into three components according to the nature of coupling. If the wire and soil were perfect conductors, then  $\eta = 0$  and  $\gamma = jk$ , and the short-circuit current in the wire at  $z_2$  would be

$$I_g(z_2) = \frac{E_o h e^{-jkz_2}}{Z_o} \left( \frac{1}{z_2} - \frac{1}{z_1} \right) \quad \left( \begin{array}{l} \eta = 0 \\ \gamma = jk \end{array} \right) \quad (16)$$

The coupling in this case is caused by the nonuniformity in the magnitude of the incident electric field along the wire, which causes the potential at the wire height at  $z_1$  to differ from the potential at the wire height at  $z_2$ .

If  $\gamma = jk$  and  $\eta \neq 0$ , we obtain an additional component,

$$I_\sigma(z_2) = \frac{E_o \eta}{Z_o \eta_o} e^{-jkz_2} \log \frac{z_2}{z_1} \quad (17)$$

which is caused by the finite conductivity of the soil ( $\eta \approx \sqrt{j\omega\mu/\sigma}$ ).

This component is the integral (between  $z_1$  and  $z_2$ ) of the  $z$ -component of the electric field induced in the finitely conducting soil by the incident wave. It exists in some form whether or not the incident wave has geometric ( $1/z$ ) variation, although the  $\log(z_2/z_1)$  term is characteristic of the  $1/z$  variation of the incident field.

Finally, if  $\gamma \neq jk$ , a third component is obtained. This component, caused by the disparity in the propagation characteristics of the incident wave and the induced responses, modifies both the geometric component and the ground-field component (since  $\gamma \neq jk$ ) and adds to these a component,

$$I_{\beta}(z_2) = -\frac{E_0}{z_0} e^{-\gamma z_2} (\gamma - jk) \int_{z_1}^{z_2} \frac{e^{(\gamma - jk)v}}{v} dv \quad (18)$$

which exists only if there is a disparity between the phase factors of the incident wave and those of the transmission line. This phase-disparity component is, in reality, a geometric component also, since the integral in Eq. (15) whose coefficient is  $\gamma - jk$  occurs because of the  $1/z$  variation of the incident field.

For typical soil conductivities and line lengths, the geometric term given by Eq. (16) is significant only at very low frequencies unless the line is very high or very close to the source, and the phase-discrepancy term given by Eq. (18) is small compared to the ground-effect term given by Eq. (17). The short-circuit current induced in the transmission line by an exponential pulse  $E_0/z e^{-t/\tau}$  is thus

$$I(z_2) \approx \frac{E_0}{z_0 \sqrt{\epsilon_r}} \log \frac{z_2}{z_1} \left[ \frac{1}{j\omega + \frac{1}{\tau}} \right] \quad \left( \omega \gg \frac{1}{\epsilon_r \tau} \right) \quad (19)$$

$$\approx \frac{E_0}{z_0} \sqrt{\tau} \log \frac{z_2}{z_1} \left[ \frac{\sqrt{j\omega}}{j\omega + \frac{1}{\tau}} \right] \quad \left( \omega \ll \frac{1}{\epsilon_r \tau} \right)$$

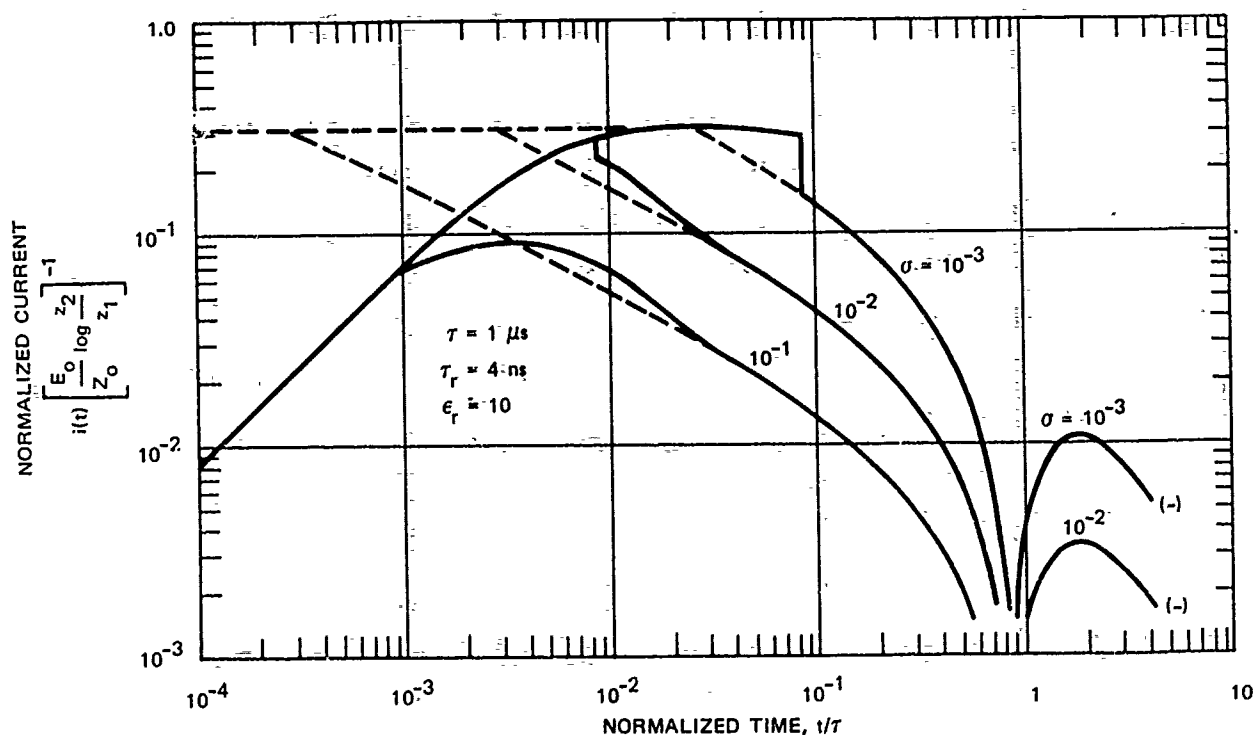
when phase is referred to the terminals at  $z_2$ .

The current waveform is thus

$$i(z_2, t) \approx \frac{E_0}{z_0 \sqrt{\epsilon_r}} \log \frac{z_2}{z_1} e^{-t/\tau} \quad (t < \epsilon_r \tau) \quad (20)$$

$$\approx \frac{E_0}{z_0} \sqrt{\frac{\tau}{\pi}} \log \frac{z_2}{z_1} \left[ \sqrt{\frac{\tau}{t}} - 2e^{-t/\tau} \int_0^{\sqrt{t/\tau}} e^{u^2} du \right] \quad (t > \epsilon_r \tau)$$

for a zero-rise-time exponential pulse. For a two-exponential pulse with non-zero rise time, the current waveform can be obtained by superposing two solutions such as in Eq. (20). The waveforms for single and double exponential transient fields are shown in Figure 9 for a pulse decay time constant of  $1 \mu s$  and soil conductivities varying from  $10^{-1}$  to  $10^{-3}$  mho/m. For the two-exponential pulse (solid curves), the rise time constant is  $4 ns$ . The early time and late time approximations do not meet at  $t = \epsilon_r \tau_e$  for the lower conductivities, so they have been joined by a vertical line. The dashed curves are the zero rise time (single exponential) responses.



LA-7995-111

FIGURE 9 SHORT-CIRCUIT CURRENT AT THE TERMINALS OF A LINE 1000 METERS LONG AND 1000 METERS FROM THE SOURCE WITH 1 V/m INCIDENT ON THE END NEAREST THE SOURCE ( $Z_0 = 300 \Omega$ ,  $z_1 = 1000 m$ ,  $z_2 = 2000 m$ )

The waveforms of Figure 9 are such short, high-amplitude pulses that it was necessary to plot them on a log-log scale to view significant details. It is noted that the peak value and the time to reach the peak value both increase as soil conductivity decreases. This is because the poorer conducting soil behaves as a dielectric longer and supports a larger z-component of electric field when it behaves as a conductor. Also interesting is the fact that the short-circuit current waveform has a negative undershoot beginning at about one decay time-constant.

For comparison of the end-on illumination of the finite-length transmission line with the oblique incidence on the semi-infinite line, we will compute the peak current and time-to-peak for a soil conductivity of  $10^{-2}$  mho/m and an exponential pulse decay time of 1  $\mu$ s. Assume the finite-length line is 1 kilometer from the source and 1 kilometer long, and that the field strength at the end nearest the source is 1 V/m ( $E_0 = 1000$ ). The characteristic impedance of the line is taken to be 300  $\Omega$ s. Then the peak short circuit current from Eq. (20) and Figure 9 is 0.65 A occurring at  $t \approx 10^{-8}$  seconds. From Figures 4 and 5, the lossless semi-infinite transmission line illuminated with a plane wave of 1 V/m at  $\psi = 10^\circ$  will have a peak short-circuit current of about 2.3 A occurring at  $t \approx 6 \times 10^{-7}$  seconds.

Although some of the difference between these two results can be attributed to the non-uniform illumination, most of it can be attributed to the finite length of the line in one case and its infinite length in the other. On the semi-infinite line, the peak current occurring at  $t = 6 \times 10^{-7}$  seconds contains current that was induced  $ct/(1 - \cos \psi) = 11.8$  kilometers away from the terminals. Thus, unless the transmission line is straight and at least 11.8 kilometers long, the short-circuit current will never attain the peak value predicted for a semi-infinite line. One should, therefore, use caution in interpreting the currents and voltages predicted for semi-infinite lines with small angles of incidence.<sup>4</sup>

### E. Response of Vertical Element

Vertical elements such as ground wires and service entrance conduits also interact with the incident wave and, thus, have current induced in them. Because only the vertically polarized wave has a component of electric field in the vertical direction, the vertical elements actively interact with only the vertically polarized wave; for horizontally polarized waves, the vertical elements behave as passive impedances with delay times associated with their length. The vertical element is considered to be a biconic transmission line with its upper end terminated in its characteristic impedance and its lower end short-circuited to the ground. The current induced in this biconic transmission line by the vertical component of the electric field can then be determined in the same way as the current in the horizontal transmission line over ground. As was pointed out in Technical Memorandum 22,<sup>2</sup> the current induced in the vertical riser opposes the current induced in the horizontal conductor when  $|\varphi| < \pi/2$  and aids it when  $|\varphi| > \pi/2$ . Since the coupling to the horizontal conductor is greatest for  $|\varphi| < \pi/2$ --when  $D(\psi, \varphi)$  is large--the current induced in the vertical element tends to reduce the maximum current calculated for the horizontal conduction alone.

For a vertically polarized wave incident at an elevation angle  $\psi$  on a vertical element of height  $h$ , the current at the top will be

$$I(h) = \frac{E_o c \cos \psi}{2Z_o} \frac{1}{j\omega} \left[ \frac{1 - e^{-j\omega \frac{2h}{c} (1 + \sin \psi)}}{1 + \sin \psi} + \frac{e^{-j\omega \frac{2h}{c} \sin \psi} - e^{-j\omega \frac{2h}{c}}}{1 - \sin \psi} \right] \frac{1}{j\omega + 1/\tau} \quad (21)$$

for an exponential pulse  $E_o e^{-t/\tau}$ . In the expression above,  $Z_o$  is the characteristic impedance of the biconic transmission line given by

$$Z_o \approx \frac{\eta_o}{2\pi} \log \frac{2h}{a} \quad (22)$$

and the ground is assumed to be a perfect conductor ( $R_v = 1$ ). The waveform of the current at the top of the vertical element is

$$i(h, t) = \frac{E_o c \tau \cos \psi}{2Z_o} \left\{ \frac{1}{1 + \sin \psi} \left[ \left( 1 - e^{-t/\tau} \right)_{t > 0} - \left( 1 - e^{-(t-t_1)/\tau} \right)_{t > t_1} \right] + \frac{1}{1 - \sin \psi} \left[ \left( 1 - e^{-(t-t_2)/\tau} \right)_{t > t_2} - \left( 1 - e^{-(t-t_3)/\tau} \right)_{t > t_3} \right] \right\} \quad (23)$$

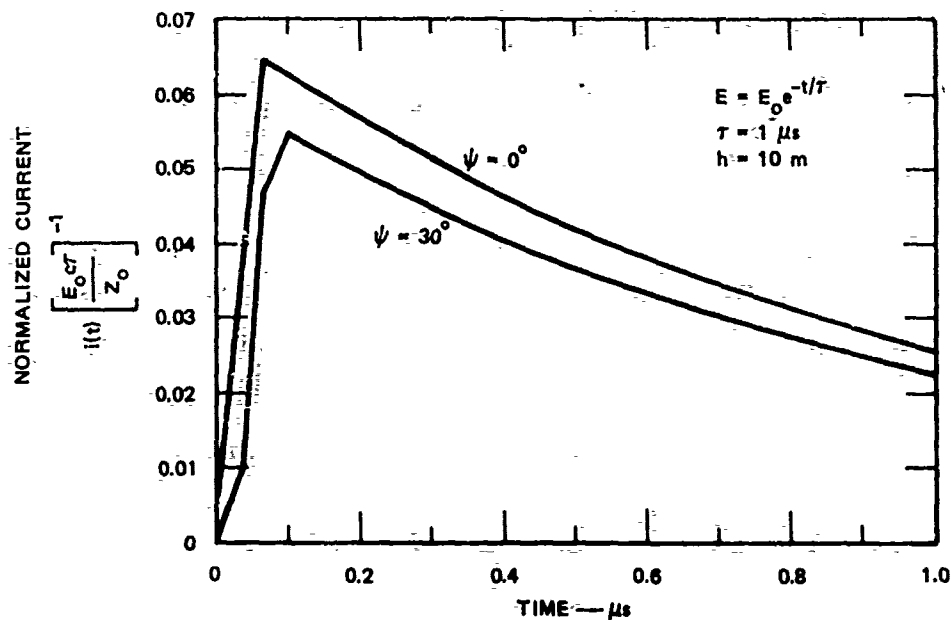
where  $t_1 = 2h/c (1 + \sin \psi)$ ,  $t_2 = 2h/c \sin \psi$ , and  $t_3 = 2h/c$ .

For a vertically polarized wave at grazing incidence ( $\psi = 0$ ),

$$i(h, t) = \frac{E_o c \tau}{Z_o} \left[ 1 - e^{-t/\tau} - \left( 1 - e^{-(t-t_3)/\tau} \right)_{t > t_3} \right] \quad (24)$$

Plots of the current waveform are shown in Figure 10 for  $\psi = 0$  and  $\psi = 30^\circ$  for an incident exponential pulse with a decay time constant  $\tau = 1 \mu s$  and a riser height  $h = 10$  m. The waveforms for these two angles of incidence are quite similar, but the leading edge of the waveform for  $\psi = 30^\circ$  is more complex because of the difference in time of arrival of the upward and downward traveling current waves induced by the direct and ground-reflected electric-field waves.

A comparison of the current induced in the riser for conditions similar to those used earlier for comparing the current between the



LA-7995-112

FIGURE 10 CURRENT DELIVERED TO A MATCHED LOAD AT THE TOP OF A VERTICAL RISER BY A VERTICALLY POLARIZED INCIDENT WAVE

horizontal conductor of finite length and the semi-infinite conductor shows that the peak current induced in the riser by a 1-V/m incident exponential pulse ( $\psi = 0$ ,  $h = 10$  m,  $\tau = 1 \mu s$ ) is about 0.064 A. The peak current in the finite-length horizontal conductor was 0.65 A and, in the semi-infinite conductor, it was 2.8 A ( $\sigma = 10^{-2}$  mho/m). The peak current induced in the riser is thus only about 10 percent of the peak ground-effect current induced in a 1000-meter-long horizontal conductor, but it is flowing in the opposite direction from the ground-induced current. For perfectly conducting ground, however, the peak current induced in the riser is one-half as large as that induced in a semi-infinite horizontal conductor, so that the higher the soil conductivity, the more significant the riser current.

### SECTION III

#### PROPAGATION OF CURRENTS INDUCED IN POWER LINES

##### A. Introduction

In previous reports the coupling of incident electromagnetic energy onto power lines has been analyzed and the analysis confirmed with measurements.<sup>2,3,5</sup> This report discusses how these induced currents propagate down a power line over real earth and with discontinuities. The induced current will be changed by attenuation and dispersion due to the real earth. In addition, the waveform will be altered by a variety of discontinuities that occur in actual power lines--bends, junctions, spurs, and grounded neutrals. Since propagation is important for wavelengths that are short compared to the height above ground, the transmission line solutions are not strictly correct. In this chapter, the significance of these effects is experimentally evaluated. In the final section some consideration is given to coupling to multi-wire lines.

##### B. Real Earth Effects

The propagation of a signal down a wire over real earth has been worked out by Sunde.<sup>1</sup> An analysis that gives similar results was presented in Technical Report 5.<sup>3</sup> We shall not repeat these analyses but will give the results from Sunde's analysis.

The propagation constant,  $\gamma$ , is given by

$$\gamma = \gamma_0 H(j\omega)$$

where  $\gamma_0 = jk = j(\omega/c)$  = free-space propagation constant,  $c$  = velocity of light in vacuum, and  $H(j\omega)$  is a function that contains the earth and the line parameters:

$$H(j\omega) = \left[ 1 + \left( \ln \frac{2h}{a} \right)^{-1} \left( \ln \frac{1 + (j\omega\tau_h)^{1/2}}{(j\omega\tau_h)^{1/2}} + \frac{1}{(j\omega\tau_a)^{1/2}} \right) \right]^{1/2} \quad (25)$$

For most cases of interest the second term on the right is small compared to 1 so that

$$H(j\omega) \cong 1 + 1/2 \left( \ln \frac{2h}{a} \right)^{-1} \left( \ln \frac{1 + (j\omega\tau_h)^{1/2}}{(j\omega\tau_h)^{1/2}} + \frac{1}{(j\omega\tau_a)^{1/2}} \right) \quad (26)$$

$$\tau_h = \mu \sigma h^2$$

$$\tau_a = \mu \sigma_i a^2$$

where  $h$  = line height over ground,  $a$  = line radius,  $\mu$  = permeability,  $\sigma$  = soil conductivity, and  $\sigma_i$  = wire conductivity. The terms  $\sqrt{j\omega\tau_h}$  and  $\sqrt{j\omega\tau_a}$  may be recognized as complex and related to the line height,  $h$ , and conductor radius,  $a$ , normalized to the appropriate skin depth, since

$$\sqrt{j\omega\tau_h} = \frac{h}{\delta} (1 + j1) \quad \delta = \text{soil skin depth} = \left( \frac{\omega\mu\sigma}{2} \right)^{-1/2}$$

$$\sqrt{j\omega\tau_a} = \frac{a}{\delta_i} (1 + j1) \quad \delta_i = \text{wire skin depth} = \left( \frac{\omega\mu\sigma_i}{2} \right)^{-1/2}$$

To gain some insight into the propagation over real earth, Sunde calculates the step function response of a line. Although there is no closed form solution for all times, an analytic solution may be found for both small times and for large times, where the distinction between small and large times depends upon the value of  $h/\delta$ . If  $h/\delta \gg 1$ , the small-time solution is appropriate. If  $h/\delta \ll 1$ , the large-time solution is appropriate.

For small times, the current at a point  $z$  down the line normalized to the current at  $z = 0$  is

$$\frac{I(z, j\omega)}{I(0, j\omega)} = \exp - \frac{j\omega z}{c} \cdot \exp \left[ \sqrt{j\omega} z \left( 2c\sqrt{\tau_1} \ln \frac{2h}{a} \right)^{-1} \right] \quad (27)$$

where

$$\sqrt{\tau_1} = \frac{\sqrt{\tau_h \tau_a}}{\sqrt{\tau_h} + \sqrt{\tau_a}}$$

For most cases,  $\tau_a \gg \tau_h$  so that  $\tau_1 \approx \tau_h$ . The transform of this expression for current when a step function of current is introduced at  $z = 0$  is

$$\frac{I(z, t)}{I(0, t_0)} = \operatorname{erfc} \left[ z \left( 4\sqrt{\tau_1} c t_0^{1/2} \ln \frac{2h}{a} \right)^{-1} \right] \quad (28)$$

for small times, where  $\operatorname{erfc}(z)$  = complimentary error function of  $z$ , and  $t_0 = t - z/c$ .

For large times the normalized current in the frequency domain is

$$\frac{I(z, j\omega)}{I(0, j\omega)} \cong \exp - \frac{j\omega z}{c} \left[ 1 + \frac{j\omega z}{4c \ln \frac{2h}{a}} \left( \ln(j\omega \tau_h) - \frac{2}{\sqrt{j\omega \tau_a}} \right) \right] \quad (29)$$

The time domain solution with step-function input is

$$\frac{I(z, t)}{I(0, t_0)} = 1 - z \frac{1 + 2 \left( \frac{t_0}{\pi \tau_a} \right)^{1/2}}{4c t_0 \ln \frac{2h}{a}} \quad (30)$$

for large times.

For many cases  $2(t_0/\pi\tau_z)^{1/2} \ll 1$ , which further simplifies the solution. Note that for large times the response is independent of the value of soil conductivity and only weakly dependent on the height above ground through the logarithmic term in  $h/a$ . This contrasts with the small time solution, which is a function of both  $\tau$  and  $h$ .

The contrast between small- and large-time solutions can be illustrated by looking at the attenuation constant as a function of frequency for different values of  $\sigma$  and  $h$  as shown in Figures 11 and 12. This constant is derived from the expression for  $H(j\omega)$ . The values for which computations were carried out encompassed the parameters for which measurements, which are described in a subsequent section, were made. These same charts can be used for other ranges of parameters by employing the following scaling relations. For a line height and wire radius  $k$  times greater than those given in Figures 11 and 12, divide the frequency, attenuation and conductivity scales by  $k$ . If the wire radius is not scaled exactly, the attenuation constant should also be multiplied by  $(\ln 2h/a)_{\text{figure}} / \ln 2kh/a'$  where  $a'$  is the actual radius. The values for 100:1 scaling (full scale values) are shown in the parentheses.

In Figures 11 and 12, the attenuation due to the wire has been omitted since it changes the result by only a few percent.

The large-time solution is most prominent in Figure 11 at frequencies below about 100 MHz. The attenuation constant varies less than a factor of 2 when  $\tau$  is increased 100 times. The variation of  $\alpha$  with frequency is almost linear.

In Figure 12, where the height is increased by a factor of 6, the attenuation constant depends much more strongly on  $\tau$ , approaching a  $\tau^{-1/2}$  dependence at very high frequencies. In this case,  $\alpha$  also varies with  $f^{1/2}$ , not with  $f^1$  as previously mentioned.

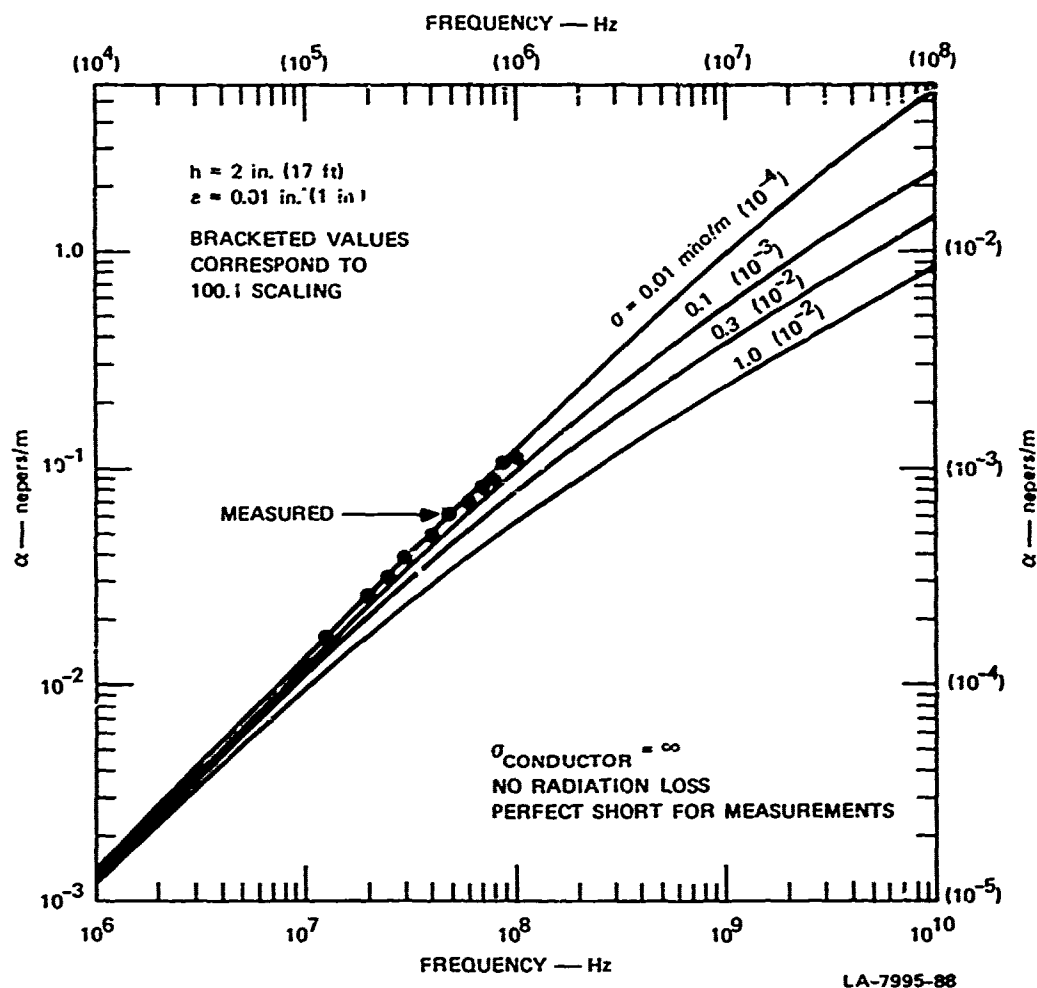


FIGURE 11 ATTENUATION CONSTANT OF A LINE OVER GROUND AS A FUNCTION OF FREQUENCY, WHERE  $h = 17$  FEET FULL SCALE

A comparison of Figures 11 and 12 also shows that at low frequencies  $\alpha$  is relatively independent of  $h$ , while at high frequencies  $\alpha$  varies approximately as  $h^{-1}$ .

If the complete expression for  $\gamma$  is manipulated to extract the attenuation and phase constant separately, rather simple expressions result when the wire loss is neglected.

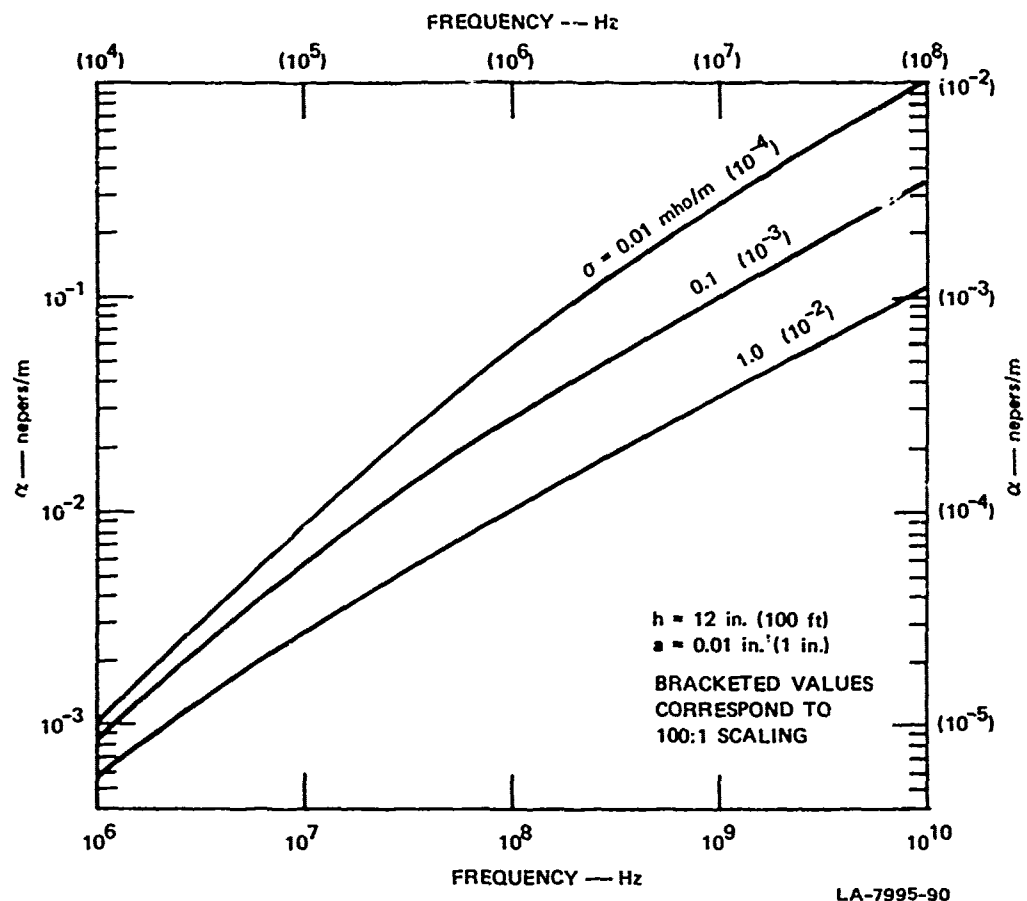


FIGURE 12 ATTENUATION CONSTANT OF A LINE OVER GROUND AS A FUNCTION OF FREQUENCY, WHERE  $h = 100$  FEET FULL SCALE

$$\alpha = \frac{k \left[ \arctan \frac{1}{1 + 2h/\delta} \right]}{2 \ln \frac{2h}{a}} \quad (31)$$

$$\frac{\beta}{k} = 1 + \frac{\ln \left[ 1 + \frac{1}{h/\delta} + \frac{1}{2(h/\delta)^2} \right]^{1/2}}{2 \ln \frac{2h}{a}} \quad (32)$$

These expressions are accurate for the entire frequency range of applicability of Equation 26. The key parameter is seen to be  $h/\delta$ , since  $\ln 2h/a$  is a slowly varying quantity with line parameters. The only other parameter is  $k = \omega/c$ , which is simply related to the frequency.

The asymptotic behavior of  $\alpha$  when  $h/\delta$  is very small and very large compared to 1 illustrates how the line and soil parameters affect the small- and large-time solutions. When  $h/\delta \ll 1$ , the arc tangent term reaches a constant value of  $\pi/4$ . Therefore

$$\alpha = \frac{k\pi}{8 \ln \frac{2h}{a}} \quad (33)$$

for late times. For this condition  $\alpha$  is independent of  $\sigma$  and only weakly dependent on  $h$  through the  $\ln 2h/a$  term;  $\alpha$  is linearly dependent on frequency.

When  $h/\delta \gg 1$ , the arc tangent term reaches  $1/(2h/\delta)$  so that

$$\alpha = \frac{k}{4h/\delta \ln \frac{2h}{a}} \quad (34)$$

for early times. Under these conditions  $\alpha$  varies with  $\sigma^{-1/2}$  and with  $f^{1/2}$ . In addition,  $\alpha$  is inversely proportional to  $h$  when the variation of  $\ln 2h/a$  is neglected.

A good analytic approximation for all frequencies is

$$\alpha = \frac{8.2 \times 10^{-9} f}{\ln \frac{2h}{a} [1 + 1.47 h/\delta]} \quad \text{nepers/m} \quad (35)$$

### C. Measurements of Propagation Effects

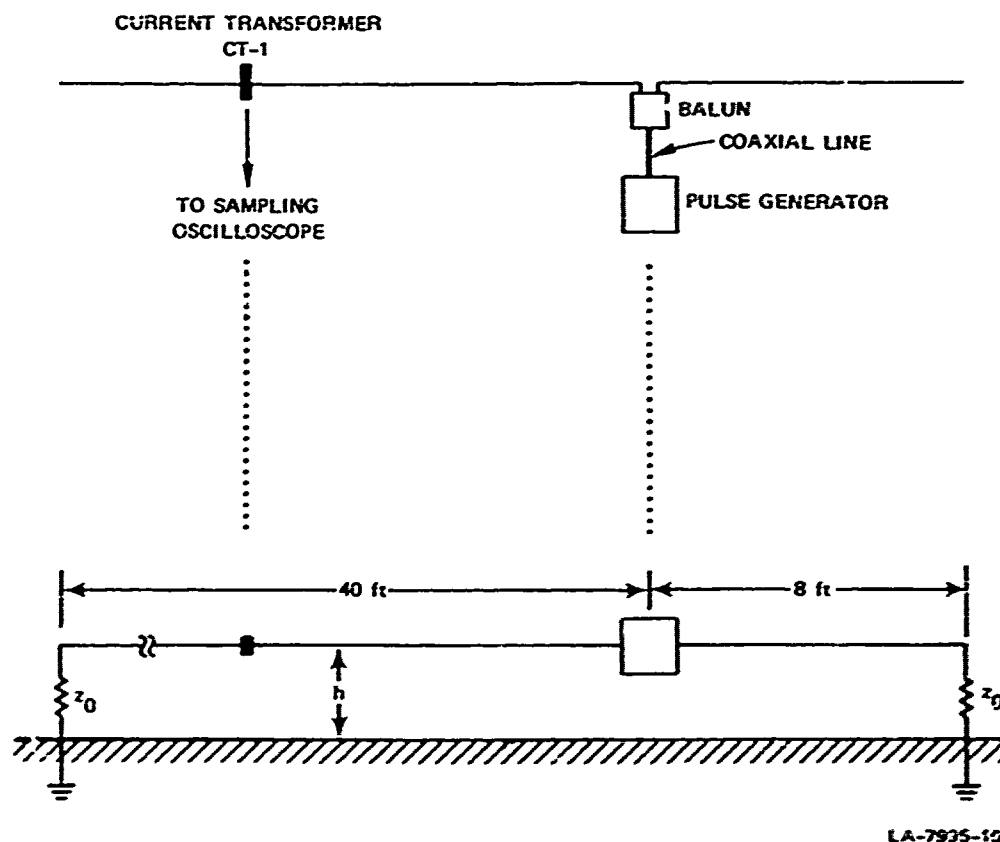
To confirm the above calculations, especially for wavelengths comparable to the line height, two types of measurement were made. The step function response of a line over real earth was measured and compared to the calculated values. This comparison was effective in checking performances at the higher frequencies. Because, however, the attenuation falls to such low values at low frequencies, this method does not insure detection of an error in the low frequency value of  $\alpha$ . In addition, therefore,  $\alpha$  was measured with CW signals over the lower range of frequencies.

### D. Step Function Response

In the experimental set-up, which is shown in Figure 13, a mercury reed pulse generator produced an approximate step function with a rise time of about 300 ps. This was fed into a balun, which in turn excited a transmission line above ground. The line was generally terminated in  $Z_0$ , but since the significant measuring time was shorter than the time required for end reflections to arrive at the measuring point, the termination point did not affect the results. A CT-1 current transformer was used to measure the current waveform along the wire.

The earth was salted to increase its conductivity to between 0.2 and 0.3 mho/m as measured by a test cell at 1 MHz.

The measured and calculated results for a single wire line 2 inches above ground and 16 feet from the feed point are shown in Figure 14. The calculated value is for the late time solution. The agreement is quite good. The early time solution gives quite a different waveform, which differs considerably from the measured waveform. For our waveform most of the energy is below 1 GHz. At this frequency  $h/\delta \sim 1$ . Thus, for most of the frequencies  $h/\delta < 1$ , and the late time solution should apply.



LA-7935-152

FIGURE 13 EQUIPMENTAL SET-UP FOR MEASUREMENT OF CURRENT WAVEFORMS OF A LINE OVER GROUND

In contrast, the same measurements made on a single wire line at a height of 12 inches showed hardly any degradation in waveshape after travelling 16 feet from the feed point. For this configuration  $h/\lambda > 1$  for frequencies down to  $10^7$  Hz, and the small time solution was appropriate. This solution showed no significant degradation in waveshape at this distance. At a distance of 40 feet, small changes could be measured that were in accord with the small time solution (see Figure 15).

Similar measurements were made with three-wire lines at both 2-inch and 12-inch heights. The results are shown in Figures 16 and 17. The agreement between the measured and calculated waveforms is quite good

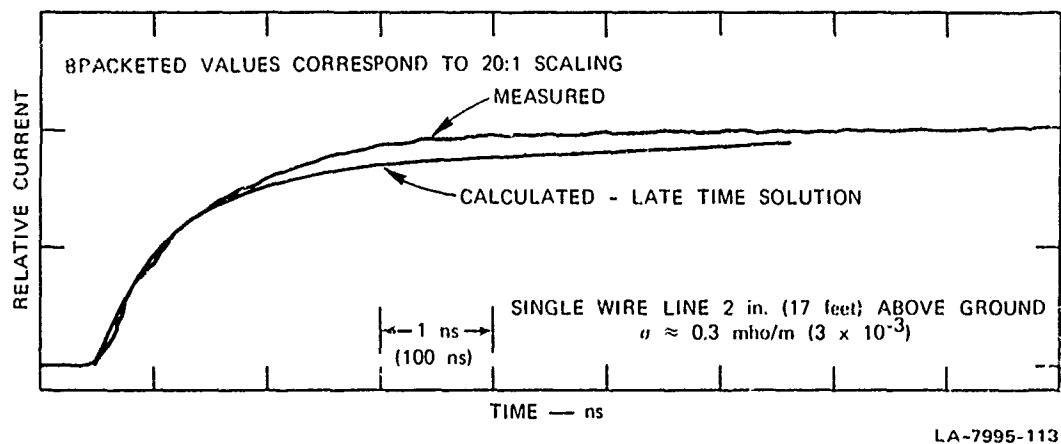
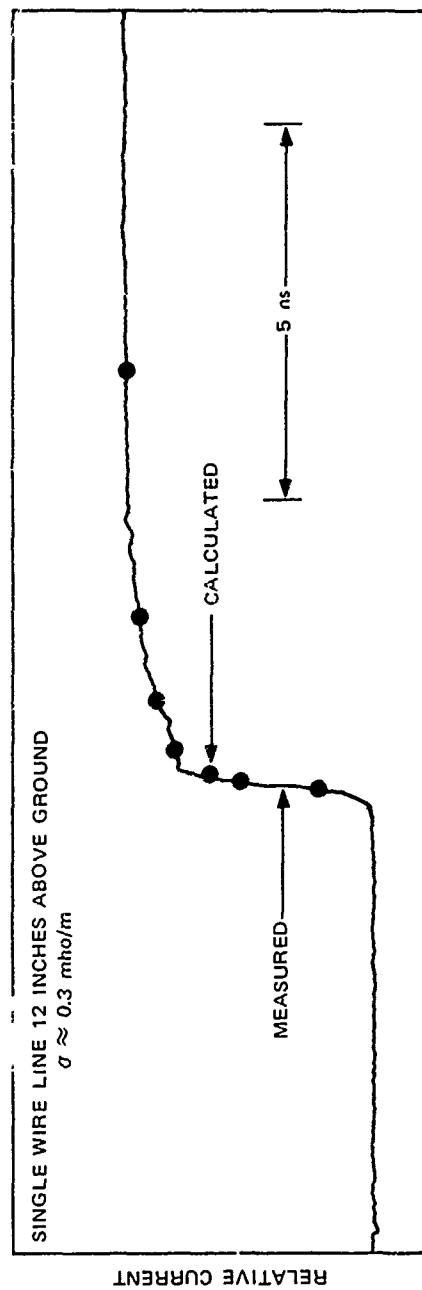


FIGURE 14 CURRENT WAVEFORM OF A SINGLE WIRE LINE 1600 FEET (full scale) FROM THE FEED POINT, WHERE  $h = 17$  FEET FULL SCALE

when the small time solution is used for  $h/\delta > 1$  and the large time solution when  $h/\delta < 1$ .

The three-wire solution is essentially the same as the single wire solution with the exception that the wire radius for the multi-wire line is an effective radius that is larger than the individual wire radius and smaller than the total distance between the wires. This difference in the effective radii accounts for the smaller impedance of the three-wire line over ground.

The conclusion from these measurements is that Sunde's formulation is accurate for predicting the change in waveshape of a signal down a transmission line. Since the formulation does not include any radiation loss terms, it is concluded that any radiation loss is negligibly small compared to the loss due to the finite conductivity of the ground. Our measurements at a height of 12 inches corresponded to a height of one wavelength at a frequency of 1 GHz. These measurements may be considered a 20:1 scale model of a three-wire line 20 feet high over soil with conductivity of about  $10^{-2}$  mho/m; the conclusion that radiation losses for pulses with rise times of greater than 6 ns are negligible still holds.



LA-7995-91

FIGURE 15 CURRENT WAVEFORM OF A SINGLE WIRE LINE 4000 FEET (full scale) FROM THE FEED POINT, WHERE  $h = 100$  FEET FULL SCALE

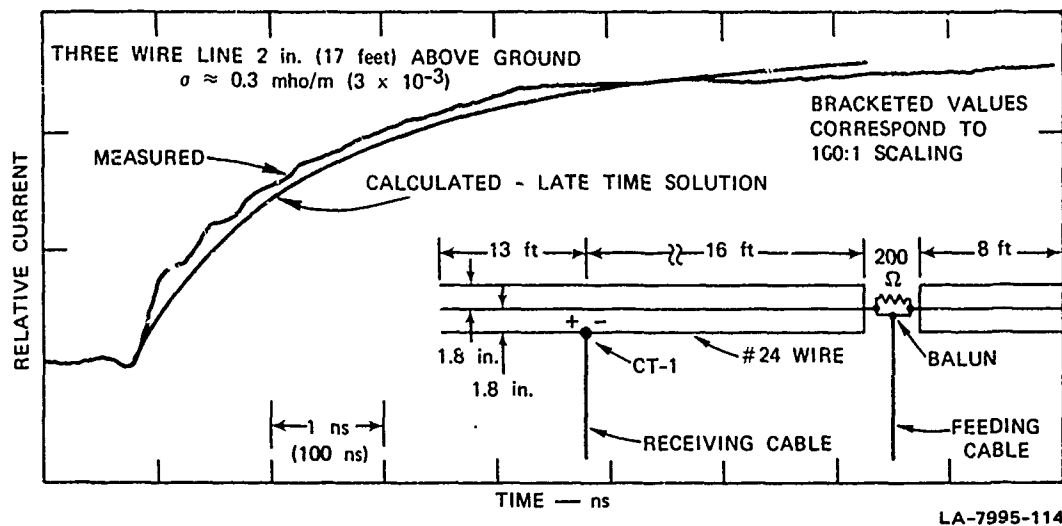


FIGURE 16 CURRENT WAVEFORM OF A THREE-WIRE LINE 1600 FEET (full scale) FROM THE FEED POINT, WHERE  $h = 17$  FEET FULL SCALE

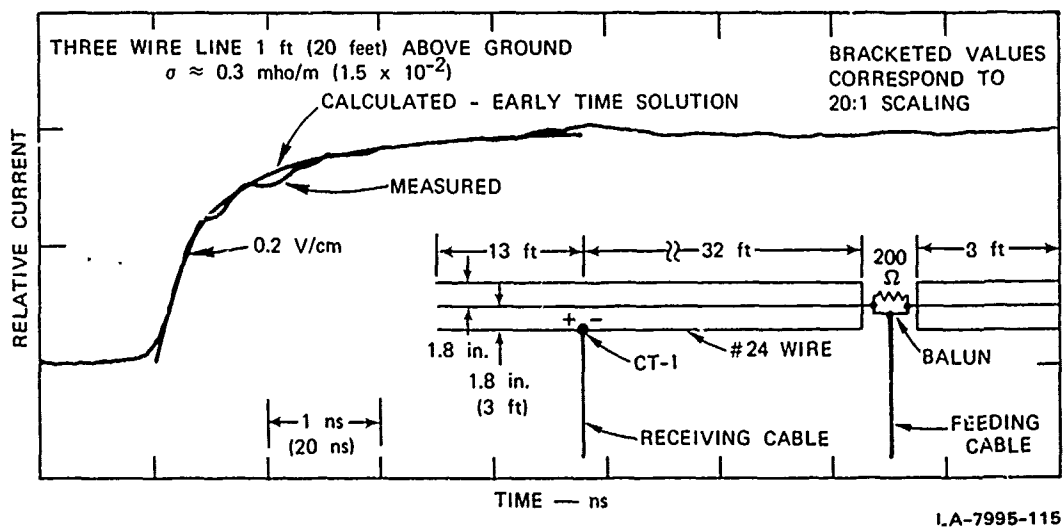
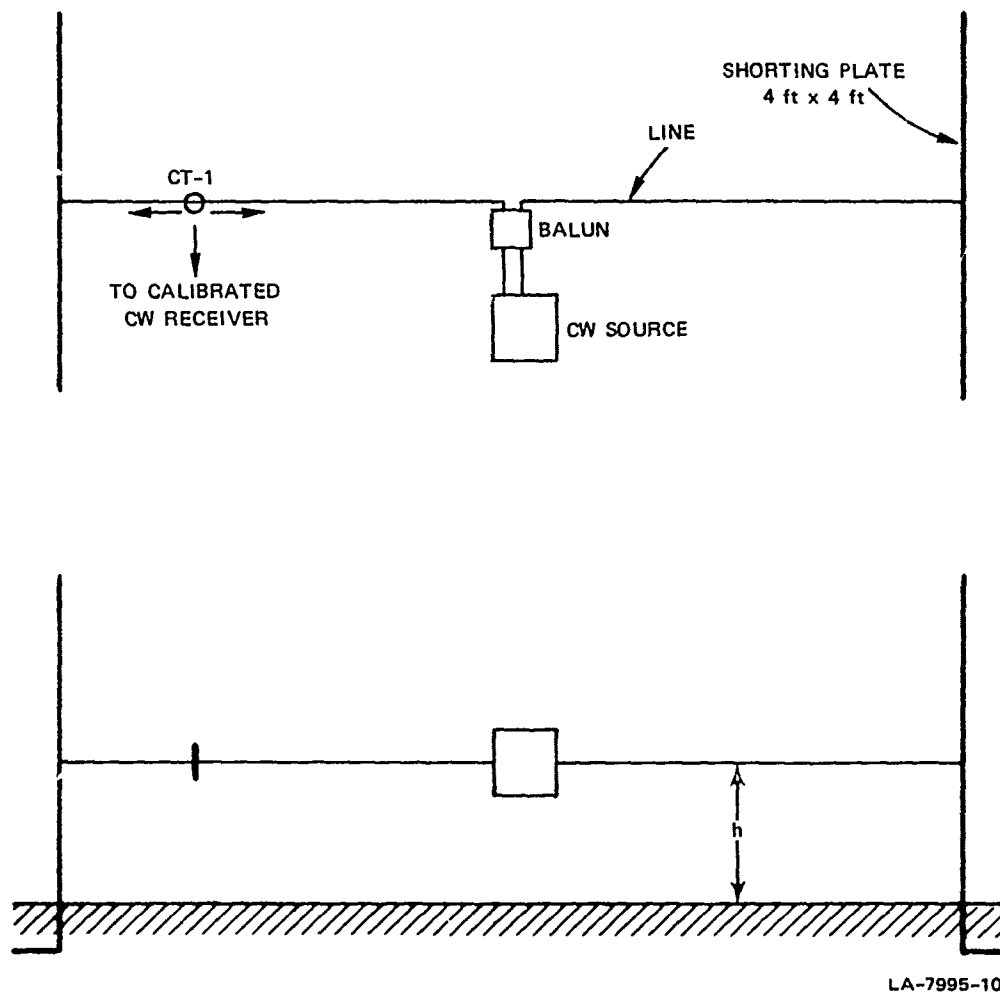


FIGURE 17 CURRENT WAVEFORM OF A THREE-WIRE LINE 640 FEET (full scale) FROM THE FEED POINT, WHERE  $h = 20$  FEET FULL SCALE

### E. Low Frequency Attenuation

Because the attenuation at low frequencies is too low to be detectable in step function measurements, the attenuation at these frequencies was measured by a CW technique. The set-up is shown in Figure 18.

A CW source feeds the balun which excites the transmission line. The line is short-circuited to produce standing waves along the line. When the three-decibel width of the current nulls is measured, the attenuation constant  $\alpha$  may be determined according to the following relation:<sup>6</sup>



LA-7995-101

FIGURE 18 EXPERIMENTAL SET-UP FOR MEASUREMENT OF ATTENUATION OF A WIRE OVER GROUND

$$\alpha w + \rho_s = \frac{\beta \Delta w}{2} \quad (36)$$

where  $w$  = distance from short circuit,  $\rho_s$  = absorption term of load (zero for a perfect short),  $\beta = 2\pi/\lambda$ , and  $\Delta w = 3$  dB width of current null. This technique allows very small values of attenuation to be measured. Large plates were used as a short circuit. These kept the value of  $\rho_s$  low by providing a low impedance to ground and by minimizing radiation from the end of the line. Measurements were made over a frequency range of 10 to 100 MHz for a line 2 inches above ground, which, on a 10:1 ratio, corresponds to a full-scale line at a height of 20 feet. Thus the full-scale frequencies correspond to 83 to 830 kHz. The full-scale conductivity corresponds to about  $2 \times 10^{-3}$  mho/m.

The measured results are shown in Figure 11, which also shows calculations based on Sunde's analysis. Wire conductor losses and radiation losses are assumed negligible in the calculation. A perfect short circuit was assumed in reducing the measurements. At the higher frequencies, it was possible to measure the null width at more than one null. In this way  $\rho_s$  was estimated and found to be small at these frequencies.

When a conductivity of about 0.2 mho/m is assumed, it can be seen that the measured values are slightly higher than the calculated values (at most 30 percent higher) and follow the theoretical variation with frequency quite well.

The phase constant  $\beta$  was also checked by measuring the position of the null. With a perfect short circuit and free space propagation, the current nulls should occur at  $(2n+1)\lambda_0/4$ . The deviation from these locations is proportional to the deviation in phase constant. Figure 19 shows the measured and calculated values of the deviation from free space phase constant for the line 2 inches above ground. The points in

reasonably close to the value for a conductivity 0.2 mho/m. The measured value of conductivity was between 0.2 and 0.3 mho/m.

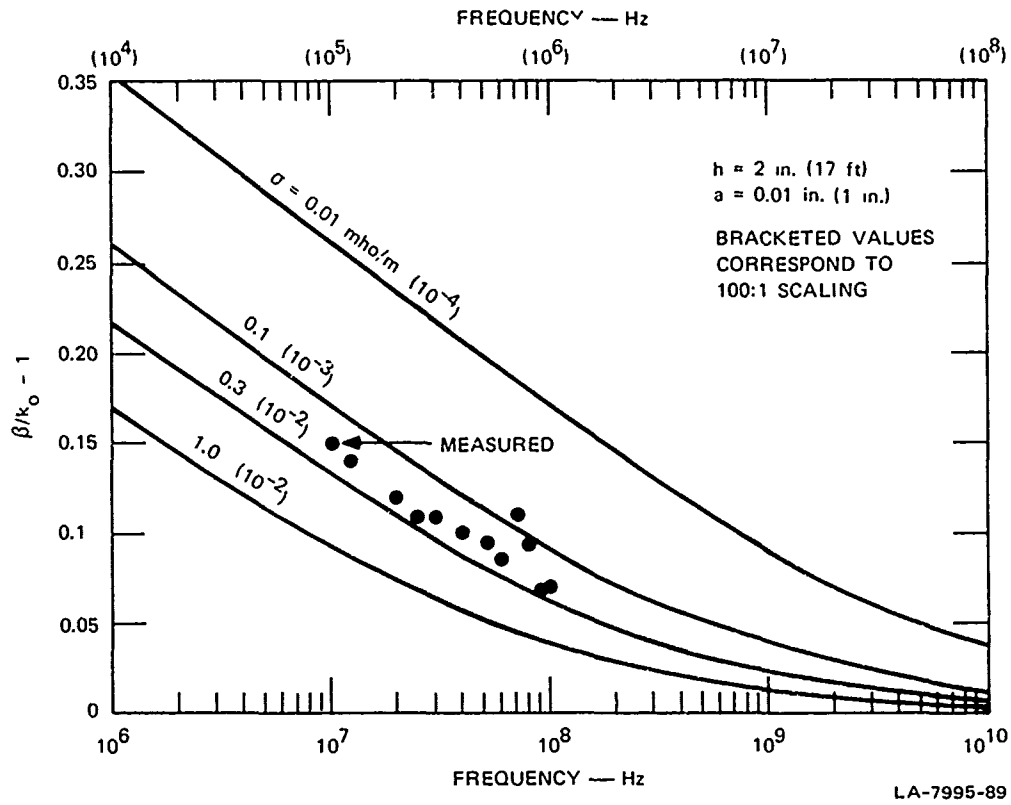


FIGURE 19 PHASE CONSTANT AS A FUNCTION OF FREQUENCY FOR A SINGLE WIRE LINE OVER GROUND

## SECTION IV

### DISCONTINUITIES ON POWER LINES

The signals coupled to the power lines will not always propagate straight to the load. There may be a variety of discontinuities including bends, junctions, and spurs. In this section, we present theoretical and experimental results for propagation of signals when discontinuities are present.

Analysis is usually restricted to the case where the line height is small compared to the wavelength. Thus, one purpose of the measurements was to see if significant deviations from theory could be found when the line height was comparable to the wavelength.

#### A. Bends

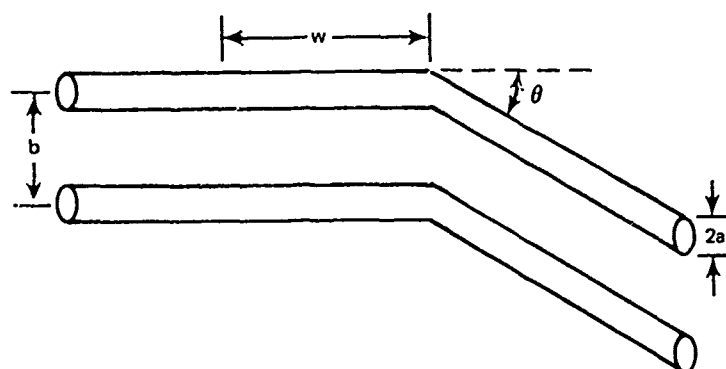
The simplest discontinuity is a bend in the line. King, treated this type of discontinuity when  $\beta h \ll 1$ , considered the geometry shown in Figure 20.<sup>7</sup> His analysis shows that the bend has the effect of lowering the inductance  $\ell(w)$  and capacitance  $c(w)$  per unit length of line in the region around the bend. The values of  $\ell(w)$  and  $c(w)$  are

$$\ell(w) = \frac{K - F_1(w) + F_2(w) \cos \theta}{2\pi v} \quad (37)$$

$$c(w) = \frac{2\pi\epsilon}{K - F_1(w) + F_2(w)} \quad (38)$$

where

$$K = 2\ell n \frac{b}{a}$$



LA-7995-96

FIGURE 20 TWO-WIRE LINE WITH A BEND

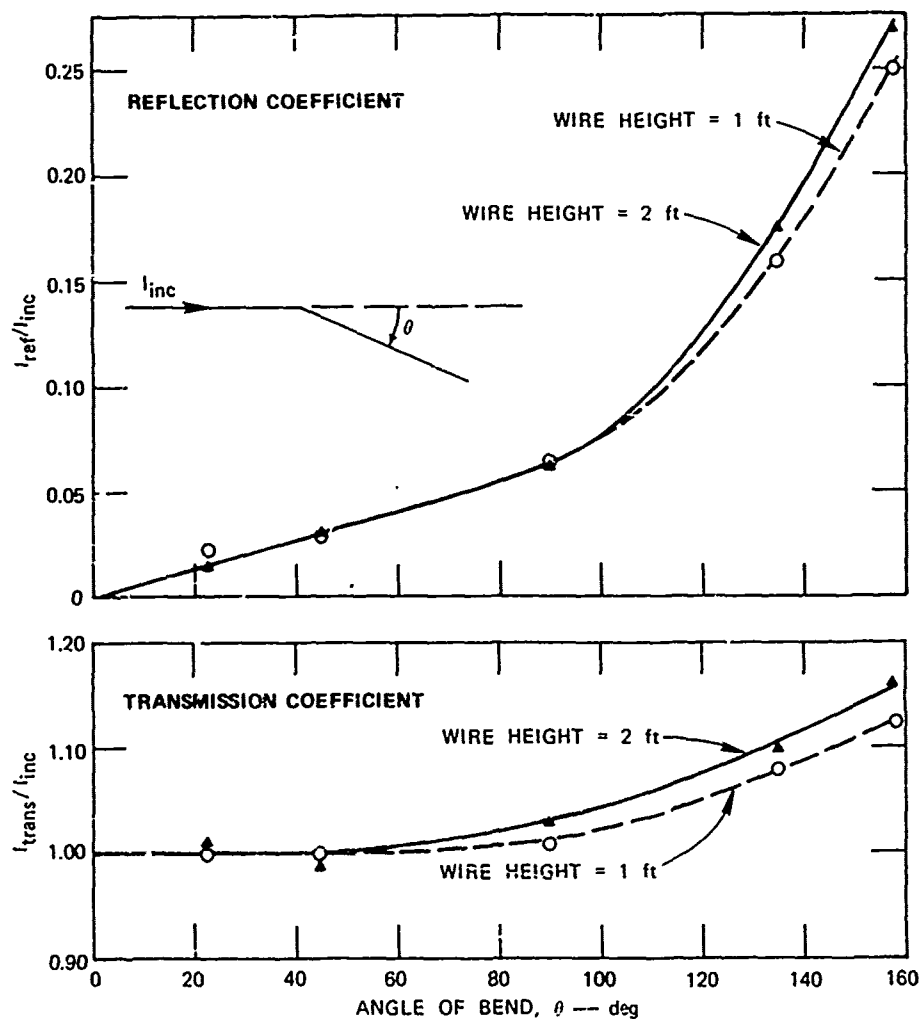
$$\nu = \frac{1}{\mu} = \frac{1}{\text{permeability}}$$

$$F_1(w) = \ln \frac{w + \sqrt{w^2 + b^2}}{w + \sqrt{w^2 + a^2}}$$

$$F_2(w) = \ln \frac{w \cos \theta + \sqrt{w^2 + b^2}}{w \cos \theta + \sqrt{w^2 + a^2}}$$

Measurements were made with a single wire line 1 foot and 2 feet above ground for a range of bend angles from  $0^\circ$  to  $157.5^\circ$ . A step function signal with rise time of about 300 ps was fed onto the line. A current transformer was mounted 1 foot from the junction to monitor the reflected and transmitted waveform.

The results are shown in Figure 21. The reflected signal added to the incident signal (voltage reflection coefficient was negative) and the transmitted signal increased when a bend was introduced into the line. The reflection is small (less than 6 percent) for bends up to 90 degrees.



LA-7995-116

FIGURE 21 REFLECTION AND TRANSMISSION COEFFICIENT OF A BEND IN A SINGLE WIRE LINE OVER GROUND AS A FUNCTION OF BEND ANGLE

Similarly, the transmitted signal varied only a few percent up to  $\theta = 90^\circ$ . At angles greater than 90 degrees, the reflection and transmission coefficients increased sharply. Of course, for  $\theta > 90^\circ$ , the wave on the incident arm can couple to the transmitted arm before the incident signal reaches the bend.

The variation of results with height was small and within the data uncertainties.

The perturbation due to the bend was time dependent. The values shown in Figure 21 are peak values. Generally the effect of the bend was relaxed within a few ns (or equivalently, a few line heights). This result is consistent with King's analysis, which shows that the effects on  $\ell(w)$  and  $c(w)$  are strong only near the junction. At later times--or longer wavelengths--the strong effects near the junction are smoothed, since perturbances that extend over only a small fraction of a wavelength cannot be resolved. The results of King's analysis are compared to measured results in Figure 22. Since the measured and calculated results are in reasonable agreement, the effect of the line height's comparability to the wavelength must be small for the rise times considered. In any case, the effect is small for  $\theta \leq 90^\circ$ .

The effect of radius of curvature on the reflection coefficient was briefly investigated. A line of 0.01-inch diameter was shaped into a

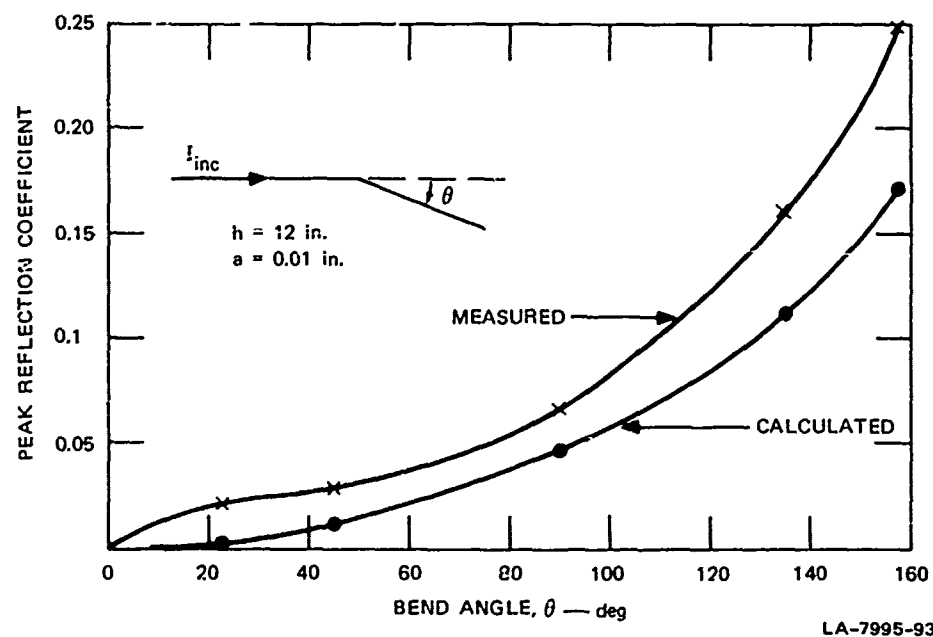


FIGURE 22 COMPARISON OF CALCULATED AND MEASURED REFLECTION COEFFICIENTS OF A BEND AS A FUNCTION OF BEND ANGLE

90-degree bend with the radius of curvature varying from 24 inches to ~0.01 inch. The results are shown in Figure 23. The reflection coefficient decreases monotonically as the radius of curvature is increased.

#### B. Symmetrical Junctions

The reflected and transmitted signals were also measured at symmetrical junctions. The line configuration and results are shown in Figure 24. The line height used was two feet, or six times the equivalent length of the rise time ( $L_{eq} = c\tau_{rise}$ ).

If the two lines forming the junction are considered as two lines of characteristic impedance  $Z_0$  in parallel and are fed by a single input line of  $Z_0$ , then the reflection coefficient would be 0.33 and the transmission coefficient would be 0.667. These values are indicated in Figure 24. The results show that this model accurately reflects the interaction

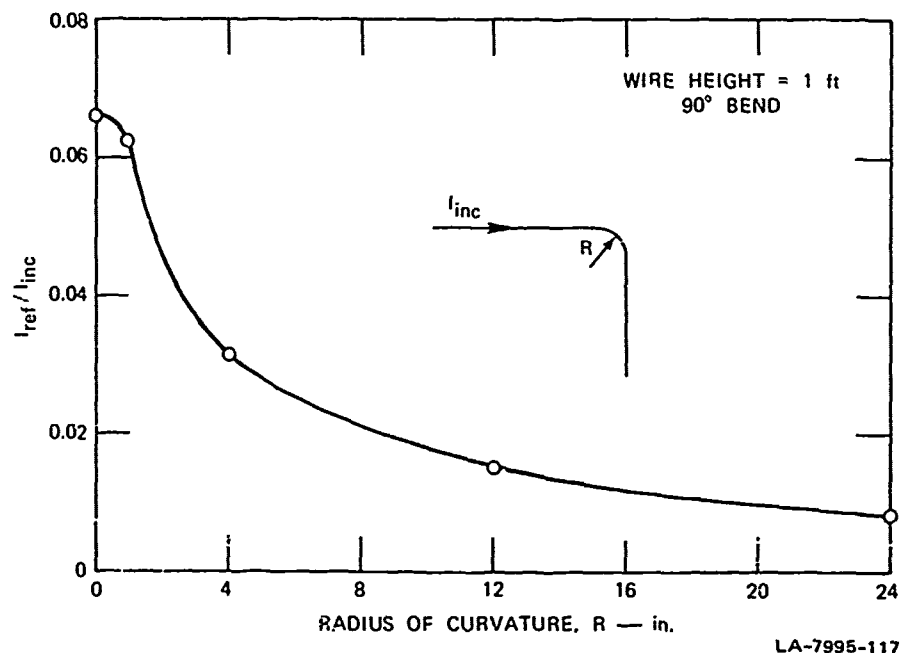


FIGURE 23 REFLECTION COEFFICIENT FOR A 90° BEND AS A FUNCTION OF RADIUS OF CURVATURE

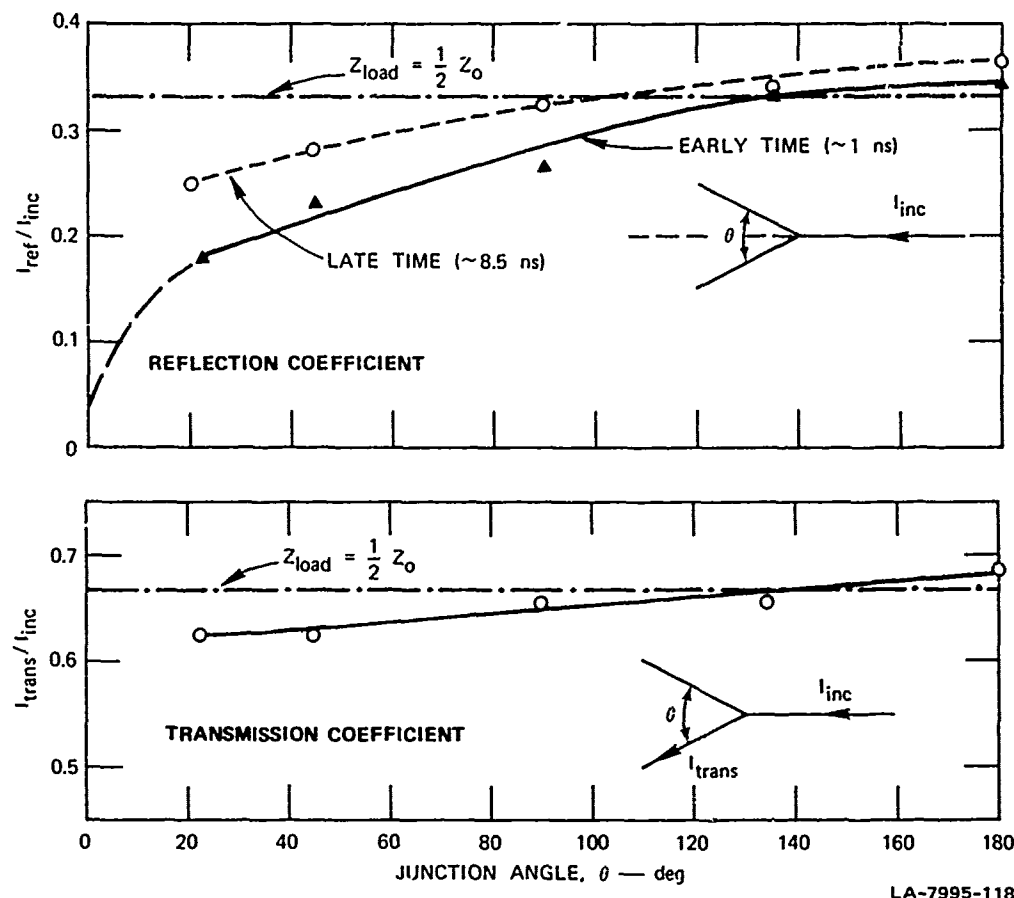


FIGURE 24 REFLECTION AND TRANSMISSION COEFFICIENT AT A SYMMETRICAL JUNCTION, WHERE  $h = 2$  FEET

at the junction when the junction angle is large. This result is reasonable since at large angles the junction lines are relatively independent. However, when the angle is small, the junction lines are more tightly coupled to each other, making the net impedance closer to  $Z_0$ . This reduces the reflection and transmission coefficients. The reflection coefficient is shown for early times ( $\sim 1$  ns) and for late times ( $\sim 8.5$  ns). At early times the reflection coefficient is much lower than would be expected from the uncoupled line of characteristic impedance  $Z_0$ . In the limit as  $\theta \rightarrow 0$ , the wire diameter roughly doubles and, since  $Z_0$  is proportional to  $\ln 2h/a$ , the value of  $Z_0$  for the junction

wire almost equals the value of  $Z_0$  for the input line, resulting in only a very small reflection. This is shown as the dashed portion of the early time curve from  $\theta = 0^\circ$  to  $\theta = 22.5^\circ$ .

One may calculate the local  $Z_0$  of the junction lines considered as two wires over ground. The  $Z_0$  for this configuration is<sup>8</sup>

$$Z_0 = 30 \ln \left[ \frac{4h}{d} \left( 1 + \left( \frac{2h}{D} \right)^2 \right)^{1/2} \right] \quad (39)$$

where  $h$  = line height,  $d$  = line diameter, and  $D$  = line spacing for the diverging junction wires,  $D$  increases as the distance from the junction increases. As  $D \rightarrow \infty$ ,  $Z_0$  reaches 1/2 that of the input line and the reflection coefficient reaches 0.33.

We have computed the local impedance at distances corresponding to 1 ns and 8.5 ns after the wave reaches the junction. The reflection coefficient  $\rho$  was then calculated based on this local  $Z_0$  as a function of the input line. The calculated and measured results are shown in the following tabulation:

$\theta$	$t = 1 \text{ ns}$		$t = 8.5 \text{ ns}$	
	$\rho_{\text{calc}}$	$\rho_{\text{meas}}$	$\rho_{\text{calc}}$	$\rho_{\text{meas}}$
22.5°	0.192	0.181	0.285	0.25
45	0.224	0.234	0.311	0.283
90	0.264	0.266	0.328	0.325
135	0.30	0.334	0.334	0.342
180	0.333	0.344	0.333	0.367

Since the calculation does not include the effect of cumulative reflection from the continuously varying impedance, it is to be expected that the values would not be in perfect agreement. But the agreement is reasonably good and certainly shows the correct trends.

The transmission coefficient may be calculated from the reflection coefficient. The result of this calculation and the measured values are shown in the following tabulation:

$\theta$	$T_{\text{calc}}$	$T_{\text{meas}}$
22.5°	0.596	0.625
45	0.612	0.525
90	0.632	0.656
135	0.65	0.656
180	0.666	0.687

Once again, the agreement is reasonably good, and the trend is correct.

Similar measurements were carried out at a line height of one foot with the results shown in Figure 25. Calculations as outlined above gave similarly close agreement with the measurements.

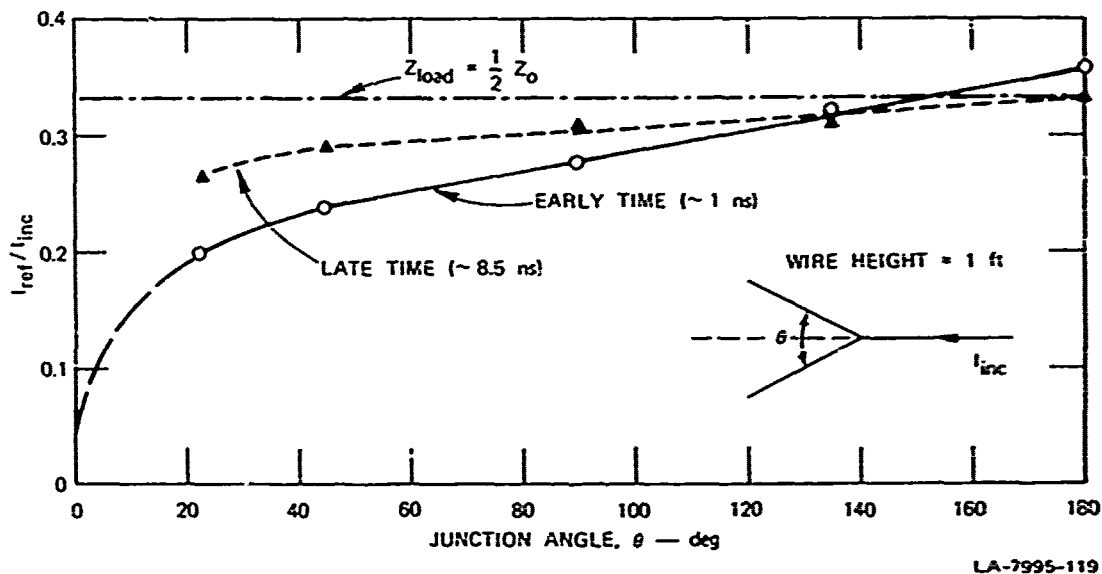
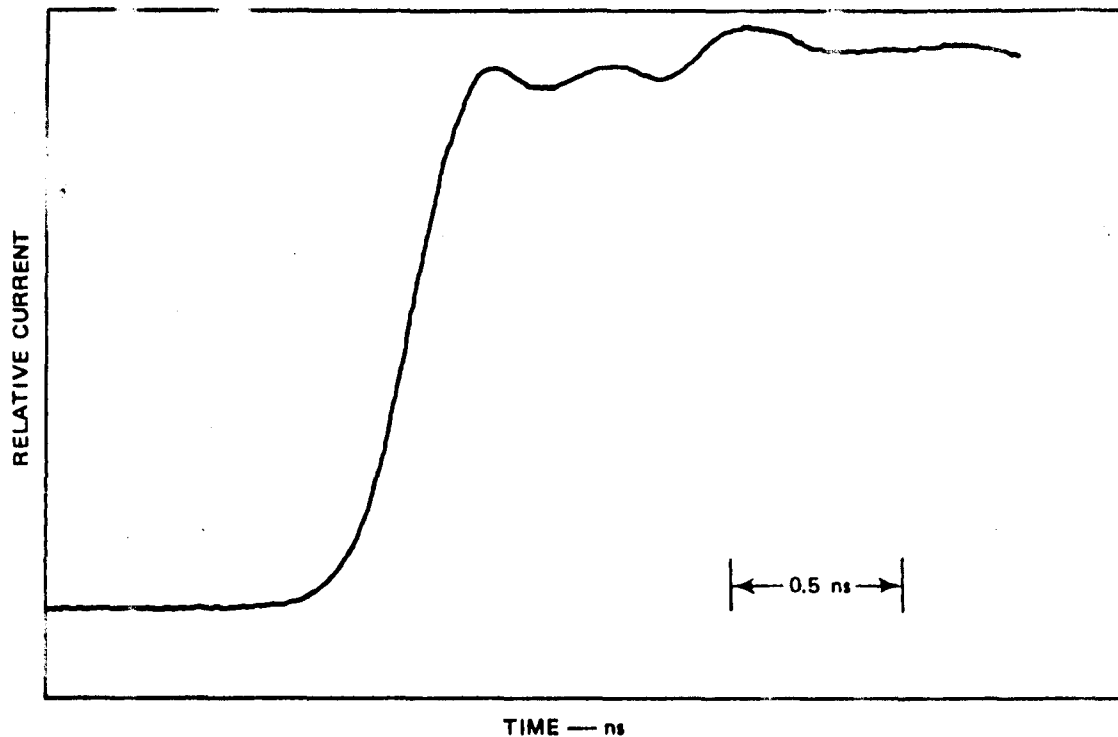


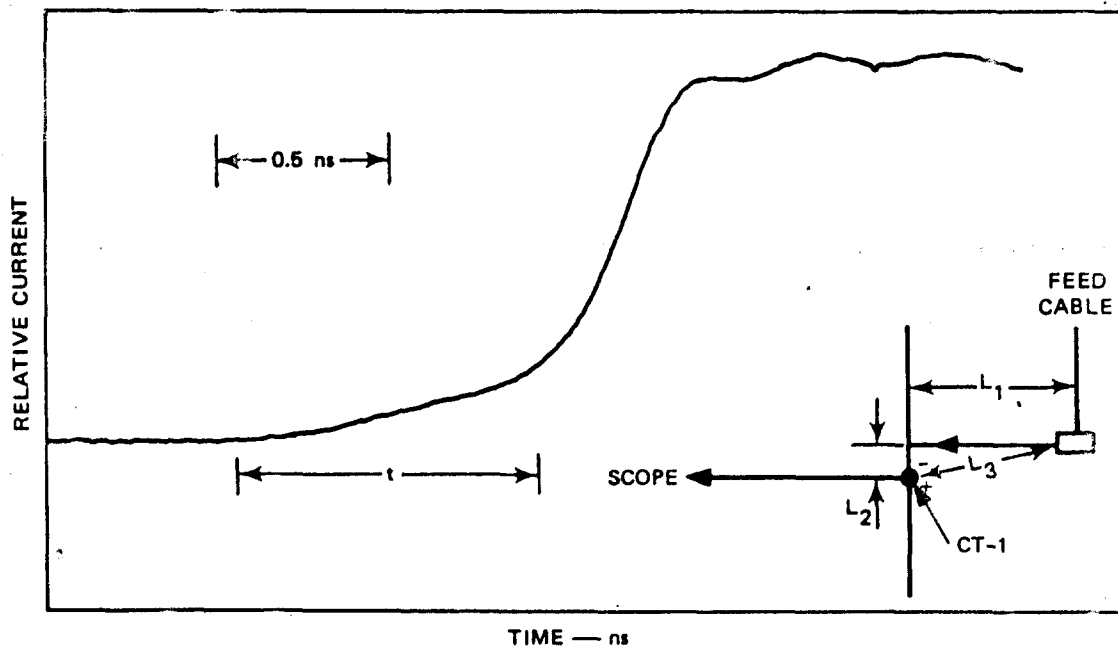
FIGURE 25 REFLECTION COEFFICIENT AT A SYMMETRICAL JUNCTION, WHERE  $h = 1$  FOOT

### C. Rise Time Characteristics

The waveform of the incident signal is shown in Figure 26. The rise time is 310 ps. For  $\theta$  of 22.5 degrees and 45 degrees the rise time was measured as 320 ps, which is within experimental error. As  $\theta$  was increased beyond 45 degrees, a marked degradation in rise time was noted. This is illustrated in Figure 26 for  $\theta = 180^\circ$ . A long, slow rise is observed. It precedes a rapid increase of signal with a rise time approximately equal to the input rise time. The difference between the calculated time it would take a signal to radiate directly from the feed point to the observation point and the calculated time it would take a signal to propagate along the line to the observation point equals the time ahead of the fast rise portion of the pulse at which the signal is first observed. We conclude that the slow rising "precursor" signal is due to coupling directly from the feed point radiation. Even when the feed point is infinitely far away, the electric field lines associated with the transmission line mode of the incident wave will couple to the junction arms producing a current flow before the current on the transmission line flows around to the observation point. We thus expect that spur lines will see such a "precursor" even when the signal coupled to the main line is very far from the spur.



(a) INCIDENT SIGNAL



(b) TRANSMITTED SIGNAL

LA-7995-92

FIGURE 26 CURRENT WAVEFORM ON SIDE ARM LINE OF A JUNCTION

## SECTION V

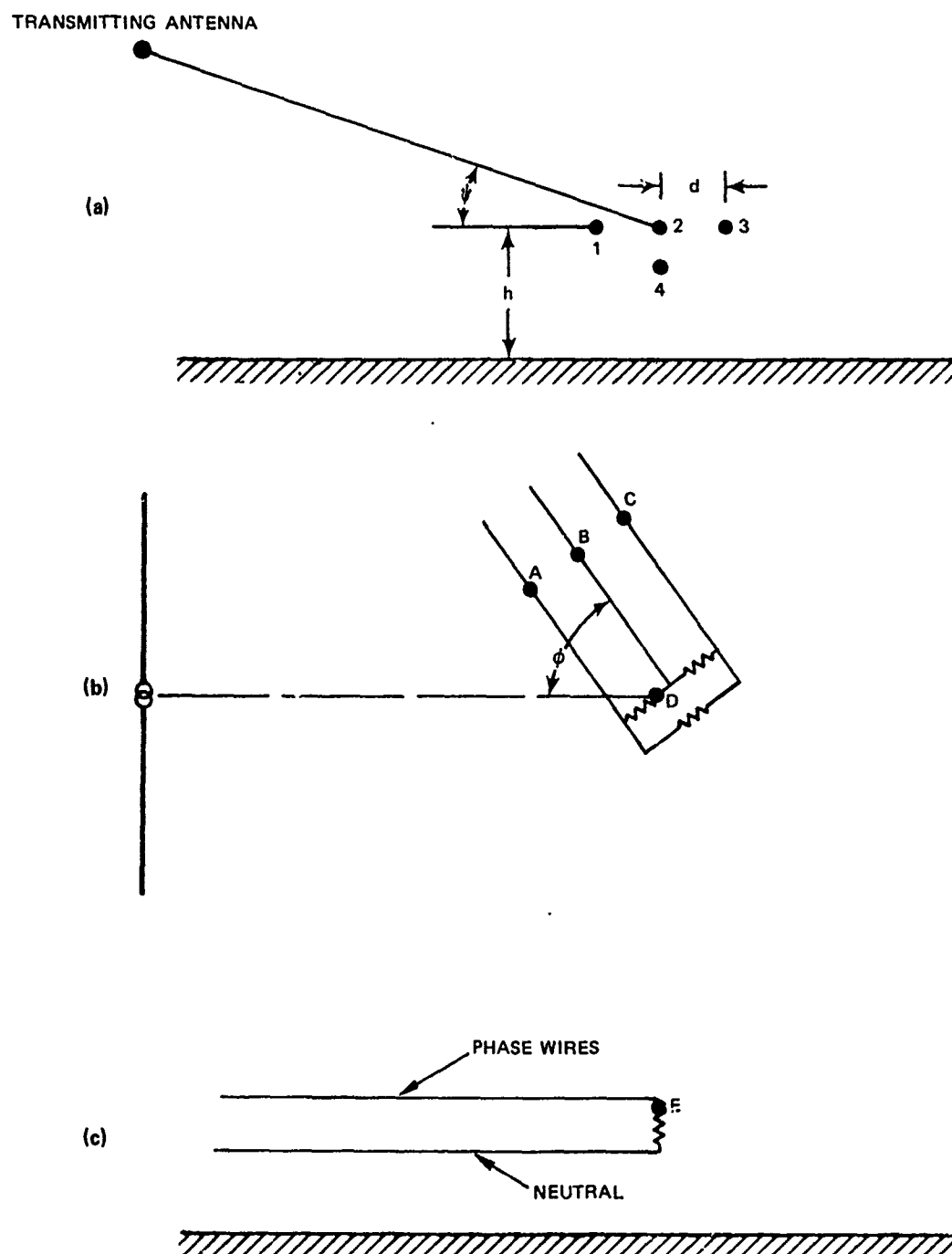
### COUPLING TO MULTI-WIRE LINES

Measurements were made on several types of multi-wire lines for both vertical and horizontal polarization and for a range of azimuth angles. A sketch of the three wire set-up for horizontal polarization is shown in Figure 27, which illustrates some of the nomenclature.

The phase wires are labeled 1, 2, and 3 while the neutral is labeled 4. The height of the phase wires above ground is  $h$  and the spacing between wires is  $d$ . The electric field at the loads was 54 V/m.

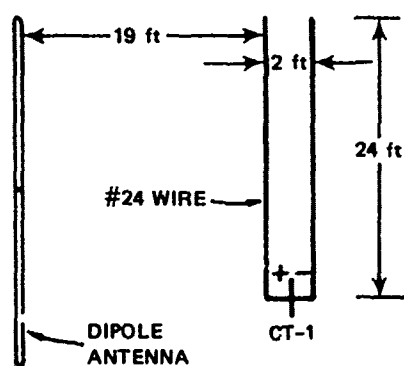
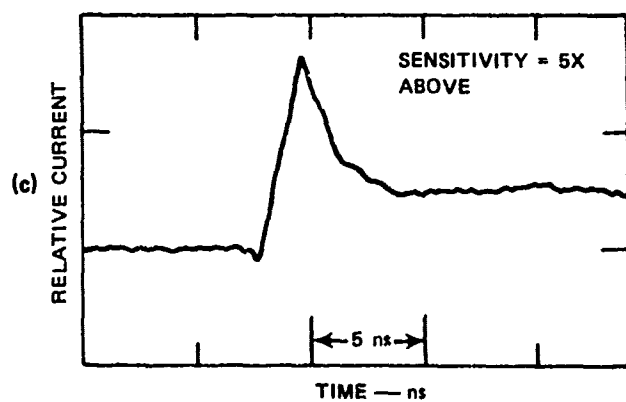
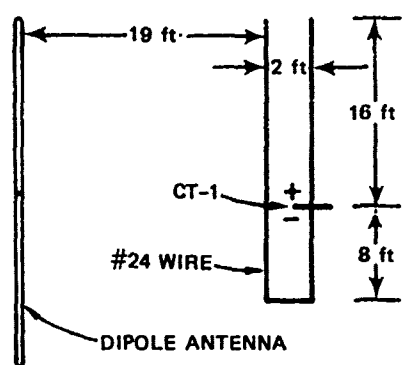
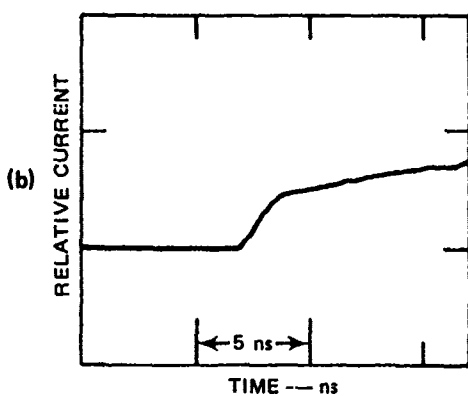
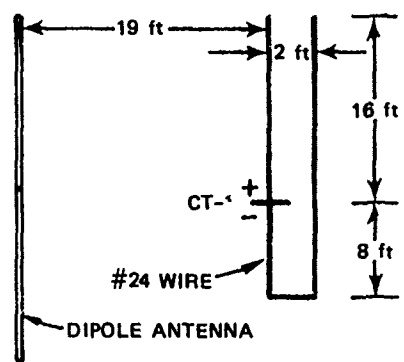
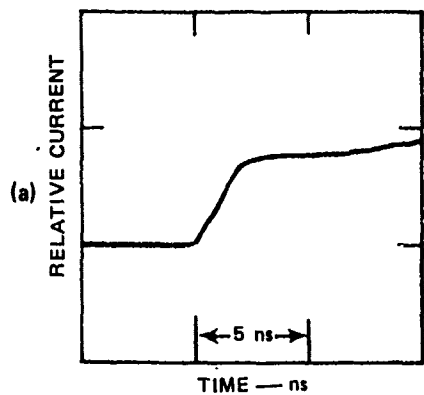
The azimuth angle is  $\phi$ . Currents were monitored at points A, B, and C on the phase wires. This point was about 4 feet from the load so that there was sufficient time to measure the currents before interaction with the load occurred. Current at point D (called the side-arm current) gave a measure of the differential mode current that would flow into a load. Measurements at point E monitored the current, and hence potential, that flowed from the phase to the neutral wire. As described later, some measurements were performed with the neutral wire periodically grounded.

To gain some insight into the complex interactions that occur in multi-wire lines, we first made measurements on a two-wire line where the spacing between wires,  $d$ , was 2 feet and the height above ground was also 2 feet. These spacings allowed us to time resolve signals. The wave shapes of the current at different positions on the line are shown in Figure 28. In Figure 28(a) the current is shown on the line closest to the transmitted signal. It rises linearly for about 2 ns, which corresponds to the time before the ground-reflected signal arrives at the wire ( $\tau = 2h/c \sin \psi$ ). After this time it slowly increases, as would be



LA-7995-100

FIGURE 27 EXPERIMENTAL CONFIGURATION FOR COUPLING TO MULTI-WIRE LINES OVER GROUND



LA-7995-95

FIGURE 28 CURRENTS COUPLED TO TWO-WIRE LINES OVER GROUND

expected for reflection from an imperfect ground. The measured current at 2 ns is just what one would calculate for a single wire over ground.

In Figure 28(b) the current is shown for the wire that is farthest from the transmitter. Its waveform is similar to the previous one except it is only about two-thirds the amplitude at a given time after the arrival of the wave. This reduction in amplitude is due to the scattered fields from the first wire inducing a current that opposes the current due to the incident field.

Figure 28(c) shows the current at the short circuit load at a point midway between the wires. The current reaches a peak at 2 ns, as the current from the first wire arrives at the current probe. At this time, current from the second wire arrives and opposes the current to a reduced value. The current does not go to zero but is much less than would be collected from two wires in free space as analyzed by Harrison.<sup>9</sup> Their analysis shows that for two wires in free space the differential mode current is

$$I_d = \frac{E_o d}{Z_o} \cos \psi \quad (40)$$

The measured value in Figure 28(c) where the wires are over ground, is about 0.2 of this value. We believe that this value is due to the ground reflection coefficient's being about -0.8 instead of -1 as it would be for perfect ground. Our reasoning is explained as follows.

The differential current flowing in the short-circuit load of a two-wire line in free space is as given in Eq. (40). Placing these wires over ground is approximately equivalent to exciting these wire from an angle,  $-\psi$ , and with a field strength of  $RE_o$ , where R is the

ground reflection coefficient. Therefore, the differential current due to presence of ground is

$$I_{dg} = \frac{RE_o d \cos(-\psi)}{Z_o} = \frac{RE_o d \cos \psi}{Z_o} \quad (41)$$

Since R is a negative number less than one, the net differential current after the ground reflection will be

$$I_{d \text{ net}} = \left(1 - |R|\right) \frac{E_o d \cos \psi}{Z_o} \quad (42)$$

This equation is only approximately true in this case since the presence of ground will change  $Z_o$  somewhat. Nevertheless, the predominant effect of ground will be to reduce the differential current.

Measurements on four-wire lines consisting of three phase wires and a neutral were made with the results shown in Figure 29. The wires were terminated in 400 ohm loads. Once again the conductor closest to the transmitter had the largest current flowing in it. Figure 29 shows the current in the side arm, which would produce differential voltages. The peaks values are about 10 percent of the current flowing on the lines while the late time currents are only a few percent of the line currents.

For this 20:1 model of a power line, the full scale currents are shown in parentheses for an incident field of 54 V/m. If the incident field is higher the current will also be higher by the ratio of the fields.

The phase to neutral currents are shown in Figure 30. These currents, even at late times are at least 10 percent of the line currents.

The same measurements were made with the neutral grounded every 2 feet. The currents are shown in Figure 31. The line current has not

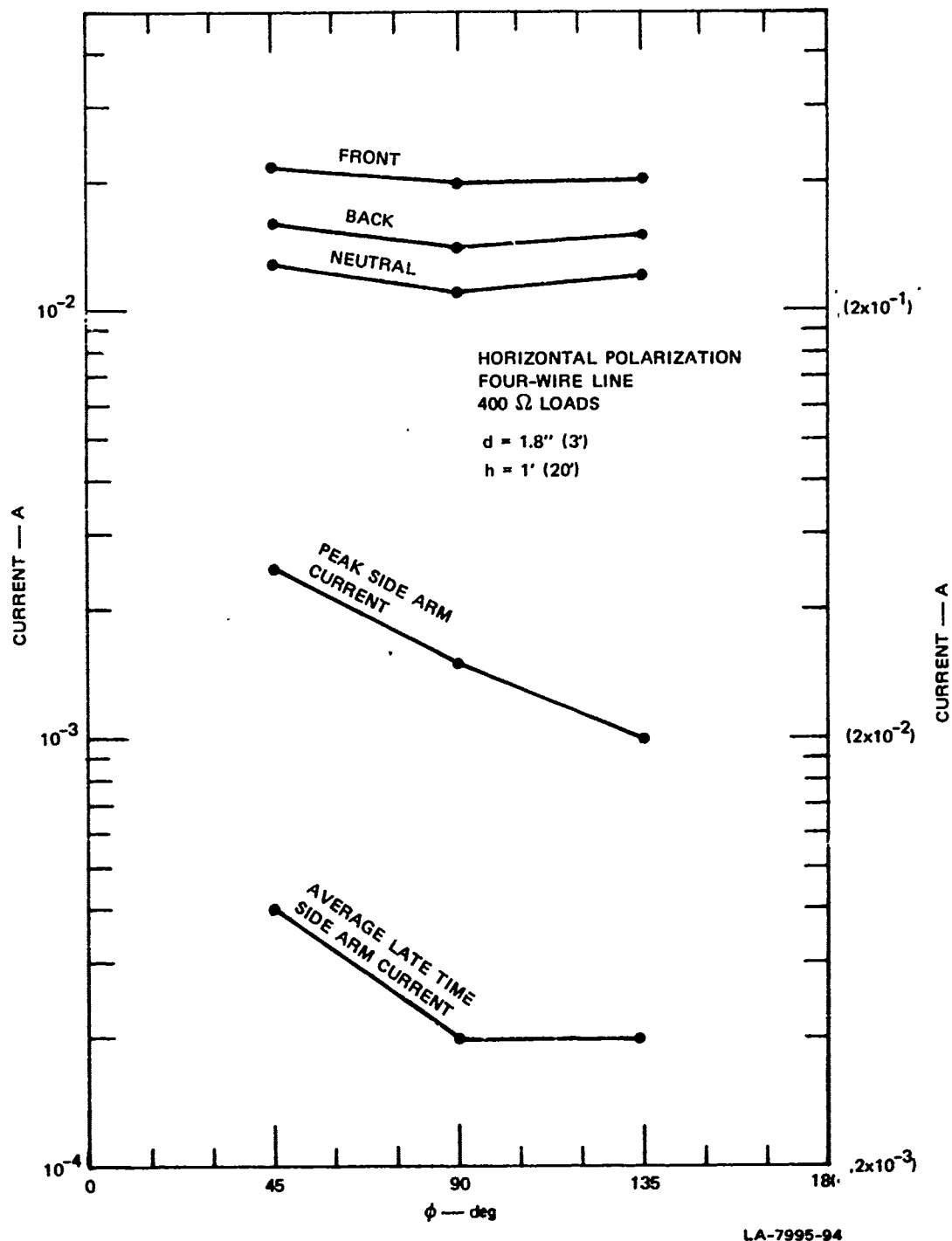


FIGURE 29 CURRENTS COUPLED TO A FOUR-WIRE LINE WITH 400  $\Omega$  LOADS AND HORIZONTAL POLARIZATION

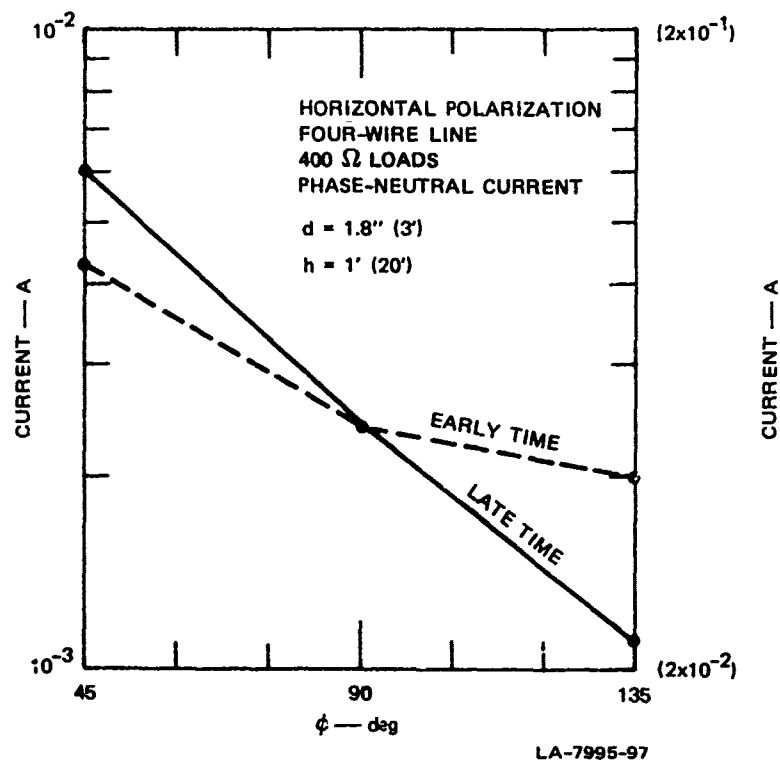
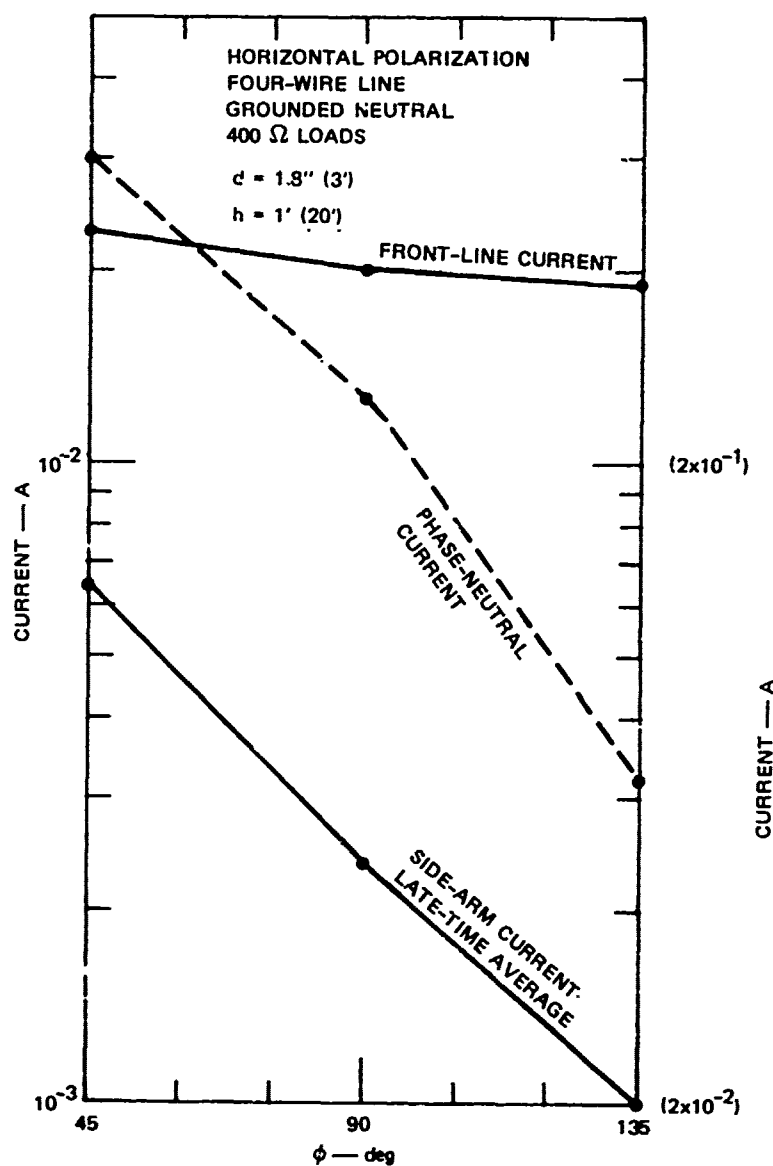


FIGURE 30 PHASE-NEUTRAL CURRENTS ON A FOUR-WIRE LINE WITH 400  $\Omega$  LOADS AND HORIZONTAL POLARIZATION

changed much from the line current in the ungrounded case. However, the late time and the phase to neutral current has increased significantly over the ungrounded case. The direction of current is such that current is being driven from the neutral into the phase wires.

The four-wire system with multiply grounded neutral was also excited with vertical polarization. The results are shown in Figure 32. The line current is a maximum at 0 degrees and dips to a minimum at 90 degrees, where the wires are cross polarized to the wave. The side arm currents at 0 degrees are reduced to about 10 percent of the line current. The phase to neutral currents, however, are quite large, being equal to the line currents at 0 degrees. They are larger by an order of magnitude at



LA-7995-98

FIGURE 31 CURRENTS COUPLED TO A FOUR-WIRE LINE WITH 400  $\Omega$  LOADS, MULTIPLY GROUNDED NEUTRAL, AND HORIZONTAL POLARIZATION

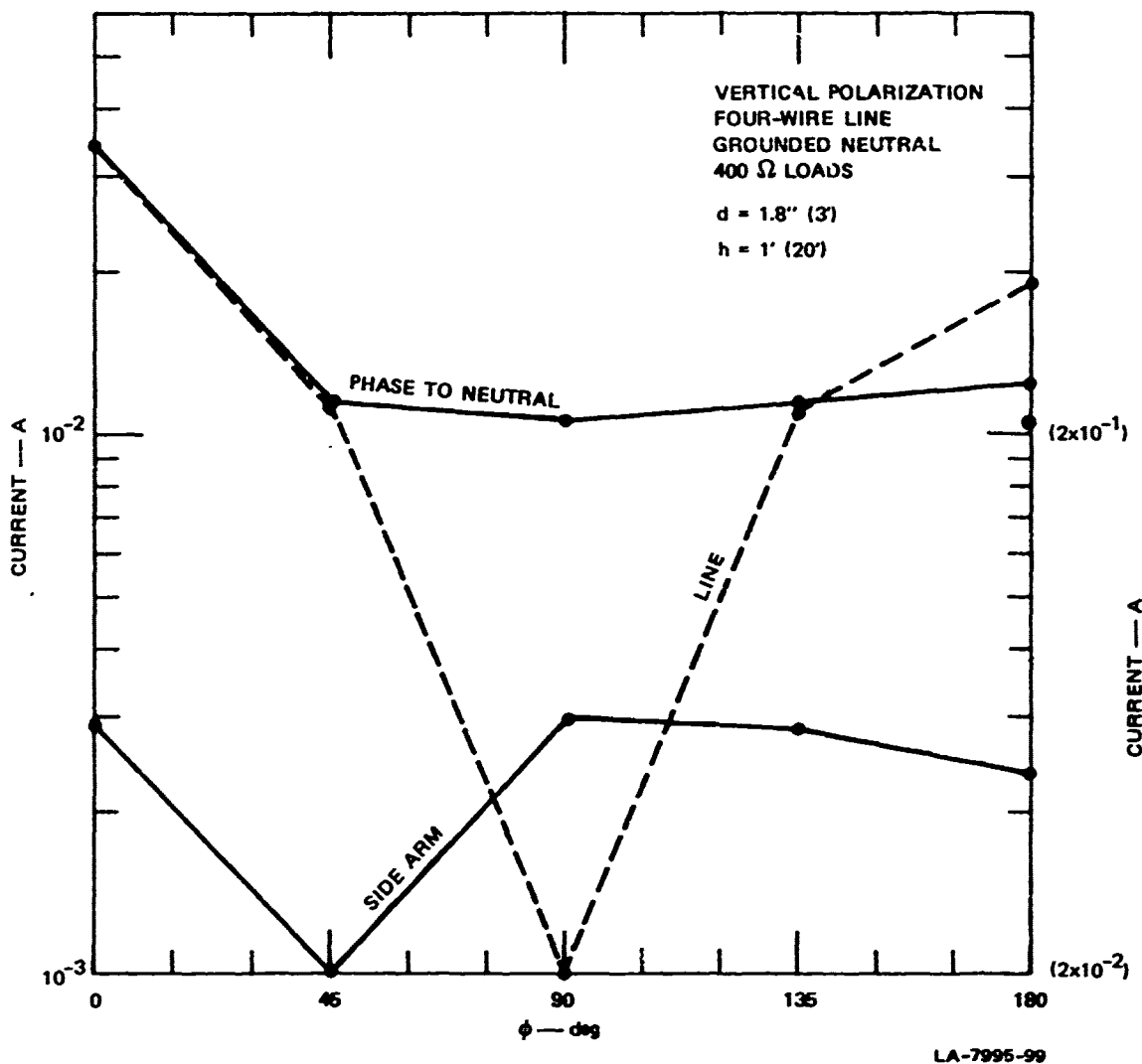


FIGURE 32 CURRENTS COUPLED TO A FOUR-WIRE LINE WITH 400  $\Omega$  LOADS, MULTIPLY GROUNDED NEUTRAL, AND VERTICAL POLARIZATION

90 degrees because the vertical grounding elements pick up current at 90 degrees.

Thus the differential currents in ungrounded systems are typically an order of magnitude below the line currents. However, in grounded neutral systems, large currents, comparable to the line currents, can flow from the neutral to the phase wires.

## SECTION VI

### CONCLUSIONS AND RECOMMENDATIONS

As a result of the work described in this report and in earlier documents prepared under this task,<sup>3</sup> it is believed that the coupling mechanisms by which the EMP interacts with open transmission lines such as power distribution lines is well understood and is adequately described for engineering purposes by the low frequency analysis used heretofore. It is apparent from the theoretical analysis and experimental verification of this analysis, that the strongest common-mode coupling to the power distribution lines occurs for a vertically polarized wave incident almost along the axis of the transmission line. For this rather special case, the short-circuit current induced in a straight line 1 kilometer long is of the order of 1 ampere for an incident field strength of 1 volt per meter.

In addition to verifying the coupling theory, the work reported here demonstrated the effects of several common perturbations to the ideal straight transmission line. These include bends and junctions, as well as periodic grounds, and differential mode coupling. The effects of a bend in the transmission line were found to be measureable and interesting, but of little significance in terms of propagation of the EMP-induced common mode current except when the bend angle approaches 180 degrees. Likewise, the effects of junctions of two lines with a third were, for most cases, found to be adequately described by conventional transmission-line theory, although deviations from ideal transmission-line behavior were noted when the two load lines were quite close together. Differential mode currents, on the other hand, could be significant since they can be as much as 1 percent of the maximum common-mode current. The

maximum differential current occurs for broadside incidence, however, whereas the maximum common-mode current occurs for end-on incidence.

One of the results of this study was to have been recommendations for full-scale tests to obtain additional information on coupling to power lines or propagation on power lines. It is felt, however, that the results of the scale-model experiments and analysis have adequately established the coupling and propagation characteristics of typical transmission-line configurations. Furthermore, the return from full-scale tests is so low (in relation to cost) that such testing should be reserved to testing related to weapon systems, in which the interaction of the existing power system with the weapon system and the local terrain is to be determined. There are few aspects of the physics of coupling to, and propagation along, power lines that cannot be determined more efficiently under controlled laboratory conditions than under field-test conditions. Parameters such as soil conductivity and stratification or local terrain in the vicinity of a particular system are not easily assessed in the general scale-model study; however, these peculiarities of a specific system or site could not be evaluated from an arbitrary full-scale test, either. Only a full-scale test on the site of interest would provide the information necessary to assess those site-peculiar aspects of the power system. Therefore, full-scale tests for the purpose of evaluating coupling and propagation characteristics are not recommended, although continued testing of the weapon system response to the coupled signal will be necessary.

## Appendix A

### COMPARISON OF TRANSMISSION-LINE APPROXIMATION WITH THE EXACT SOLUTION

The transmission-line analysis of the current induced in the power line is based on the assumption that the characteristic impedance of the line remains constant at the value defined by the electrostatic capacitance per unit length and the magnetostatic inductance per unit length. When the line height is comparable to or greater than a wavelength, the characteristic impedance so defined is no longer valid. As has been shown in this report, however, the deviation of predicted values from the measured values is so small that, within the accuracy of the measurement, it is not detectable. A more rigorous analysis of the current induced in a perfectly conducting cylinder over a perfectly conducting ground plane has recently been made by Flammer and Singhaus.<sup>10</sup> The purpose of this appendix is to compare the results of the transmission-line analysis with the exact solutions obtained in Ref. 10.

The comparison will be made for a conductor height-to-radius ratio  $h/a = 100$ , which corresponds to a transmission line whose effective radius is 10 cm at a height of 10 m. The characteristic impedance of this line is 317 ohms. The transmission-line solutions for the step-function response of the current are, for vertical polarization,

$$\frac{\eta_1 i}{2\pi a E_0} = \frac{\sin \psi \cos \phi}{1 - \cos^2 \psi \cos^2 \phi} \frac{1}{\log \frac{2h}{a}} \times \begin{cases} \frac{ct}{a} & 0 \leq t \leq \frac{2h \sin \psi}{c} \\ \frac{2h \sin \psi}{a} & t \geq \frac{2h \sin \psi}{c} \end{cases}$$

and for horizontal polarization,

$$\frac{\eta i}{2\pi a E_0} = \frac{\sin\varphi}{1 - \cos^2\psi \cos^2\varphi} \frac{1}{\log \frac{2h}{a}} \times \begin{cases} \frac{ct}{a} & 0 \leq t \leq \frac{2h \sin\psi}{c} \\ \frac{2h \sin\psi}{a} & t \geq \frac{2h \sin\psi}{c} \end{cases}$$

The characteristic impedance has been expressed as

$$Z_0 = \frac{\eta}{2\pi} \log \frac{2h}{a}$$

to accommodate the current normalization used by Flammer and Singhaus.

Flammer and Singhaus also use a dimensionless time-space parameter

$$u = \frac{ct - z \cos\gamma}{a \sin\gamma}$$

which, when the spatial variation is suppressed, becomes

$$u_v = \frac{ct}{a \sin\psi} \quad (\text{for vertical polarization, } \varphi = 0)$$

or

$$u_h = \frac{ct}{a} \quad (\text{for horizontal polarization, } \varphi = 90^\circ)$$

(The angle  $\gamma$  used by Flammer and Singhaus is the polar angle measured from the axis of the wire; see Figure 1 for the elevation and azimuth convention used in this report.) In the examples that follow, time will be expressed in graduations of  $(h \sin\psi)/c$  or  $h/c$  instead of the dimensionless parameter  $u$ .

The transmission-line solution and the exact solution for the current induced in an infinitely long conductor by a step function of incident field are shown in Figures A-1 and A-2. Figure A-1 shows the response for a vertically polarized incident field for an azimuth angle of incidence of  $\varphi = 0$  and arbitrary elevation angle of incidence. Figure A-2

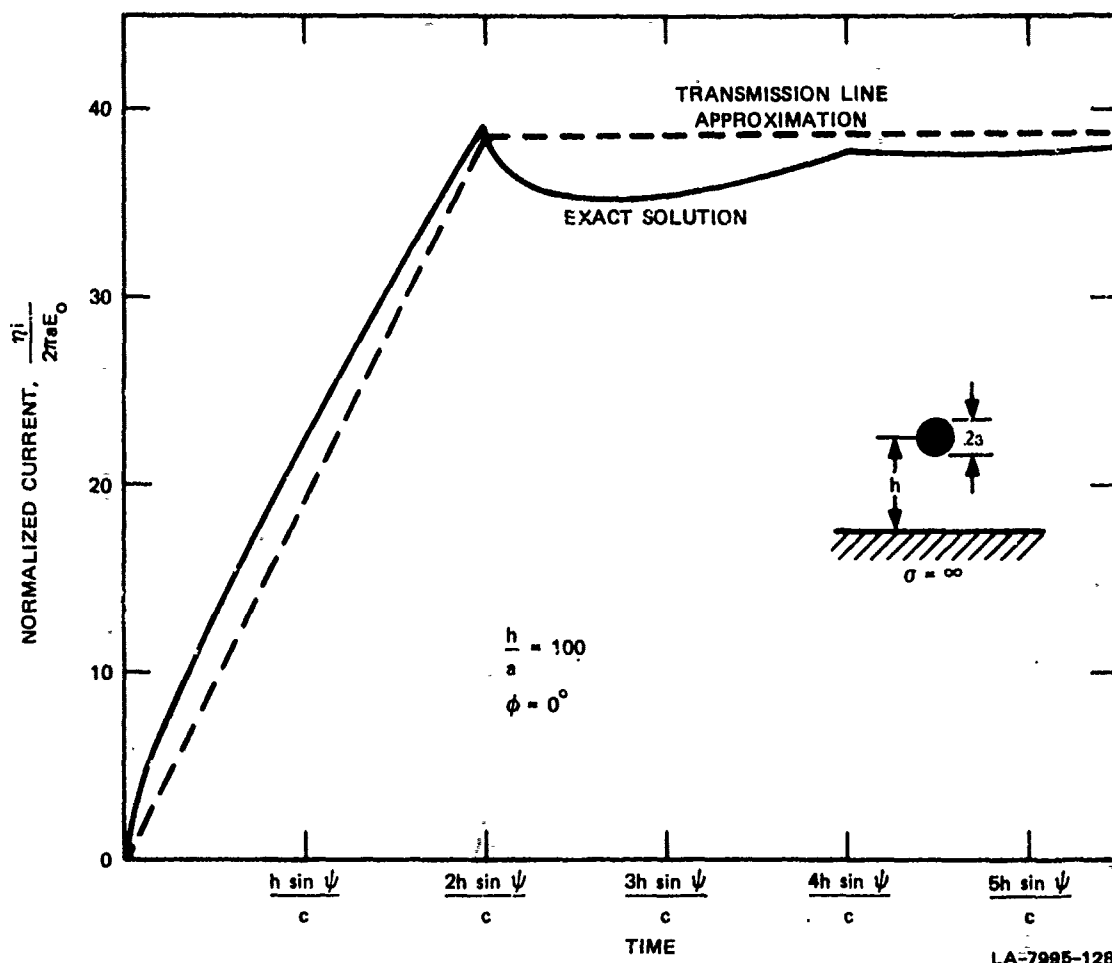


FIGURE A-1 COMPARISON OF THE TRANSMISSION-LINE APPROXIMATION AND THE EXACT SOLUTION FOR THE CURRENT IN A WIRE OVER A PERFECTLY CONDUCTING GROUND PLANE — STEP-FUNCTION INCIDENT FIELD, VERTICALLY POLARIZED

shows the response for a horizontally polarized incident field at an azimuth angle of  $90^\circ$  (broadside) for selected elevation angles of incidence. It is apparent from these illustrations that the transmission-line approximation is a good approximation to the current induced in a wire over a ground plane even for the zero-rise-time step function. For realizable finite rise-time pulses, the difference between the exact solution and the transmission-line approximation should be so small that

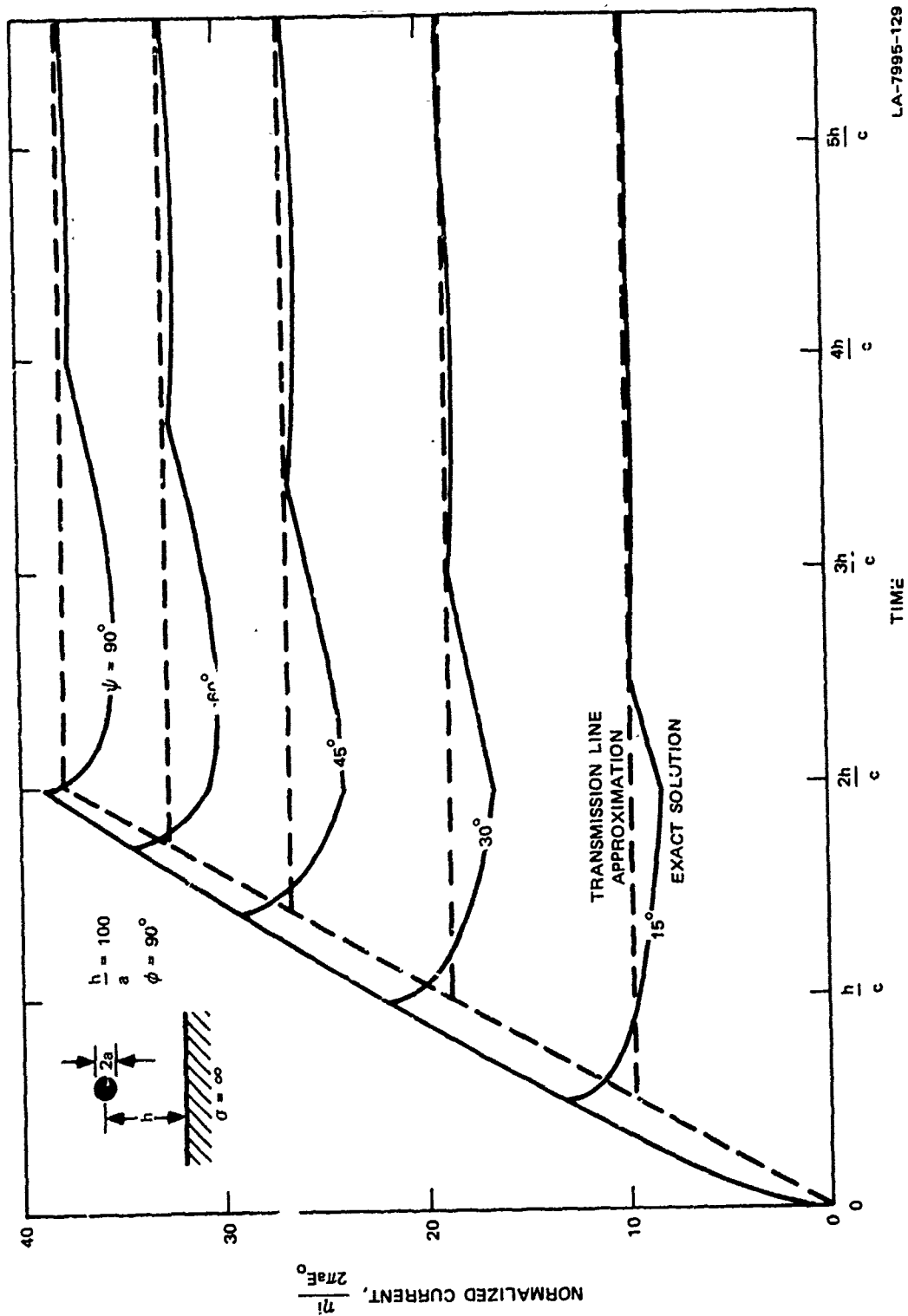


FIGURE A-2 COMPARISON OF THE TRANSMISSION-LINE APPROXIMATION AND THE EXACT SOLUTION FOR THE CURRENT IN A WIRE OVER A PERFECTLY CONDUCTING GROUND PLANE — STEP-FUNCTION INCIDENT FIELD, HORIZONTALLY POLARIZED

it would be difficult to detect experimentally (as has been observed). The exact solution does provide interesting insight into the behavior of the scattered waves before the structure "settles down" to a transmission line. In Figure A-2, for example, one can see the discontinuity that occurs as the ground-reflected wave arrives at  $(2h \sin \psi)/c$ , a second discontinuity when the scattered direct wave reflected from the ground returns at  $2h/c$ , and a third discontinuity when the ground-reflected wave scattered from the wire and reflected back from the ground arrives at  $(1 + \sin \psi) 2h/c$ . Subsequent multiply-scattered waves have a very weak influence, but they eventually bring the exact late-time response into coincidence with the transmission-line solution.

A comparison of the impulse responses for a vertically polarized wave incident at  $\phi = 0$  is shown in Figure A-3. The zero-width impulse induces a very large spike when the direct wave arrives, but the current quickly decays to a value comparable to that predicted by the transmission-line approximation. Since the zero-width impulse is not realizable, the difference between the exact and approximate solutions for practical short pulses of finite width and height and of non-zero rise and fall times is probably not very significant. The exact solution shows a small follow-on current not predicted by the transmission-line theory.

A further comparison is shown in Figure A-4, where the response to a vertically polarized incident exponential pulse is shown. This waveform was obtained by the convolution of an exponential waveform

$$E(t) = E_0 e^{-t/t_0}$$

where

$$t_0 = \frac{20 h \sin \psi}{c}$$

with the step function responses of Figure A-1. Because the time constant  $t_0$  of the exponential waveform was chosen for ease of computing, it is a

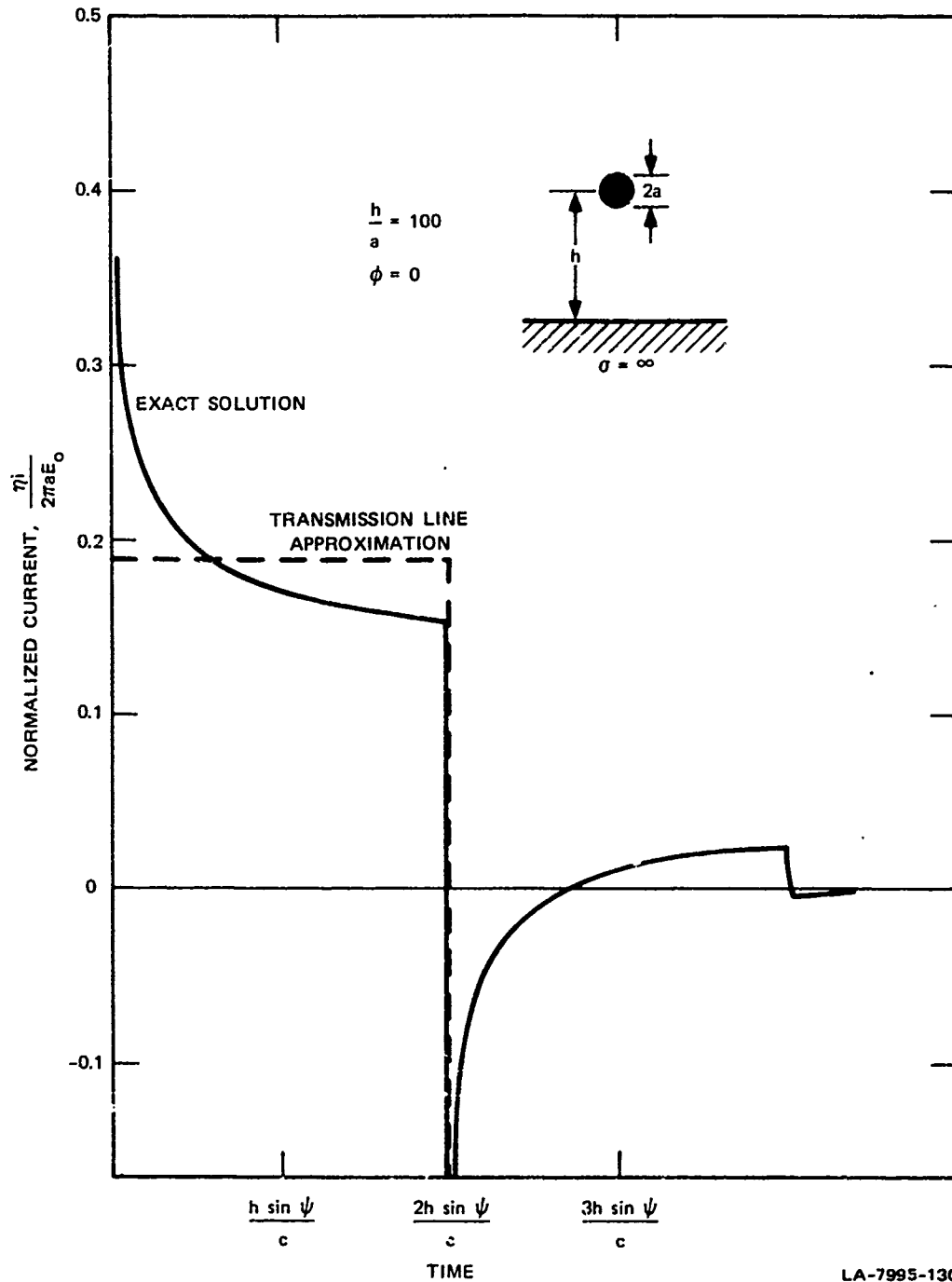


FIGURE A-3 COMPARISON OF THE TRANSMISSION-LINE APPROXIMATION AND THE EXACT SOLUTION FOR THE CURRENT IN A WIRE OVER A PERFECTLY CONDUCTING GROUND PLANE — IMPULSE INCIDENT FIELD, VERTICALLY POLARIZED

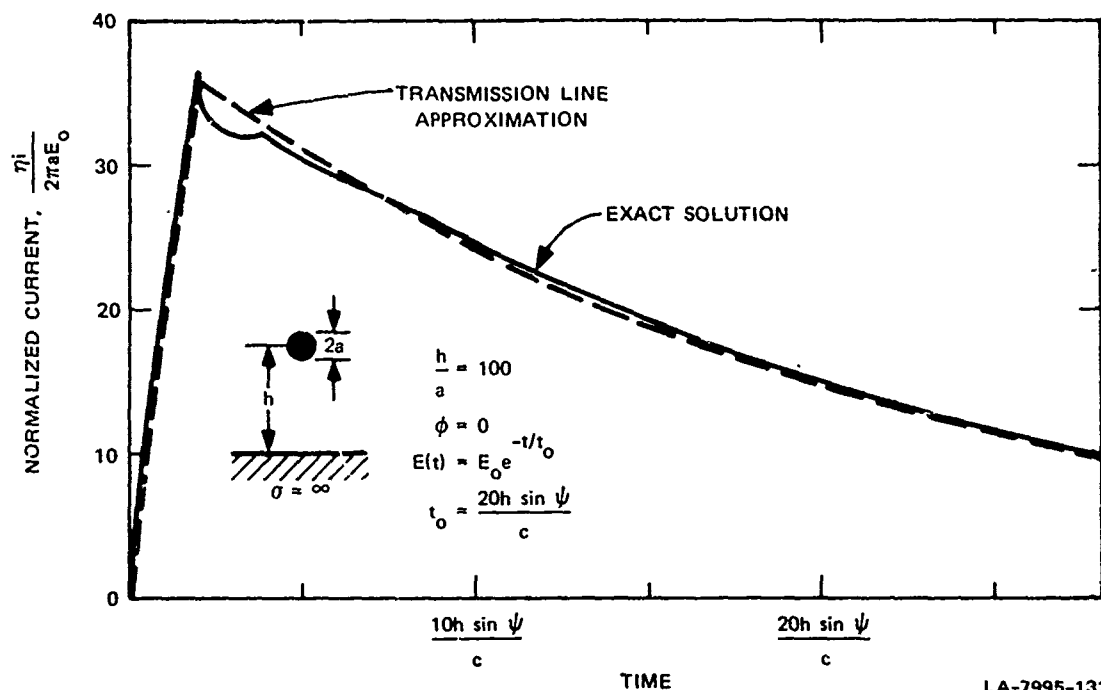


FIGURE A-4 COMPARISON OF THE TRANSMISSION-LINE APPROXIMATION AND THE EXACT SOLUTION FOR A VERTICALLY POLARIZED INCIDENT EXPONENTIAL PULSE

function of the angle of incidence for this example. It is ten times the "clear time" between the beginning of the pulse and the arrival of the ground-reflected wave, so that for a 10-m-high line with the wave incident from directly overhead,  $t_0 = 610$  ns, whereas for incidence at a  $30^\circ$  elevation angle,  $t_0 = 305$  ns. The exponential pulse has zero rise time.

A comparison of the frequency spectra of the exact solution and the transmission-line approximation is shown for a horizontally polarized wave incident at an elevation angle of  $45^\circ$  in Figure A-5. This comparison of the current spectra is consistent with the time-domain comparisons in that the low-frequency spectra, corresponding to the late-time response, are similar, while the high-frequency spectra, corresponding to the early-time response, differ somewhat. Both spectra are characterized by similar maxima and zeros.

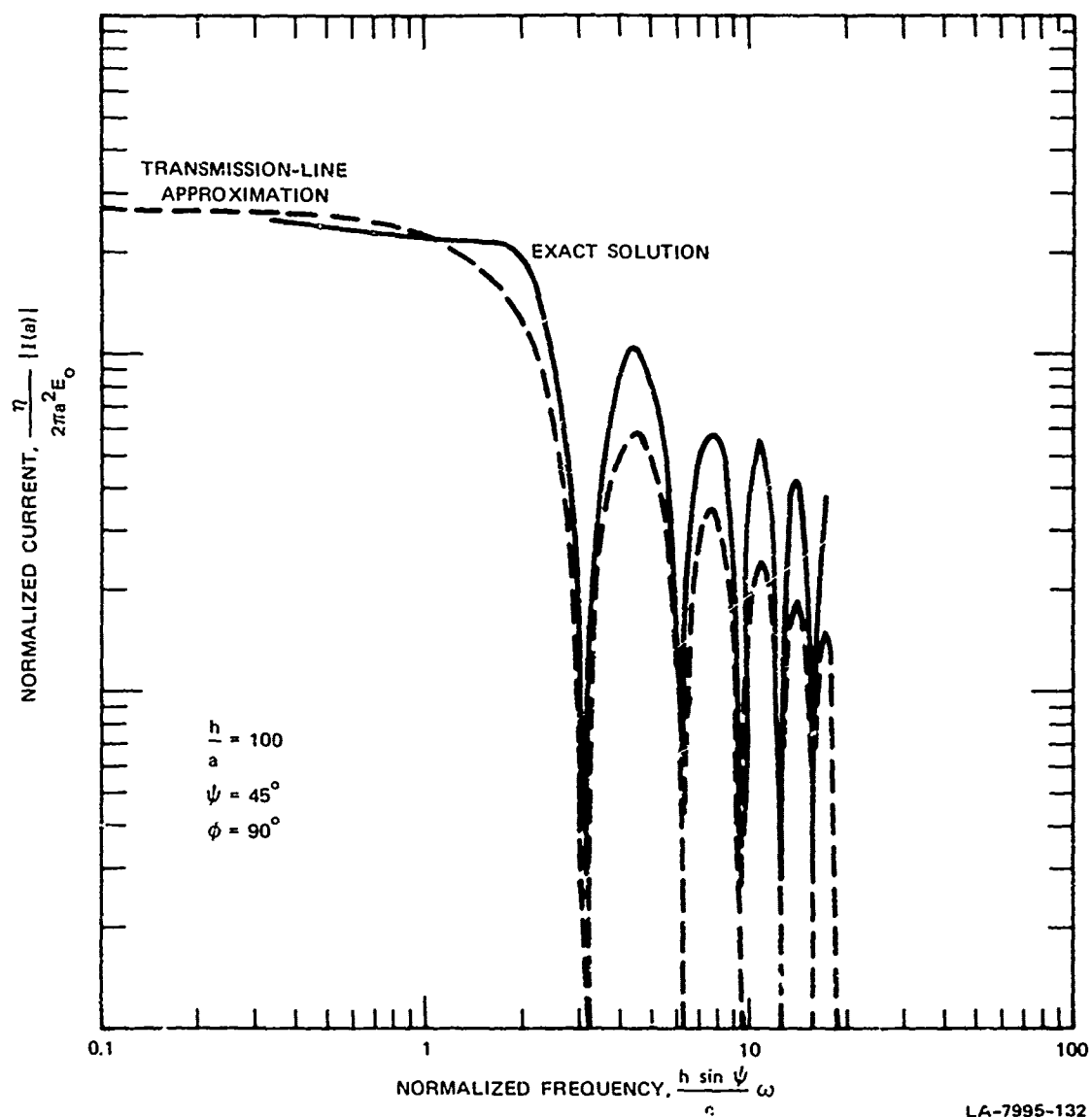


FIGURE A-5 COMPARISON OF THE INDUCED-CURRENT SPECTRA FOR HORIZONTAL POLARIZATION

## Appendix B

### THEORY OF ELECTROMAGNETIC SCALING

The theory of models is widely used in many branches of engineering, especially where the theoretical difficulties make a problem intractable to analytical solution. Before discussing the modeling relations for Maxwell's equation, a discussion of modeling in the context of the familiar RC circuit will illustrate some of the features of modeling. The differential equation for this circuit is

$$V = Ri + \frac{1}{C} \int_0^t i dt \quad (B-1)$$

Differentiating with respect to time, and rearranging, we obtain

$$\frac{\partial i}{\partial t} + \frac{i}{RC} = 0 \quad (B-2)$$

Now suppose that we could not solve this equation, but wanted to make measurements on this circuit to find the variation of current with respect to time and the values of R and C. This is analogous to our being unable, without great difficulty, of solving for the current as a function of time in our transmission line geometry.

If we had the proper R and C and V, we could simply measure the response. However, if it is impractical to make measurements in a laboratory (say, because C is so large), we could still study the response by using a model and the full-scale system can be derived as follows. Assume the following relations between the parameters in the two systems:

$$\begin{aligned}
 i &= ki' \\
 t &= mt' \\
 R &= nR' \\
 C &= pC'
 \end{aligned}
 \tag{B-3}$$

The primed quantities refer to the model system and the unprimed quantities to the full-scale system. The dimensionless numbers  $k$ ,  $m$ ,  $n$ , and  $p$  are the scale factors for the current, time, resistance, and capacitance, respectively.

For the model system the differential equation is

$$\frac{\partial i'}{\partial t'} + \frac{i'}{R'C'} = 0
 \tag{B-4}$$

If we wish to make the current-time response similar for both systems, then we should be able to apply the scaling relations of Eq. (B-3) to Eq. (B-4) and thus show under what conditions Eq. (B-2) and Eq. (B-4) are equal.

For  $i'$  we substitute  $i/k$ . Similarly, with  $R'$  and  $C'$  we substitute  $R/n$  and  $C/p$ . For  $\partial i'/\partial t'$  we use

$$\frac{\partial}{\partial t'} = \frac{\partial}{\partial t} \frac{\partial t}{\partial t'} = m \frac{\partial}{\partial t}
 \tag{B-5}$$

Equation (B-4), with these substitutions, becomes

$$\frac{m}{k} \frac{\partial i}{\partial t} + \frac{np}{k} \frac{i}{RC} = 0$$

This equation will be identical to Eq. (B-2) if

$$\frac{m}{k} = 1$$

$$\frac{np}{k} = 1
 \tag{B-6}$$

These define the scaling relations for similitude.

The first condition says that the current is scaled by the same factor as is the time. If the time is compressed by a factor of 100, the model system current will be decreased by the same factor. Full-scale currents can be found from model-measured currents by multiplying by  $m$ .

The second condition says that the product of the resistance and capacitance scale factors must equal the current scale factor. Since the current and time factors are the same from the first condition, this is the same as saying that the resistance and capacitance is changed in the same proportion as the time. If time is compressed by a factor of 100, the product of resistance and capacitance must be decreased by the same factor.

This, of course, is just restating the result known from the solution of Eq. (B-2) that the current depends on the ratio  $t/RC$  and not  $t$  or  $RC$  separately. Note that this conclusion may be derived from an analysis of the scaling relations without actually solving the equation.

This procedure can be applied to Maxwell's equations to find the scaling relations for electromagnetic problems. The conditions for similitude will lead to relations between the parameters in Maxwell's equations. When these conditions hold, the relation between the full scale fields and parameters will be similar to those for the model system. The scaling relations will enable one to apply results from the model system to the full scale system.

The most complete discussion of electromagnetic scaling is given by Sinclair.<sup>11</sup> We shall draw on his discussion for most of what follows. Consider a full scale system that is described by spatial coordinates  $x, y, z$ , time coordinate,  $t$ , and electric and magnetic field vectors

$E(x, y, z, t)$ , and  $H(x, y, z, t)$ . The corresponding quantities in the model system are primed. Sinclair shows that if there are scale factors that relate the full scale to the model system quantities such that

$$\begin{aligned}x &= px' \\y &= py' \\z &= pz' \\t &= \gamma t' \\E(x, y, z, t) &= \sigma E'(x', y', z', t') \\H(x, y, z, t) &= \beta H'(x', y', z', t')\end{aligned}\tag{B-7}$$

a set of relations between the scale factors  $(p, \gamma, \sigma, \beta)$  may be found that ensure that the model is an accurate simulation of the full-scale system. This is done by equating Maxwell's equations in the full-scale system to a set of equations derived from Maxwell's equation in the model system that are transformed to full-scale quantities by the appropriate scale factors.

Thus Maxwell's equations in the full-scale system are

$$\begin{aligned}\text{curl } H &= \sigma E + \epsilon \frac{\partial E}{\partial t} \\ \text{curl } E &= -\mu \frac{\partial H}{\partial t}\end{aligned}\tag{B-8}$$

In the model system they are

$$\begin{aligned}\text{curl}' H' &= \sigma' E' + \epsilon' \frac{\partial E'}{\partial t'} \\ \text{curl}' E' &= -\mu' \frac{\partial H'}{\partial t'}\end{aligned}\tag{B-9}$$

To illustrate the procedure, consider the term

$$\text{curl}'_{x'} H' = \frac{\partial H'_{z'}}{\partial y'} - \frac{\partial H'_{y'}}{\partial z'}\tag{B-10}$$

Since  $H = \beta H'$  and

$$\frac{\partial}{\partial y'} = \frac{\partial}{\partial y} \frac{\partial y}{\partial y'} = p \frac{\partial}{\partial y}$$

$$\text{curl}'_{\mathbf{x}}, H' = \frac{p}{\beta} \text{curl } H \quad (\text{B-11})$$

In this way each of the model system terms are related to the full-scale system.

A set of three equations that must be satisfied ensures accurate simulation. These are

$$\sigma' = p \frac{\alpha}{\beta} \sigma$$

$$\epsilon' = \frac{p\gamma}{\gamma\beta} \epsilon$$

$$\mu' = \frac{p}{\gamma} \frac{\beta}{\alpha} \mu \quad (\text{B-12})$$

Sinclair's article continues with the general scaling properties, but for our cases we can deduce several important conclusions from the above set of equations. If permittivity and permeability are to be the same in both the model and the full-scale system, then  $\alpha/\beta = 1$ ,  $p/\gamma = 1$ , and  $\sigma' = p\sigma$ . The first condition says that the ratio of  $E/H$  in the two systems is the same. This is satisfied if the  $\epsilon$  and  $\mu$  in both systems are the same. The second condition requires that the length scale and the time scale must vary by the same factor. If the model dimensions are 1/100 of full scale, then the time must also be compressed by a factor of 100.

The third condition says that the conductivity in the model system must be changed directly with the length scale factor. The model conductivity must be 100 times the full-scale conductivity if the model dimensions are 1/100 of the full scale dimension.

If the above relations are satisfied, then many other relations can be derived, such as Poynting vector, power, gain, echo area, current density, etc. The quantity most important for us is that for current:

$$I = \beta p I' \quad (B-13)$$

The full-scale current is equal to the model current multiplied by the length scale factor and the ratio of the full-scale magnetic field to the model magnetic field. Since  $\sigma = \beta$  we could as well use the ratio of electric fields.

$$I = \sigma p I' \quad (B-14)$$

If one multiplies and divides by  $E$ , one obtains

$$I = E p \frac{I'}{E'} \quad (B-15)$$

In our measurements we will determine  $I'/E'$ , so that full-scale currents may be found by multiplying by  $E p$ .

The restrictions on such modeling require that the media be linear. The media may vary from point to point in space but must be independent of time.

A practical restriction that is usually unimportant is that if the full-scale system has conductors (like antenna elements) as well as a conducting ground, the conductivity of the conductors should be modeled for perfect simulation. This is difficult to do if the full-scale conductors are copper. However, in cases where the losses on the conductors are negligible, the effect of not modeling the conductor conductivity is unimportant. For example, with a rod-over-ground transmission line it is usually unimportant to scale conductivity of the rod, since most of the loss is in the ground. Only the ground conductivity must then be scaled for proper simulation.

## Appendix C

### ESTIMATED ACCURACY OF THE MODEL DATA

The scale-model experiments were conducted with a pulsed dipole antenna illuminating the model, and measurements of the response of the model were made with a current probe and recorded with an oscilloscope and X-Y recorder as illustrated in Figure C-1. The components of this system that are important in evaluating the accuracy of the measurements are the current probe, the oscilloscope, and the transmitting antenna.

The current on the transmission line was measured with a Tektronix CT-1. This current probe has an accuracy of  $\pm 5$  percent. The currents were detected using a Hewlett-Packard sampling-scope system with an accuracy of  $\pm 3$  percent.

The largest error is that associated with the peak radiated field. There are frequency-dependent losses in the cable and balun that feed the dipole radiator. A measurement of the efficiency of conversion of dc supply voltage to current at the antenna terminals gave a value of about 70 percent of the theoretical value when no losses were assumed.

The dipole had tapered tips at the feedpoint for 4 inches of length and then was a uniform cylinder of 1 inch diameter. This structure was treated as a uniform bicone of diameter equal to 1 inch and length associated with the ground clear time ( $2h/c \sin \phi$ ) to evaluate the peak field. It is estimated that the peak field per dc charge volt could be in error by  $\pm 15$  percent.

The  $1/e$  decay time of the current at the antenna feedpoint is 35 ns. This represents a decrease in field of about 4 percent in  $2h/c \sin \phi$  for

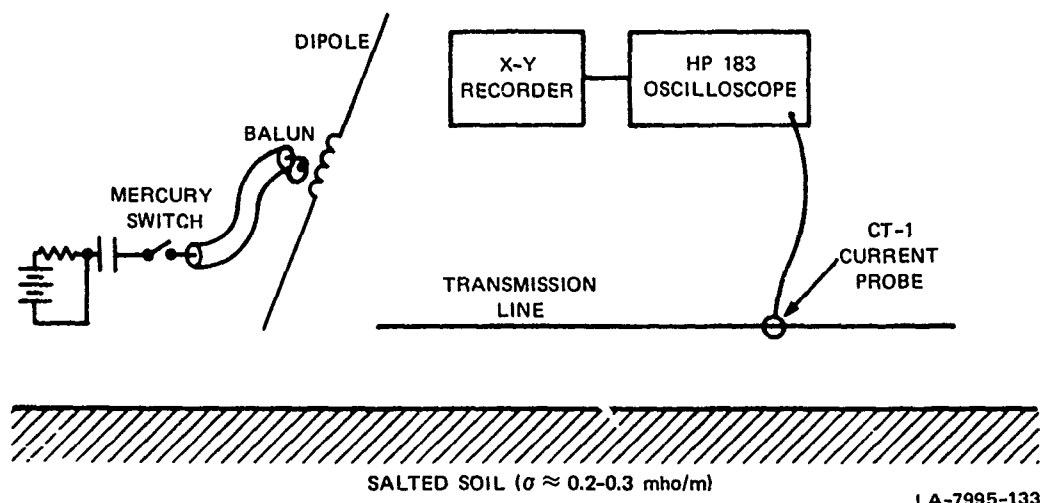


FIGURE C-1 SCALE-MODEL EXPERIMENT TO STUDY COUPLING TO TRANSMISSION LINE

the 2-foot-high line, and was accounted for in Ref. 2. At much later times, the waveform will have larger deviations from a step-function input that will also include a decrease in radiated field due to increasing impedance of the cylindrical dipole antenna.

Because the radiating source was a finite distance from the power-line model, different parts of the line were illuminated with different amplitudes and polarizations. For  $\phi = 90^\circ$  illumination, the errors were quite small (a few percent) for the peak values, increasing slowly with time. At  $\phi$  close to  $0^\circ$  the errors were larger, although even there, the peak field error was estimated to be no more than about 10 percent.

Therefore if the current probe and the oscilloscope errors are assumed to be random so that they combine in a root-mean-square fashion, the random error in the measurements will be about 6 percent. In addition, there are accountable systematic deviations due to the droop in the radiated "step function" and the nonuniformity of the field. Finally, there is an uncertainty, which is probably systematic, of about 15 percent in absolute magnitude of the incident field strength.

## REFERENCES

1. E. D. Sunde, Earth Conduction Effects in Transmission Systems, (Dover Publications, New York, 1968).
2. W. E. Scharfman, K. A. Graf, and E. F. Vance, "Analysis of Coupling to Horizontal and Vertical Wires," Technical Memorandum 22, AFWL, Contract F29601-69-C-0127, SRI Project 7995, Stanford Research Institute, Menlo Park, California (January 1973).
3. E. F. Vance and S. Dairiki, "Analysis of Coupling to the Commercial Power System," Technical Report No. AFWL-TR-72-21, Contract F29601-69-C-0127, SRI Project 7995, Stanford Research Institute, Menlo Park, California (October 1971).
4. J. K. Baird, J. H. Marable, and D. B. Nelson, "Studies of Nuclear Electromagnetic Pulse (EMP) Effects on Power Systems," ORNL-4784, Annual Progress Report, Civil Defense Research Project, Oak Ridge National Laboratory, Oak Ridge, Tennessee (December 1972).
5. E. F. Vance and W. E. Scharfman, "Investigation of Power Line Excitation," Technical Memorandum 21, AFWL, Contract F29601-69-C-0127, SRI Project 7995, Stanford Research Institute, Menlo Park, California (December 1972).
6. R. W. King, Transmission Line Theory, p. 269 (Dover Publications, New York, 1965).
7. King, op cit. pp. 382-389.
8. Reference Data for Radio Engineers, Fifth Edition, Chapter 22, p. 22 (Howards Sams, & Co., Indianapolis, 1968).
9. C. W. Harrison, Jr., "Missile With Attached Umbilical Cable as a Receiving Antenna," IEEE Trans. on Antennas and Propagation, Volume AP-11, No. 5, pp. 587-588 (September 1963).

10. C. Flammer and H. E. Singhaus, "The Interaction of Electromagnetic Pulses with an Infinitely Long Conducting Cylinder Above a Perfectly Conducting Ground," Interaction Note, Contract F29601-69-C-0127, SRI Project 7995, Stanford Research Institute, Menlo Park, California (to be published).
11. G. Sinclair, "Theory of Models of Electromagnetic Systems," Proc. IRE, Vol. 36, pp. 1364-1370 (November 1948).

## DISTRIBUTION

No. cys

	Hq USAF, Wash, DC 20330
1	(OA)
1	(RDQPM, 1C366)
1	(RDQPN, 1D425)
	Hq USAF, AFTAC, Patrick AFB, FL 32925
1	(TAP)
1	(TD-5)
1	USAF Dep, IG (SEL), Norton AFB, CA 92409
1	Dir Aerosp Safety IGDS), Norton AFB, CA 92409
1	USAF Dir Nuc Safety (SN), Kirtland AFB, NM 87117
	ArSC, Andrews AFB, Wash, DC 20334
1	(DO)
1	(DOB)
1	(DLTE)
1	SAC (OA), Offutt AFB, NE 68113
	ADC, Ent AFB, CO 80912
1	(DOA)
1	(DEE)
1	AUL (LDE), Maxwell AFB, AL 36112
1	AU (ED, Dir, Civ Eng), Maxwell AFB, AL 36112
	AFIT, Wright-Patterson AFB, OH 45433
1	(Tech Lib, Bldg 640, Area B)
1	(CES)
	USAF Academy, CO 80840
1	(DFSLB)
1	(DFCE)
3	SAMSO (MNNH), P. O. Box 92960, WWPC, LAAFS, Los Angeles, CA 90009
	ESD, L. G. Hanscom Fld, Bedford, MA 01730
1	(DEE)
1	(Capt L. West)
1	AFSWC (HO), Kirtland AFB, NM 87117
	AFWL, Kirtland AFB, NM 87117
5	(SUL)
1	(SA)
1	(SAA)
1	(SAB)
2	(SAY)
1	(DE)
1	(EL, J. Darrah)
1	(ELE, C. Baum)
5	(ELA, Capt Wilson)
1	(ELA, Lt Col Fortin)
2	(ELX)
1	(SEC)
1	(SES)

## DISTRIBUTION (cont'd)

No. cys

1	AFSC (OAR), Andrews AFB, Wash, DC 20334
1	AFOSR, 1400 Wilson Blvd, Arlington, VA 22209
1	Chief, R&D (CRDP), Dept Army, Wash, DC 20310
	Comdg Off, Diamond Lab, Wash, ED 20438
1	(Lib)
1	(Dr. J. Bombardt)
1	Redstone Sci Info Cen (Chief, Doc Sec), Redstone Arsenal, AL 35809
1	Comdg Off, BRL (AMXBR-TB, J. Meszaros), Aberdeen Prvg Gnd, MD 21005
1	Dir, NSA (C513), Ft Meade, Md 20755
1	BRL (AMXBR-RL), Aberdeen Prvg Gnd, MD 21005
1	Dir, NRL (Code 2027), Wash, DC 20390
1	Comdg Off & Dir, NEL (Code 4223), San Diego, CA 92152
1	Comdr, NOL (Code 730), White Oak, Silver Spring, MD 20910
1	Comdg Off, NWEF (Code ADS), Kirtland AFB, NM 87117
1	Dir, DNA (RAEV, Maj W. Adams), Wash, DC 20305
2	DDC (TCA), Cameron Sta, Alexandria, VA 22314
1	LLL (Lib), Bldg 50, Rm 134, Berkeley, CA 94720
1	Dir, LASL (Rpt Lib), P. O. Box 1663, Los Alamos, NM 87554
5	SRI (Dr. T. Morita), 333 Ravenswood, Menlo Park, CA 94025
1	TRW Sys Gp (J. Dahnke), P. O. Box 1310, San Bernardino, CA 92402
1	TRW Sys Gp (W. Robinette), 1 Space Park, Redondo Beach, CA 90278
1	GE TEMPO (L. Shaw), 816 State St, Santa Barbara, CA 93101
	Boeing Co, Box 3999, Seattle, WA 98124
1	(D. Isbell)
1	(J. Dicommes)
2	Oak Ridge Mat Lab (J. H. Marable, Civ Def Rsch Proj), P. O. Box X, Oak Ridge, TN 37830
1	Official Record Copy (Capt Wilson, AFWL/ELA)

UNCLASSIFIED

Security Classification

## DOCUMENT CONTROL DATA - R &amp; D

(Security classification of title, body of abstract and indexing annotation must be entered when the overall report is classified)

1. ORIGINATING ACTIVITY (Corporate author)		2a. REPORT SECURITY CLASSIFICATION	
Stanford Research Institute Menlo Park, California 94025		UNCLASSIFIED	
		2b. GROUP	
3. REPORT TITLE			
ELECTROMAGNETIC PULSE COUPLING AND PROPAGATION TO POWER LINES: THEORY AND EXPERIMENTS			
4. DESCRIPTIVE NOTES (Type of report and inclusive dates)			
Final Report; 1 May 1972-1 November 1973			
5. AUTHOR(S) (First name, middle initial, last name)			
W. E. Scharfman; E. F. Vance			
6. REPORT DATE		7a. TOTAL NO. OF PAGES	7b. NO. OF REFS
February 1974		102	11
8a. CONTRACT OR GRANT NO.		9a. ORIGINATOR'S REPORT NUMBER(S)	
F29601-69-C-0127		AFWL-TR-73-287	
b. PROJECT NO		9b. OTHER REPORT NO(S) (Any other numbers that may be assigned this report)	
133B		Contractor's rpt No: SRI Project 7995	
10. DISTRIBUTION STATEMENT			
Distribution limited to US Government agencies only because test and evaluation information concerning electromagnetic pulse coupling and propagation is discussed in the report (Feb 74). Other requests for this document must be referred to AFWL (ELA), Kirtland AFB, NM, 87117.			
11. SUPPLEMENTARY NOTES		12. SPONSORING MILITARY ACTIVITY	
		AFWL (ELA) Kirtland AFB, NM 87117	
13. ABSTRACT			
(Distribution Limitation Statement B)			
Coupling of transients to aboveground transmission lines is analyzed and measured experimentally. Measurements were made using scale models approximately 1-foot high to represent power transmission lines. The coupling to the line and the propagation characteristics of the line were measured. The effects of bends and junctions on the transmitted signals were measured and analyzed. Periodically, grounded lines and multiconductor lines were also examined. The variation of the induced-voltage waveforms with soil conductivity, line height, and pulsewidth were calculated.			

DD FORM 1473

1 NOV 65

UNCLASSIFIED

Security Classification

UNCLASSIFIED

Security Classification

14	KEY WORDS	LINK A		LINK B		LINK C	
		ROLE	WT	ROLE	WT	ROLE	WT
	Transmission lines Electromagnetic pulse Power lines Coupling Transients						

UNCLASSIFIED

Security Classification